Universidad Autónoma de Madrid
Facultad de Ciencias – Departamento de Biología Molecular

Structural studies on adenovirus: the human adenovirus packaging motor, and characterization of two reptilian adenoviruses.

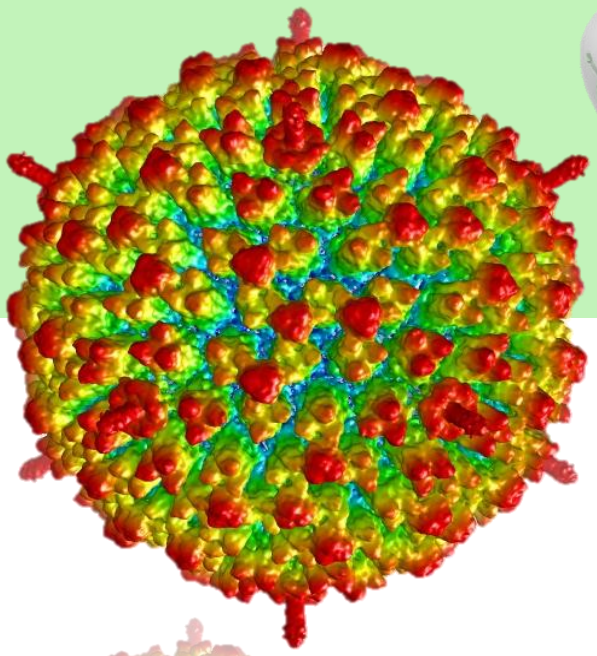

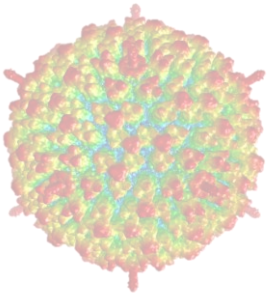

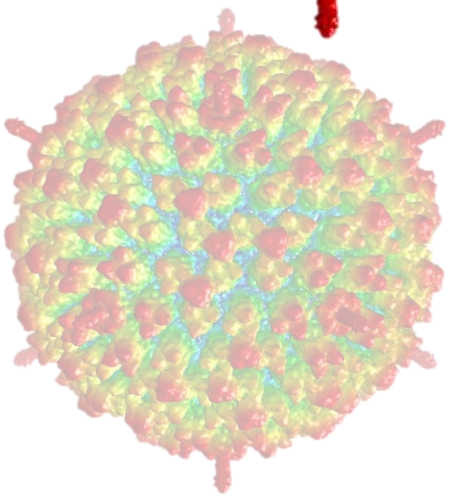

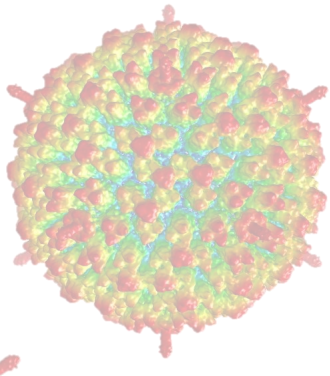

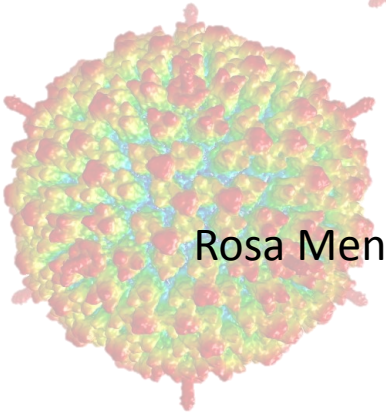

Rosa Menéndez-Conejero
Madrid, 2013

Universidad Autónoma de Madrid

Departamento de Biología Molecular

Facultad de Ciencias

"Structural studies on adenovirus: the human adenovirus packaging motor, and characterization of two reptilian adenoviruses."

-TESIS DOCTORAL-

Rosa Menéndez-Conejero

Madrid, 2013

Universidad Autónoma de Madrid

Departamento de Biología Molecular

Facultad de Ciencias

Memoria presentada para optar al grado de Doctor en Ciencias Biológicas por

Rosa Menéndez-Conejero

Universidad Autónoma de Madrid

Febrero de 2013

Directora de tesis:

Mª Carmen San Martín Pastrana

CNB-CSIC

El trabajo recogido en esta memoria ha sido realizado en el Centro Nacional de Biotecnología (CNB-CSIC) bajo la dirección de la Dra. MªCarmen San Martín Pastrana. Su financiación corrió a cargo de una beca pFIS del Instituto de Salud Carlos III (ISCIII). También se contó con la ayuda de una beca EMBO para la realización de estancias breves y con la aportación de diversos proyectos: PIE 2004-2-OE-337 (CSIC), BFU 2007-60228 (MICINN), CCG08-CSIC/SAL-3442 (CSIC-CAM), DE2009-0019 (MICINN-DAAD), BFU2010-16382 (MICINN).

Contents

Index of figures

Index of tables

Introduction

1 Introduction

1.1 A general view on adenoviruses

Adenoviruses (AdVs) were first isolated from adenoid human tissue in 1953 by Rowe et al. (Rowe et al., 1953) as a novel viral agent associated with respiratory infections. Since then, a large number of adenoviruses have been detected infecting a wide range of vertebrates, and classified in five genera approved so far ("Virus Taxonomy", 2011). Due to their dual role as pathogens and as tools for therapies, the human adenoviruses are the most extensively studied.

There are 51 different serotypes of adenovirus infecting humans, some of them producing eye, gut and respiratory infections which are mostly not clinically relevant for healthy individuals, but can be fatal for immunocompromized ones (Leen and Rooney, 2005).

AdVs as experimental systems have been useful for investigating fundamental processes in the eukaryotic cell life, such as splicing and apoptosis. Recombinant human viruses are widely studied as vehicles for gene transfer, oncolysis and vaccination (Dobbelstein, 2004; Draper and Heeney, 2010; Goncalves and de Vries, 2006; Lasaro and Ertl, 2009; Shiver et al., 2002; Stadtfeld et al., 2008; Yamamoto and Curiel, 2010). However, their successful use in humans is impaired by pre-existing immunity to the most common vectors. An approach to solve this problem is the use of recombinant viruses of non-human origin (Loser et al., 2002). Increasing the scarce characterization of AdVs infecting hosts remote from humans (reptile, amphibian or fish) is required to estimate their possible use as vectors. Also from the clinical point of view, there is a need to develop anti-adenoviral drugs, since there are no approved therapies at present. Apart from the morbidity in immunocompromized patients and other susceptible populations in humans, the ecological risk of losing threatened animal species and the economic interest to preserve the health of farm animals must also be considered. For example, fowl AdVs can have significant economic impact (Hess, 2000).

1.2 Human adenovirus

1.2.1 Genome

Adenovirus genomes are linear double-stranded DNA molecules of approximately 35 kpb in the viruses infecting humans, covalently attached at both 5' ends to one molecule of the terminal protein (TP). The terminal regions of the genome are inverted repeats (ITR) varying from 50 to 170 bp, which contain the origins of viral DNA replication.

Adenovirus genes are encoded in overlapping transcription units, in both directions, and undergo extensive alternative splicing to yield multiple unique mRNA products (Berget, Moore, and Sharp, 1977; Chow et al., 1977). The genome (**Figure 1**) is divided into early functions (E1A, E1B, E2A, E2B, E3, and E4 regions), which are expressed first during infection, and late functions (L1 to L5 regions), which are usually expressed after the early functions and after the beginning of viral DNA replication. The late genes encode the viral structural proteins, except for IX and IVa2, which are intermediate genes.

The left end of the genome encodes cis-acting sequences that appear to contribute to the directed packaging of the genome into the empty capsids (Hammarskjold and Winberg, 1980). The precise mechanism by which genome encapsidation occurs, however, remains poorly understood (see section 1.2.4).

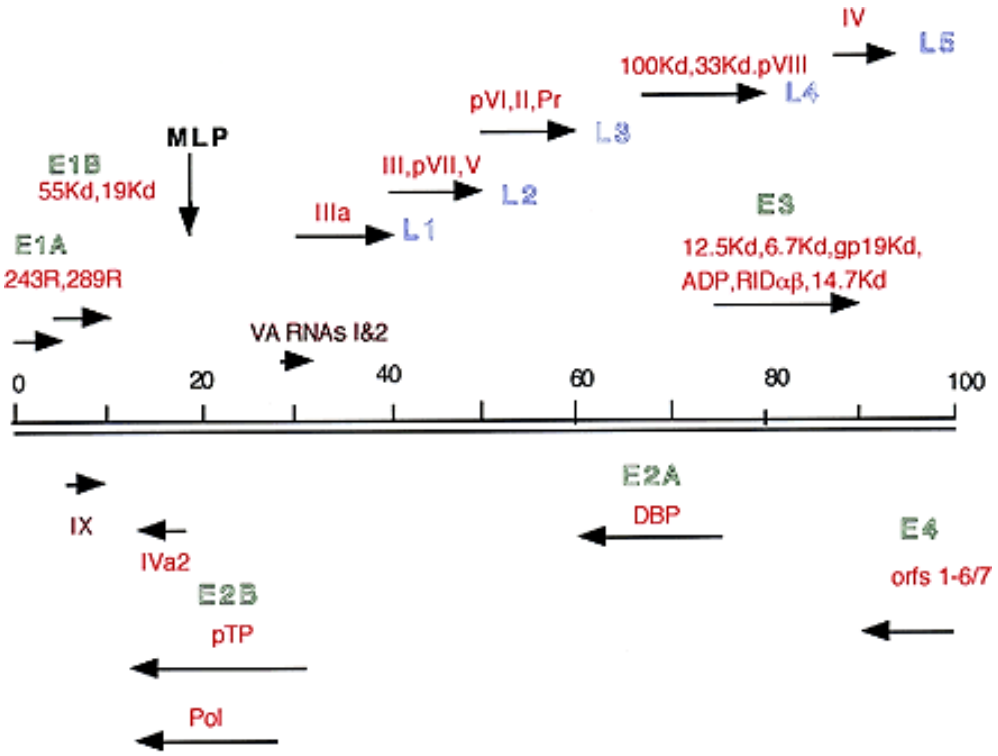

Figure 1.- Transcription of the adenovirus genome (Russell, 2000). Early transcripts are outlined in green, late ones in blue. Arrows indicate the direction of transcription. MLP, Major Late Promoter.

1.2.2 Structure

Adenoviruses have non enveloped, icosahedral capsids approximately 90 nm in diameter, with fibers projecting from the vertices of the icosahedron (Stewart et al., 1991). Most structural studies have focused on the closely related human adenoviruses type 2 and 5 (Ad2 and Ad5). The particles (virions) of Ad2 and Ad5 have a mass of approximately 150 x 10^6 Da and contain one molecule of dsDNA (13% of mass), protein (87% of mass), no lipids, and trace amounts of carbohydrate because the virion fiber protein is modified by addition of O-linked N-acetyl-glucosamine. Virions consist of a protein shell (capsid) surrounding a DNA-containing core **(Figure 2).**

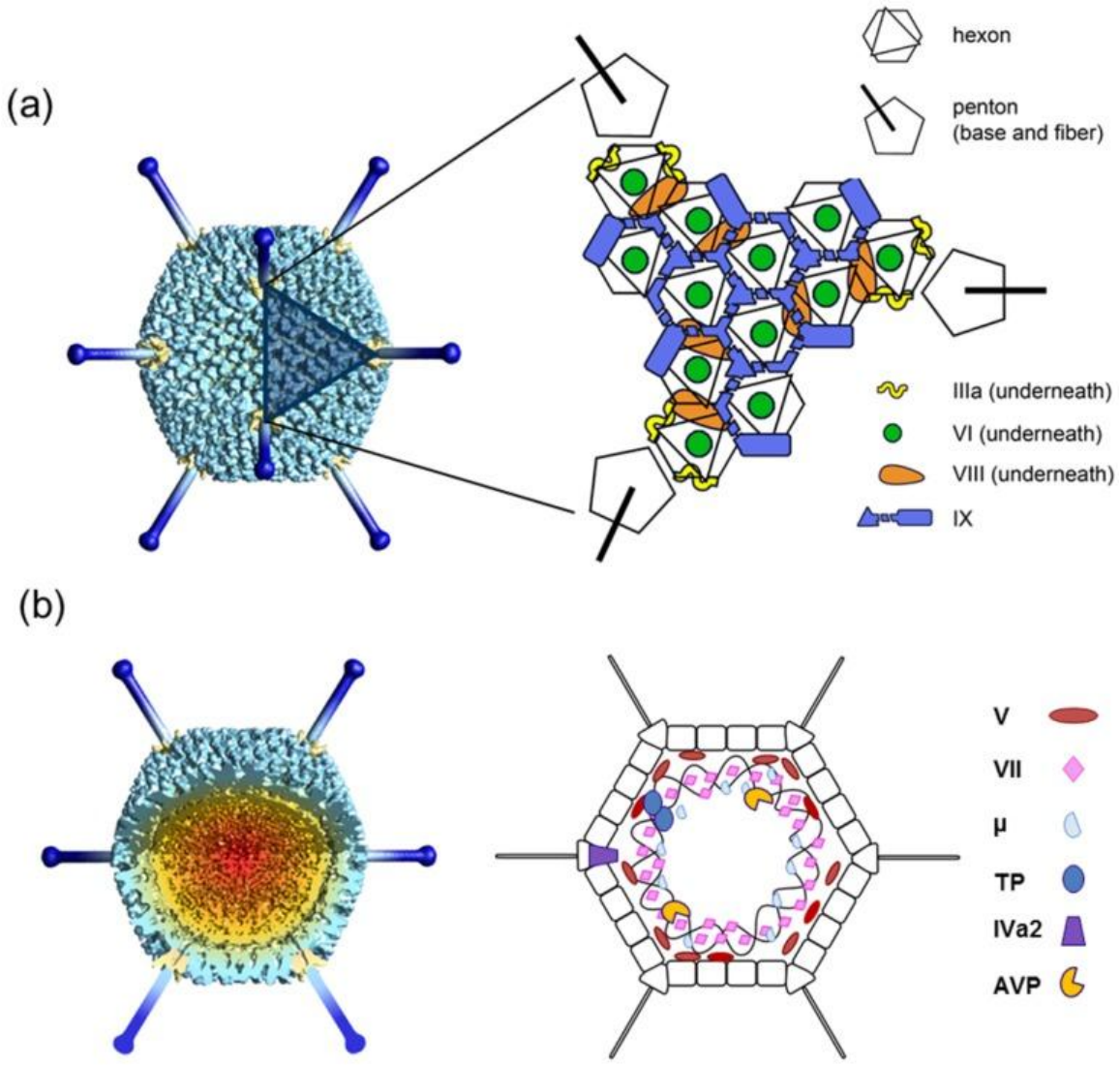

Figure 2.-Overall AdV structure and components. (San Martin, 2012) (**a**) Icosahedral shell organization according to current structural knowledge. The left hand side panel is a model built from a low resolution cryoEM map, with penton bases highlighted in yellow, and fibers built from the crystal structure of the knob and distal shaft (van Raaij et al., 1999) in dark blue. The shaded triangle indicates one facet. (**b**) Non-icosahedral components. A segment has been removed from the cryoEM map to show the inner capsid contents. The schematics on the right hand side indicate tentative positions, as little is known about the structure and organization in the virion of the genome and accompanying proteins. Polypeptide IVa2, which binds to the specific packaging sequence in the viral genome, has been reported to occupy a singular vertex in the capsid (Christensen et al., 2008).

Electrophoretic analyses of purified virions disrupted with sodium dodecylsulfate were used initially to identify structural polypeptides (Maizel, White, and Scharff, 1968). The adenovirus virion is composed by at least 11 different proteins. The major capsid protein, hexon, builds the 20 facets of the icosahedron. Penton base is present at the twelve vertices from which the third major adenoviral protein protrudes: the fiber.

1.2.2.1 Fiber

Three copies of the fiber gene product are assembled forming the homotrimeric fiber protein, which protrudes from the penton base at each of the 12 vertices of the capsid. All adenovirus fiber proteins present a common architecture: an N-terminal tail attached non-covalently to the penton base, a central shaft made of repeating sequence motifs, and a C-terminal segment folded in a globular knob domain (**Figure 3-A**). The function of the fiber is the initiation of infection by binding to cellular receptor(s); thus determining tissue tropism (Cupelli and Stehle, 2011).

Fiber density is usually absent or blurred in structural studies of the complete virion, due to its intrinsic flexibility and the symmetry mismatch between the trimeric fiber and the 5-fold icosahedral vertex (Ruigrok et al., 1990; van Oostrum and Burnett, 1985). A pseudo-atomic model of the entire human Ad5 fiber has been built based on the crystal structures of the penton base and the knob, together with a homology model from the crystal structure of the Ad2 fiber shaft to merge with the cryoEM density from the Ad5 fiber. It has been proposed that the three N-terminal tails of each fiber act as stay-cables, residing inside three of the five grooves between neighboring penton base monomers (Liu, Wu, and Zhou, 2011) (**Figure 3-B**).

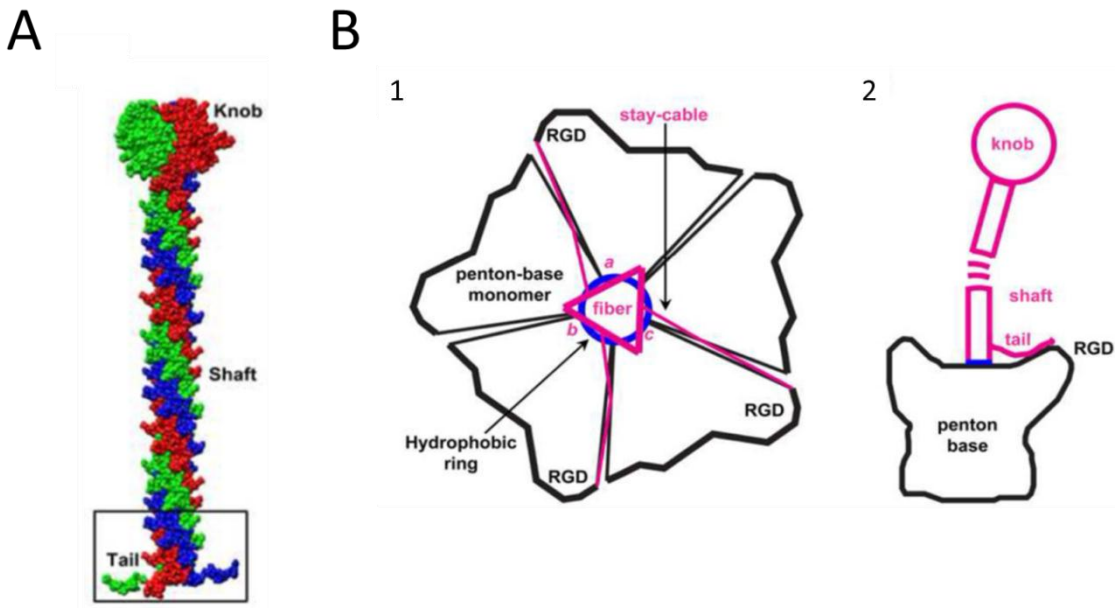

Figure 3.-Fiber model and attachment of the trimeric fiber to the pentameric penton base. (Favier et al., 2002) (A) Full space filling model of the Ad5 fiber consisting of a globular knob, a long shaft, and three short N-terminal tails. The three subunits are coloured red, green and blue. (B) Schematic illustrations of the attachment of the trimeric fiber (magenta) to the pentameric penton base (black). (B-1) Top view showing the trimeric fiber attached to the pentameric penton base at a hydrophobic ring (blue) and three fiber tails (stay-cables). The three sides (*a*–*c*) of the magenta triangle denote the three subunits of each fiber. (B-2) Side view of (B-1), showing the locations of the hydrophobic interaction (blue), 'stay-cable'/tail, and the flexible fiber shaft.

Most of the adenoviruses sequenced so far present one single gene coding for fiber protein. The previous description of one fiber attached to the penton base can accomodate the symmetry mismatch for this general case, but there are exceptions of adenoviruses with more than one fiber gene. Human adenovirus type 41 presents two different fiber products encoded by two fiber genes (Kidd et al., 1993; Song et al., 2012). There are three possible ways to explain how two trimeric fibers can fit into the viral vertices. The first one is that, despite being two different fibers, there is only one per penton, as in Ad41 (Favier et al., 2002). The second possibility is that only one fiber is attached to the penton base and the second fiber is attached to the first one. Finally, that both fiber tails are attached to the penton base, forming a mismatch of five penton base to six fiber monomers.

1.2.2.2 Minor coat proteins

There are other coat proteins whose particular function is not fully characterized yet, but they are likely to play essential roles for the virus. The most informative AdV

structural data comes from a cryo-EM study at atomic resolution published in 2010, allowing the tracing of polypeptide chains to reveal in detail the different minor coat proteins and their interactions (Liu et al., 2010) (**Table 1**).

Protein	Localization	Reported or proposed function(s)
IIIa	– Underneath each vertex, at the inner capsid surface.	– Stabilizing the vertex region and the packaged genome upon assembly. – Signaling for vertex and genome release during uncoating.
VI	– Bound to the inner cavity of the hexon trimer and to dsDNA, bringing the core to the icosahedral shell.	– Viral escape from the endosome. – Trafficking to the nucleous along the microtubular network. – Activator of the adenoviral gene expression. – Transport of newly synthesized hexon bound to VI to the nucleous. – Substrate and cofactor of the adenoviral protease.
VIII	At the inner capsid surface: – Around the icosahedral 3-fold symmetry axis, stabilizing groups of nine hexons (GONs) – Wedged between polypeptide IIIa and the hexon bases located at the periphery of the vertex region.	– Architectural contribution to the capsid as cementing protein.
IX	On the outer part of the AdV capsid forming a hairnet: – Binds hexons within one GON, and adjacent GONs across the edge.	– Viral entry: interaction with kinesin-1, allowing the partially disrupted virion to travel along the microtubule network. – Modulation of the viral tropism and/or interfering with the immune response. – Cementing protein of the GON, capsid stabilization.

Table 1.- Localization and functions of adenovirus minor coat proteins. See (San Martin, 2012) for original references.

1.2.2.3 Core

The human adenovirus core contains a single molecule of linear double stranded DNA and four viral proteins: polypeptides V, VII, μ and the TP. Two copies of the TP are covalently linked to the 5' genome ends, circularizing it and acting as a primer for DNA replication (Rekosh et al., 1977). Polypeptides V, VII and μ bind DNA (Chatterjee, Vayda,

and Flint, 1986b), and their high proportion of basic residues makes them similar to histones, although at present the disposition of DNA and proteins in the core is still unclear. Additionally, the viral protease in charge of the virion maturation and the minor protein IVa2 are also bound to DNA in the core..

1.2.3 Infectious cycle and assembly

Adenovirus infects epithelial cells by receptor mediated endocytosis. For most of the human adenoviruses, the first step is the binding of fiber knob to a CAR type receptor in the cell surface. Afterwards, penton base binds integrin and the endocytosis takes place. Inside the endosome, because of the low pH, the viral capsid suffers modifications, releasing some internal proteins and triggering the release from the vesicle. Once liberated from the endosome, the subviral particle travels along the cytoskeleton to the nucleus, where the viral DNA is inserted through the nuclear pore (**Figure 4**). This viral DNA is replicated and transcribed in the nucleus and once the new viral proteins are produced in the cytoplasm, they are transported to the nucleus to assemble new viruses (Flint, 2009). How the assembly of the new capsids and the packaging of DNA happens is not yet fully understood.

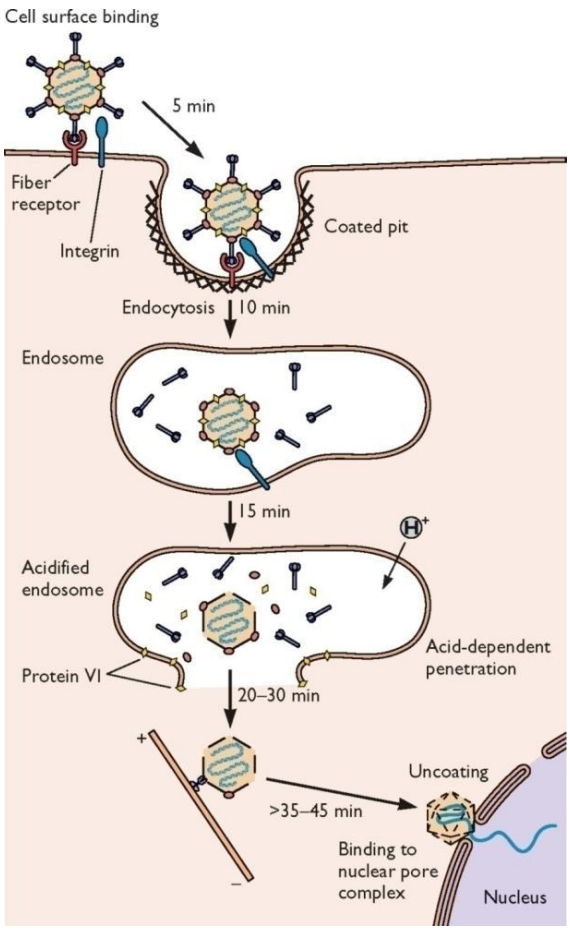

Figure 4.- Adenovirus infection pathway (Flint, 2009).

The last step of the adenovirus maturation consists in a proteolytic processing of the virion. Adenoviruses, like many other viruses, encode an endoproteinase which is required for virus maturation and infectivity (Weber, 1995). This proteinase cleaves some of the capsid and core protein precursors to produce to the mature form of the virus.

1.2.4 Adenovirus genome packaging

Adenovirus purification by CsCl density gradient centrifugation led to the observation of viral particles with buoyant densities significantly lower than those of the infectious virions. The lightest of these particles were identified by EM and polypeptide analysis as empty adenovirus capsids (Shimojo et al., 1967; Smith, 1965). The first evidence about the nature of the incomplete particles as intermediates in virus assembly came from *in vivo* pulse-chase experiments (Sundquist et al., 1973) observing that incorporation of labeled aminoacids to viral proteins was first detected in empty particles and delayed in the full ones. In addition, adenovirus particles observed at positions in CsCl density gradients between the virions and the empty capsids contain viral DNA sequences shorter than full-length virion DNA (Prage, Hoglund, and Philipson, 1972; Wadell, Hammarskjold, and Varsanyi, 1973), and are therefore considered incomplete packaged virions. These intermediates of DNA packaging and the directional encapsidation of the genome starting from its left end suggested a similarity between the adenovirus and the bacteriophage packaging mechanisms, based on the encapsidation of the dsDNA genome into pre-assembled empty capsids through a special vertex.

1.2.5 Packaging motors in phages

Most dsDNA bacteriophage and some dsDNA eukaryotic viruses (HVS, (Rochat et al., 2011)) assemble empty procapsids into which the genome is subsequently packaged, thereby compressing a large amount of negatively charged DNA into a limited space (Rao and Feiss, 2008).

In dsDNA bacteriophage, the preformed empty shell is an icosahedral structure formed by many copies of the major capsid protein. One of the 12 fivefold vertices in the shell is a special portal vertex formed by the dodecameric portal protein (Driedonks and Caldentey, 1983). During assembly, a viral enzyme complex, called terminase, is docked on the portal and the DNA is translocated through the portal channel. This DNA encapsidation process is powered by the ATP hydrolysis activity of the terminase complex. Components and characteristics of the portal complex are summarized in **table 2**.

Component		Number of subunits	Functions
Conector		12	DNA translocation into the capsid.
Terminase complex	Major terminase	5, 6	ATPase and nuclease. DNA is threaded through the central channel.
	Minor terminase	8, 10 or larger	Recognizes viral DNA and regulates enzymatic activity of the major terminase. DNA wraps around the outside of the ring and it is directed to the major terminase.

Table 2.- Portal components in dsDNA bacteriophages

There are common characteristics in most of the described packaging motors, such as a ring-shaped oligomeric conformation; conserved sequence motifs associated with binding and hydrolysis of ATP (Walker Box); and a location at a single vertex of the virus (as a transient structure in bacteriophages or as a virion component after packaging in other viruses, such as HSV and PBCV-1) (Cherrier et al., 2009; Rao and Feiss, 2008; Rochat et al., 2011; Yamada, Onimatsu, and Van Etten, 2006).

Numerous attempts to crystallize viral terminases have failed, presumably because the proteins are flexible or conformationally heterogeneous, or much too unstable to easily carry out structural studies. In the same way, the adenoviral candidate to conform the motor protein for DNA packaging, has not been crystallyzed nor structurally described by other methods.

1.2.6 IVa2 protein: the putative AdV packaging motor

IVa2 was first described as an effector of the late-phase-dependent activation of the major late promoter (Lutz and Kedinger, 1996). Later on, it was reported that IVa2 binds to L1 52/55-kDa protein (Gustin, Lutz, and Imperiale, 1996), which is an essential protein for the viral DNA packaging (Gustin and Imperiale, 1998). This led to the

hypothesis that IVa2 was something else than a transcription regulator factor in the infectious cycle.

1.2.6.1 IVa2 binds to the packaging sequence in a serotype dependent manner

Adenovirus DNA is packaged in a polar fashion, starting from the left end of the genome. Packaging requires of a region containing seven A/T rich motifs ("A-repeats"), denominated "packaging sequence" (PS). The PS is located between the ITR at the left end of the genome and the E1A transcription unit (nucleotides 194 to 358 in Ad5) (Gustin and Imperiale, 1998; Lang and Hearing, 2003) (**Figure 5**). Interaction of IVa2 from nucleolar extracts with this region, specifically to the "A-repeats" of the PS, pointed to a role of the protein in the DNA packaging process (Zhang and Imperiale, 2000). This was very soon confirmed and described as a serotype dependent functional interaction between IVa2 and PS by experiments with a chimeric virus, containing the Ad7 genome except for the ITR and the PS from Ad5. This chimeric virus only could package its DNA in 293 cells expressing the Ad5 IVa2 protein (Zhang et al., 2001).

Figure 5.- Arrangement of the left end of the Ad5 genome. The A repeats, represented as triangles, are located between nucleotides 200 and 397, upstream of the transcription start site of the E1A promoter, shown as a right-facing arrow. (Tyler, Ewing, and Imperiale, 2007)

A recombinant untagged IVa2 protein was used to further analyze binding to the PS, finding an interesting EMSA pattern of five DNA-IVa2 complexes (Tyler, Ewing, and Imperiale, 2007) (**Figura 6**).

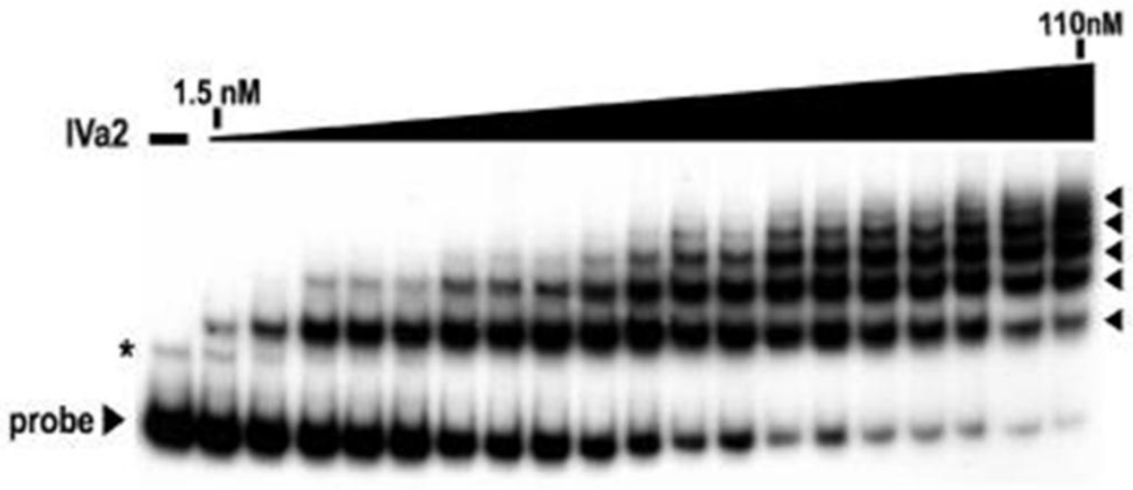

Figure 6.- Multiple complexes form as IVa2 interacts with the packaging sequence. Autoradiogram from an EMSA using a radiolabeled probe to nucleotides 200 to 397. The first lane lacks IVa2. The triangle above the lanes represents increasing concentrations of IVa2. The IVa2 packaging sequence complexes are indicated with arrowheads. (Tyler, Ewing, and Imperiale, 2007)

The DNA binding domain has been recently identified and characterized. A mutant protein that lacks a putative helix-turn-helix motif at the extreme C-terminus (440-449) is unable to bind to the PS and to pack the genome (Christensen, Ewing, and Imperiale, 2012).

1.2.6.2 IVa2 presents Walker Box motifs and binds ATP

Bioinformatics analysis show conserved motifs associated with binding and hydrolysis of ATP in the IVa2 sequence. This finding supported the idea of IVa2 acting as a packaging motor protein in adenovirus, similarly to dsDNA bacteriophages, which contain an ATPase protein to produce the energy needed for DNA packaging. (See section 1.2.5) Based on these conserved motifs, ATP binding assays and ATPase experiments were carried out in the group of Patrick Hearing, demonstrating binding to the nucleoside triphosphate, but not its hydrolysis (Ostapchuk and Hearing, 2008). Attending to the ASCE division of P-loop NTPases, adenoviral IVa2 proteins could be derived from the ABC superfamily (**Figure 7**). IVa2 presents an atypical topology in relation to other viral packaging ATPases, which fall in the families HerA/FtsK and terminases (Burroughs, Iyer, and Aravind, 2007).

Interestingly, IVa2 is required to package DNA, since mutants without IVa2 form empty particles (Ostapchuk, Almond, and Hearing, 2011).

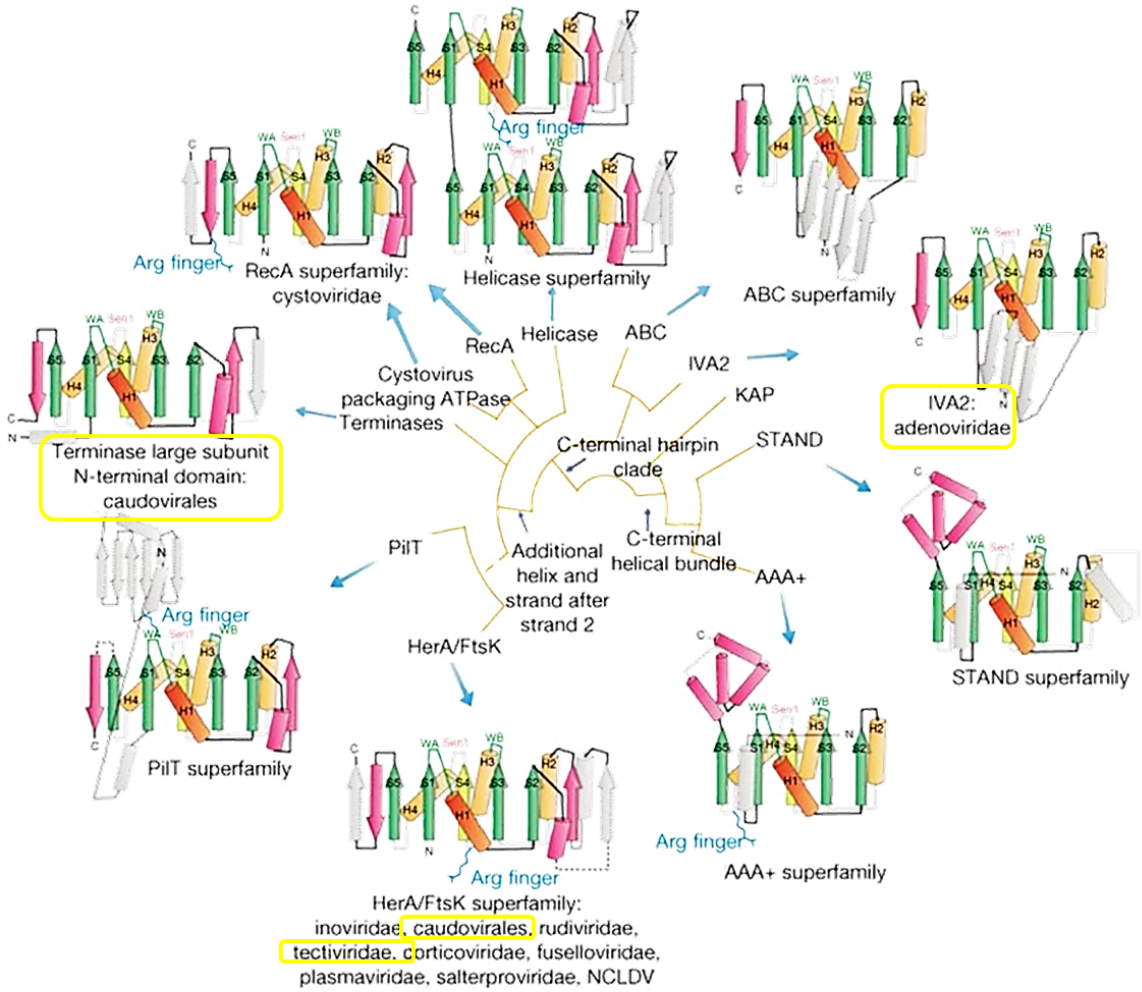

Figure 7.- IVa2 proteins within the ASCE division of P-loop NTPases. Topology diagrams depicting ASCE division of P-loop NTPases and accompanying cladogram depicting higher-order relationships. Viral lineages with packaging ATPases from a specific superfamily are listed following a colon below the superfamily name. Abbreviations: WA, Walker A; WB, Walker B and Sen1, sensor-1.

1.2.6.3 Characterized IVa2 sequence domains

IVa2 protein presents a Walker box domain and a DNA binding domain. Additionally, it has been described a N-terminus disordered domain, which is non-essential for the IVa2 activity. A mutant lacking the N-terminus domain (1-74) gives place to a 40 kDa isoform which is sufficient for viral viability (Pardo-Mateos and Young, 2004). These three domains are highlighted in the IVa2 sequence in **figure 8**.

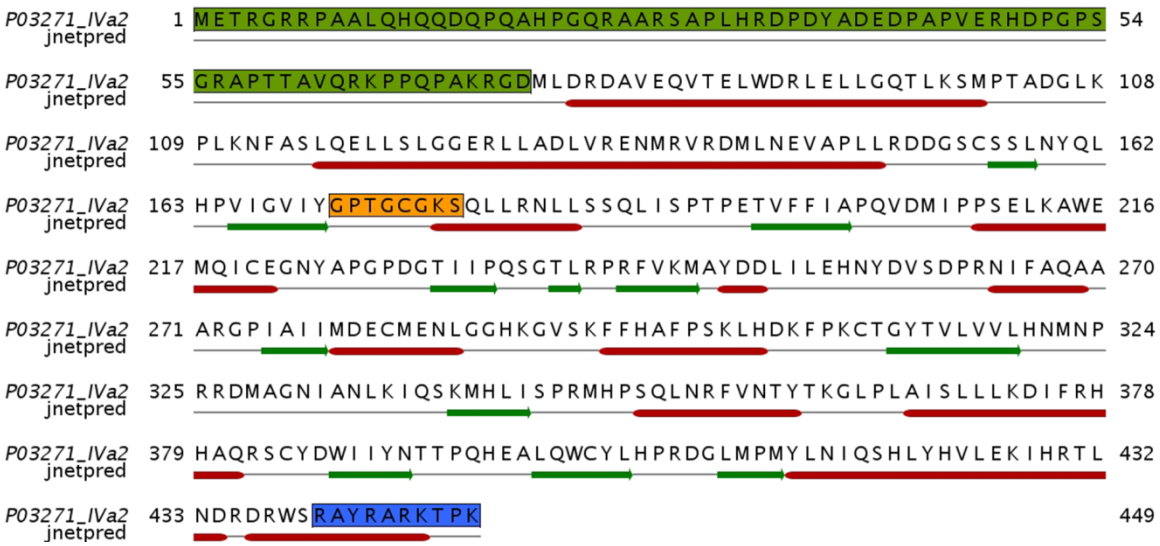

Figure 8.- IVa2 sequence domains. Ad5_IVa2 sequence showing highlighted motifs. Colour code: orange, Walker box domain (170-179); blue, DNA binding domain (440-449); green, N-terminal domain (1-78).

1.2.6.4 IVa2 copy number and proposed localization within the capsid

To further explore the possible role of IVa2 as the packaging motor, other studies focused on its copy number and location in the capsid. If an empty capsid were preceding the DNA packaging, it would be expected to find proteins involved in the encapsidation at a unique vertex, and the motor protein would have a low copy number. Quantitative WB in parallel with quantitative mass spectrometry and metabolic labeling yielded a copy number of 6.3 ± 1.5 molecules of IVa2 per virion (Christensen et al., 2008). In the same study, immune EM assays indicated the presence of IVa2 at a single vertex (**Figure 9**). However, the technique used could not unequivocally reveal the organization of IVa2 in the virion.

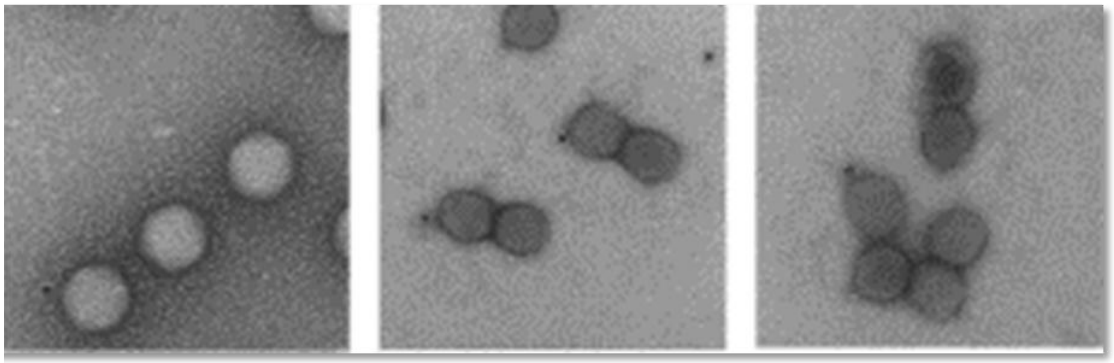

Figure 9.- Immunogold labeling of IVa2 in the viral particles. Label was detected in 19% of the particles, in one vertex of the virus (Christensen et al., 2008).

1.2.6.5 Interaction of IVa2 with other proteins involved in DNA packaging

In AdV, a complex interplay between the capsid proteins and DNA is required for a successful packaging. IVa2 does not bind alone to the PS. The previously mentioned protein L1 52/55K, along with viral proteins L4 22K and IIIa, also take part in the AdV DNA packaging process.

L1 52/55K is a nuclear phosphoprotein that is present in empty capsids, assembly intermediates and young virions, but not in mature virus, suggesting a scaffolding role for this protein. L1 52/55K is also involved in the DNA packaging process, since its absence results on production of empty capsids (Gustin and Imperiale, 1998) .

L4 22K is an AdV late gene product, associated with diverse activities during infection, including activation of late gene expression and suppression of early gene expression, viral DNA packaging (see below), infectious virus production, and regulation of adenovirus death protein expression.

Chromatin immunoprecipitation (ChIP) experiments indicated that IVa2, L1 52/55K and protein IIIa (located underneath each vertex, at the inner capsid surface) bind to the PS *in vivo* (Ma and Hearing, 2011; Ostapchuk et al., 2005; Perez-Romero et al., 2005). *In vivo* experiments also proved that IVa2 and L4 22K are dependent upon each other for PS binding, and both proteins are also required to recruit L1 52/55K to this region of the genome (Wu, Orozco, and Hearing, 2012).

In vitro experiments showed the interaction between L1 52/55K and IVa2. The DNA binding *in vitro* was positive for IVa2 alone; in contrast, L1 52/55K was not able to bind DNA but it bound protein IIIa (Ma and Hearing, 2011).

A proposed model (Wu, Orozco, and Hearing, 2012) for these protein–DNA interactions is an initial interaction of L4 22K and IVa2 bound directly to the packaging sequence, which would recruit the protein L1 52/55K and the capsid protein IIIa to promote viral packaging.

1.2.6.6 Possible mechanisms for adenovirus DNA packaging

A unique feature of adenovirus is that the histone-like protein VII both in its precursor (pVII) and mature (VII) forms, is bound to the viral DNA before it is packaged (Brown and Weber, 1980; Chatterjee, Vayda, and Flint, 1986a; Chatterjee, Yang, and Flint, 1986; Dery et al., 1985; Weber and Philipson, 1984). Having this fact in consideration, three possible ways for a DNA-protein complex encapsidation have been proposed (**Figure 10**) (Zhang and Arcos, 2005):

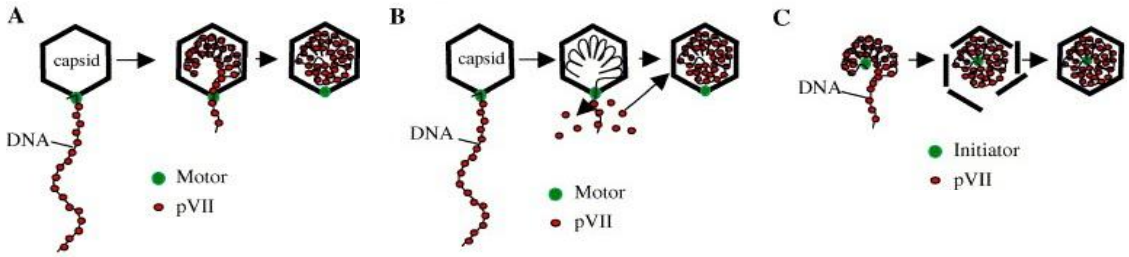

Figure 10.- Models for packaging of DNA-pVII complex. (Zhang and Arcos, 2005)

1) Viral DNA with the bound protein pVII is transferred into an empty capsid through a portal vertex (**Figure 10-A**). Although reminiscent of the bacteriophage packaging, the presence of protein bound to the dsDNA would make this a novel mechanism of DNA packaging. Supporting this idea, immunoprecipitation assays proved the interaction between proteins pVII and IVa2 in infected cells (Zhang and Arcos, 2005).

2) The second possibility is that the DNA packaging machinery only transfers naked DNA without protein VII (**Figure 10-B**), in the same way as many dsDNA bacteriophage and herpesviruses. If this were true, the DNA packaging motor should somehow strip protein pVII off to make DNA ready for the transference into the capsid, and the protein pVII would need to penetrate the capsid to associate again with the DNA and form the chromatin-like structure.

3) The third possibility does not consider a preformed empty capsid, but an initial core formation by nucleation of the DNA and pVII followed by assembly of the capsid proteins around it (**Figure 10-C**). There is no direct evidence in adenovirus for this possibility, but there are other viruses following this mechanism, such as poliovirus

(Putnak and Phillips, 1981; Rombaut, Vrijsen, and Boeye, 1990) and SV40 (Garber, Seidman, and Levine, 1980). In this case, IVa2 would be an initiator of nucleation rather than a translocation motor.

1.3 Other adenoviruses

1.3.1 Approved adenovirus genera

Based on molecular taxonomy, the family *Adenoviridae* is currently divided into five different genera (**Figure 11**).

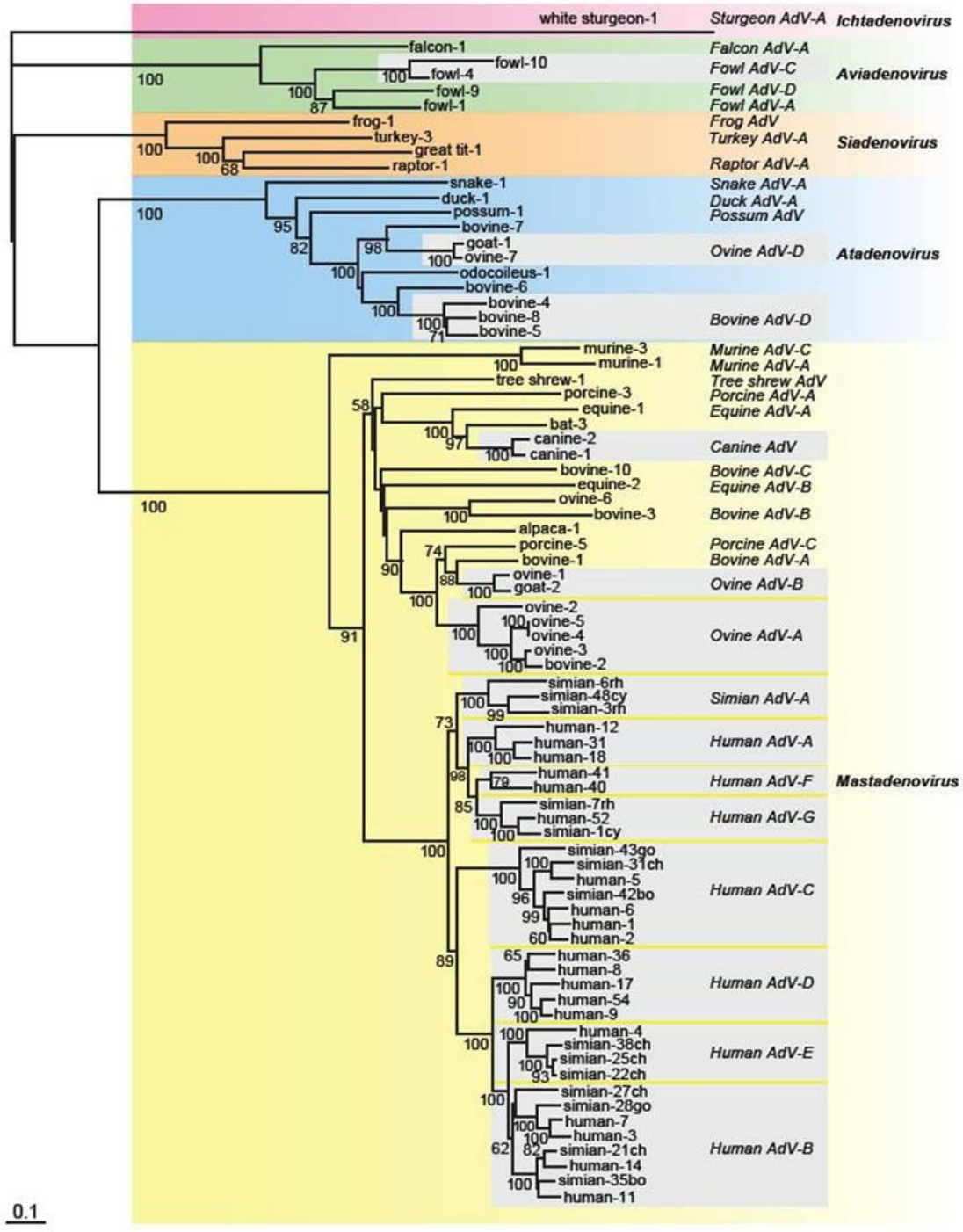

Figure 11.-Phylogenetic tree of adenoviruses. Phylogenetic tree of adenoviruses based on a distance matrix analysis of hexon amino acid sequences (www.vmri.hu/~harrach/AdVtaxlong.htm).

The largest genus in terms of assigned serotypes, mainly because it contains all the human adenoviruses, groups AdVs infecting mammalian hosts: *Mastadenovirus*. The second genus in number of identifications is *Atadenovirus*, a genus characterized by the high A + T content of their sequences (Dan et al., 1998) and a broad range of hosts (ruminant, avian, marsupial and reptilian). The next adenoviridae genus attending to the variety of hosts is *Siadenovirus*, isolated from birds and a frog (Davison, 2002) and named after the putative sialidase gene at the left terminus of the genome. Finally, *Aviadenovirus*es infect birds and the only confirmed fish adenovirus falls into the latest recognized genus: *Ichtadenovirus*.

1.3.2 Genome organization

Components of the family *Adenoviridae* present linear dsDNA genomes ranging from 26 to 45 kb in size (Davison, Benko, and Harrach, 2003). Comparative analysis of genes across this family has identified conserved protein-encoding regions, classified into genus-common and genus-specific genes (Davison, Benko, and Harrach, 2003) (**Figure 12**). Genus-common genes are centrally located in the genome, encoding proteins with functions involved in DNA replication (pol, pTP and DBP), DNA encapsidation (52K and IVa2) and architecture of the virion (pIIIa, penton base, pVII, pX, pVI, hexon, protease, 100K, 33K, pVIII and fiber). Genus-specific genes are mainly located near the ends of the genome, except for *Mastadenovirus* protein V. Other viruses with linear, double-stranded DNA genomes (*Herpesviridae* and *Poxviridae)* also present this distribution of genus-specific genes at the ends of the genome and genus-common genes in a central position. (McGeoch, 1999; Upton et al., 2003).

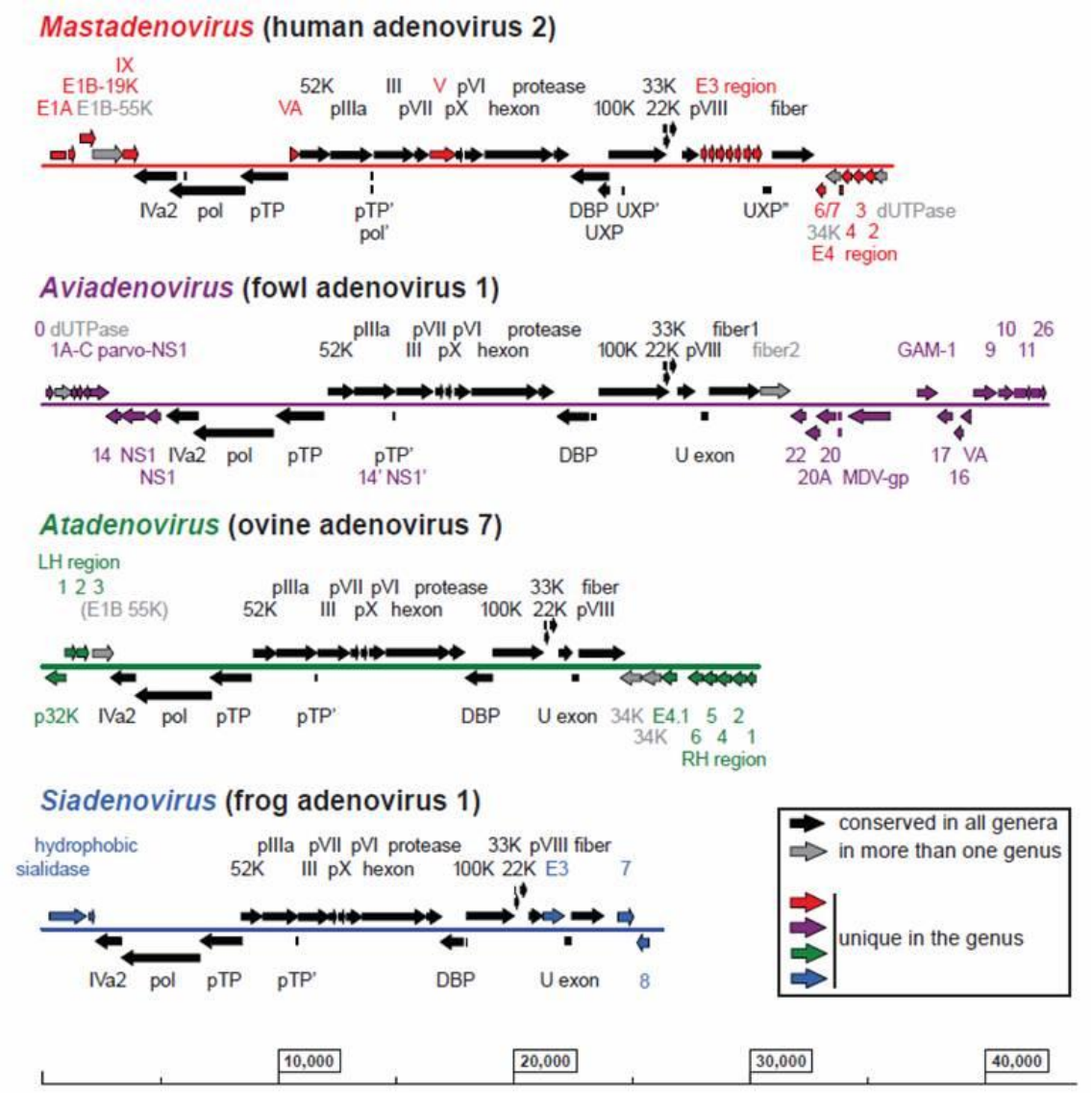

Figure 12.- Genome organizations of four adenovirus genera. Schematic illustration of the various genome organizations found in members of four adenovirus genera. Black arrows depict genes conserved in every genus, grey arrows show genes present in more than one genus, and coloured arrows show genus-specific genes (www.vmri.hu/~harrach/AdVtaxlong.htm).

1.3.3 Structural studies on non-human AdVs

The use of non-human adenoviruses has been proposed as a means to improve vector performance by avoiding pre-existing immunity. While the structure of human adenovirus has been extensively characterized by electron microscopy and crystallography studies (Liu et al., 2010; Reddy et al., 2010), little is known about the structure of other adenoviruses.

In correspondence with the ability to isolate and produce viruses in the laboratory, non-human adenovirus structural characterization is so far limited to 3DEM studies on canine adenovirus type 2 (*Mastadenovirus*) (Schoehn et al., 2008) and ovine adenovirus (*Atadenovirus*) (Pantelic et al., 2008). Crystal structures are available for canine, porcine and avian adenovirus fibers, as well as for a chimpanzee and the avian CELO virus hexon (El Bakkouri et al., 2008; Guardado-Calvo et al., 2007; Guardado-Calvo et al., 2010; Pichla-Gollon et al., 2007; Seiradake et al., 2006; Xu, Benson, and Burnett, 2007), but there are no data on the complete virion structure for any adenovirus with non-mammalian host.

1.3.3.1 Canine adenovirus type 2 (CAV-2)

The 3D structure of the CAV-2 capsid has been determined by cryo-EM and compared to the known X-ray and EM structures of human adenoviruses (AdV-2 and AdV-5) by fitting the different atomic resolution structures into the EM density. The capsid presents a slightly smoother structure than in the human adenoviruses, with shorter or absent external loops in penton base and hexon. Also in the outside of the capsid, the C-terminal region of protein IX is in a different position, making a cylindrical density sticking out of the capsid from the 3-fold axes instead of at the edges. The inner side of the capsid presents a non-attributed extra density under the penton base. Finally, the CAV-2 trimeric fiber is about 330 Å long and more complex than the ones from AdV-2 and AdV-5, with two bends in the shaft.

1.3.3.2 Ovine adenovirus (OAdV)

Minor coat polypeptide IX, and core polypeptide V are unique to *Mastadenoviruses*, but are replaced in the viral particle by unique *Atadenovirus* polypeptides LH3 and p32k (Gorman et al., 2005; Pantelic et al., 2008). LH3 is also referred to as E1B 55K, due to its placement in the analogous position to this product in the human AdV genome. However, human AdV E1B 55K is not part of the virion, but is involved in blocking apoptosis.

A 3D cryo-EM reconstruction of OAdV was the first 3D structure solved for any adenovirus not belonging to the *Mastadenovirus* genus (**Figure 13**). The structure of OAdV differs from those previously reported in having very distinctive surface

protusions (knobs) lying on the icosahedral and local three fold axes. In addition, some density extends beneath the viral capsid into the interior of the particle. A viable mutant virus lacking protein p32k presented no evident surface differences in the outer capsid surface, which has taken as evidence that the outer knobs correspond to LH3 and not p32K. The OAdV penton base is missing the Arg/Gly/Asp motif that interacts with certain cell surface integrins during human AdV uptake. No other integrin-binding motifs have been identified. Measurement of penton/fiber complexes indicated a fiber length of 380 Å, consistent with an OAdV fiber that has 25 repeats (at 15 Å per repeat) and a head domain (Vrati et al., 1996).

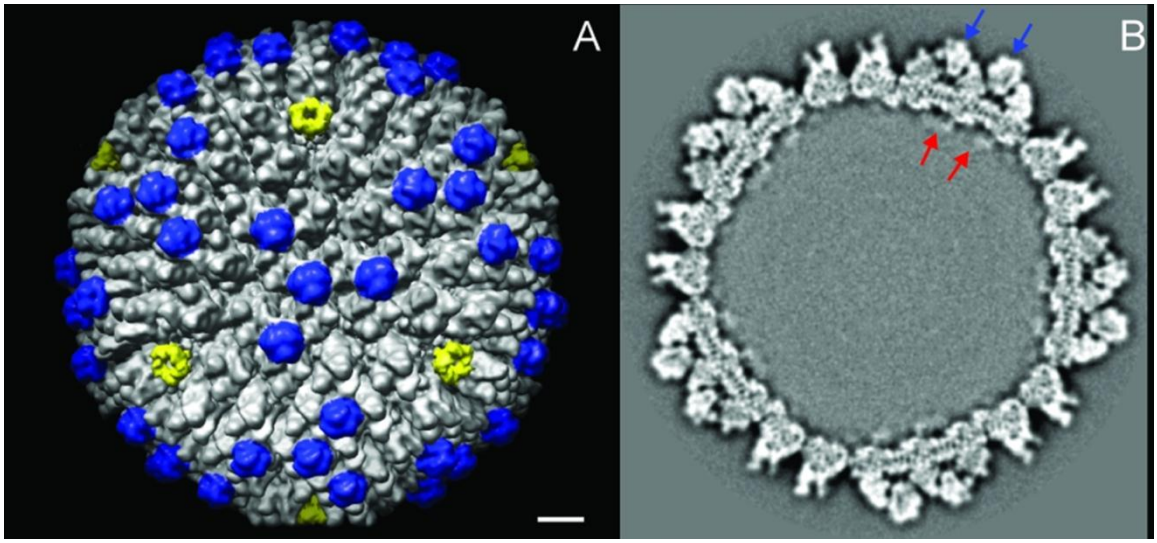

Figure 13.- Cryo-EM structure of OAdV (A) Capsid surface oriented around one of the three-fold axes. Penton complexes are marked in yellow, indicating the approximate bounds of the icosahedral facet. A major capsid protein and key distinguishing feature of OAdV is marked in blue. Scale bar, 10 nm. (B) Slice taken through the volume of the WT map viewed along a three-fold axis. Blue arrows indicate two LH3 densities, and red arrows are thought to correspond to p32k. (Gorman et al., 2005; Pantelic et al., 2008)

1.3.4 Adenoviruses infecting reptiles

1.3.4.1 Snake adenovirus

Adenoviruses have been isolated from different snake species. The first isolation was in 1985 from Boa constrictor (*Boa constrictor*) (Jacobson, Gaskin, and Gardiner, 1985), followed by isolations from a royal python (*Python regius*) (Ogawa, Ahne, and Essbauer, 1992) and from Corn snake (*Pantherophis guttatus*) (Juhasz and Ahne, 1993). The adenovirus from Corn snake (SnAdV-1) was propagated on VH-2 viper heart cell line (Juhasz and Ahne, 1993) and fully sequenced (Farkas, Harrach, and Benko, 2008). A

later study reported a complete identity between this SnAdV-1 and the virus isolated from Boa constrictor (Marschang, August 2003). The SnAdV-1 genome presents the typical *Atadenovirus* structure (**Figure 14**).

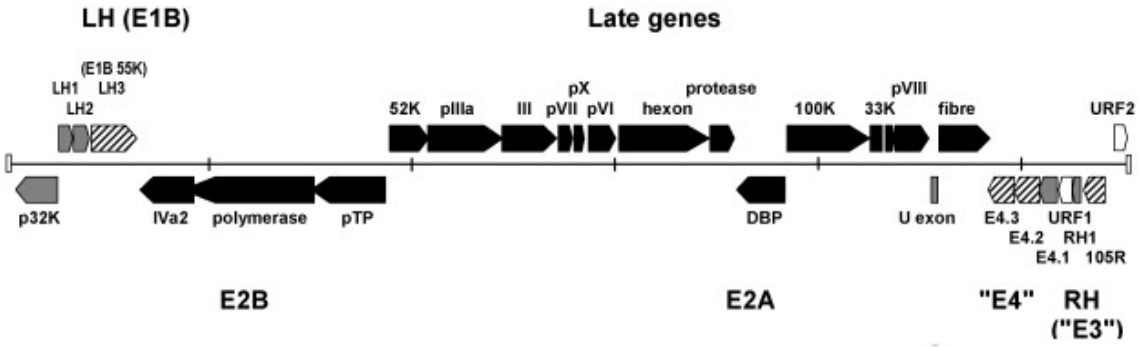

Figure 14.- Schematic genomic map of SnAdV-1. The genome is shown as a central horizontal line marked at 5 kb pair intervals. The ITRs and the putative genes are marked with rectangles and arrows of proportional in size, respectively. Different filling of the arrows shows divergent occurrence of the homologous genes within the genera. Black arrows show genes that are present in every member of the family *Adenoviridae*. Grey filling marks genes that are specific for members of the genus *Atadenovirus*. Striped filling of arrows is used to indicate genes that occur in members of more than one genus. Putative genes (URFs) specific to SnAdV-1 are delineated as empty arrows (Farkas, Harrach, and Benko, 2008).

1.3.4.2 Lizard adenovirus

The first AdV-like particles in lizard species were identified 30 years ago (Jacobson and Gardiner, 1990; Julian and Durham, 1982; Kinsel et al., 1997). However, a consensus PCR for analysis of the lizard genomes was not described till 2004 (Wellehan et al., 2004). Although adenovirus infections have been very often detected in lizards since then, isolation in cell culture has been reported only once (Papp, Fledelius et al. 2009). In that work, adenoviruses were isolated from Mexican beaded lizard (*Heloderma horridum*) and two Gila monsters (*Heloderma suspectum*) and propagated in an iguana heart cell line (IgH-2). The first whole genome sequence of a lizard AdV has just been obtained by our collaborators Dr. Mária Benkö and Dr. Balázs Harrach (paper in preparation). This sequenced genome showed the presence of two genes encoding for fiber proteins. The adenovirus isolated from *Heloderma horidum* and its recently sequenced genome were used in this thesis.

Objectives

2 Objectives

This thesis is divided in two main topics. One is the study of the protein IVa2 as the putative motor protein for DNA packaging of adenovirus, and the second one is the characterization of reptilian adenoviruses and their comparison to the human ones.

In particular, the following objectives have been pursued:

IVa2 protein:

- Determine the quaternary structure of IVa2 protein *in vitro*.
- Determine the localization of the protein IVa2 within the viral particle.

Reptilian adenoviruses:

- Optimize the propagation and purification of AdVs infecting reptiles for structural and molecular studies.
- Characterize the molecular composition of AdVs infecting reptiles.
- Characterize the stability properties of AdVs infecting reptiles.
- If possible, determine the first structure of an AdV with non-mammalian host.

Materials and Methods

3 Materials and methods

3.1 Materials

3.1.1 Viruses

Specimen	Description	Storage buffer composition
Ad5GL	Non replicative, E1 deleted, structurally wild type human Ad5. Contains GFP and firefly luciferase genes (designated by the suffix "GL").	20 mM HEPES pH 7.8, 150 mM NaCl, 10% glycerol
Ad5EZ-pIX-flag45A-6HisF5/3[1]	Encodes modified IX protein displaying both FLAG and 6His sequences separated by a 45 Å alpha-helix spacer and represents hybrid serotypes 5 and 3.	PBS 10% glycerol
SnAdV-1[2]	Snake adenovirus isolated from *Boa constrictor*.	20mM HEPES pH 7.8, 150 mM NaCl, 10% glycerol
LAdV[2] (proposed nomenclature)	Heloderma adenovirus isolated from infected *Heloderma horridum*.	20 mM HEPES pH 7.8, 150mM NaCl, 10% glycerol

Viruses were kindly provided by our collaborators [1]David T. Curiel (Division of Human Gene Therapy, Birmingham, Alabama) and initial seeds were provided by [2]Rachel Marschang (Institute for Environmental and Animal Hygiene, University of Hohenheim, Stuttgart). Adenovirus propagation protocols have been implemented in our lab to provide our experiments.

3.1.2 Proteins

Protein	Description	Buffer composition
IVa2-flag[1]	Derivative of the Ad5 IVa2 protein carrying a C-terminal FLAG tag; produced in 293FT cells.	Hepes 20 mM pH 7.5; 500 mM NaCl; 100 µg/mg FLAG tag peptide; 5µM $ZnCl_2$; 1.5mM $MgCl_2$; 10% glycerol;0.1% TRITON x-100
IVa2-strep[2]	Recombinant IVa2 protein containing a C-terminal, eight aminoacid Strep tag, expressed using a baculovirus vector following infection of Sf9 cells.	100mM Tris pH 7.6; 300 mM NaCl; DTT 1 mM; desthiobiotin 2.5 mM.
Truncated IVa2-strep[2]	Recombinant IVa2 protein containing a C-terminal, eight aminoacid Strep tag and a truncation of the 74 first aminoacids, expressed using a baculovirus vector following infection of Sf9 cells.	TRIS 100 mM pH 7.6; NaCl 300 mM; DTT 1 mM; desthiobiotin 2.5 mM.

Proteins were kindly provided by our collaborators [1]Patrick Hearing (Department of Molecular Genetics and Microbiology, Stony Brook University, New York) and [2]Jane Flint (Department of Molecular Biology-Princeton University, New Jersey).

3.1.3 Cell lines

Cell line	ATCC	Description
HEK 293	CRL-1573	Human Embrionic Kidney cell line transformed with sheared Ad5 DNA.
VH2	CCL-140	Viper Hearth cell line. Established from the hearth of a normal female Russell's viper, *Vipera Russelli*.
IgH-2	CCL-108	Iguana Hearth cell line. Established from the heart of a normal immature male *Iguana*.

3.1.4 Antibodies

Antibody	Source
Mouse anti-V	hybridoma supernatant
Mouse anti-penton base	hybridoma supernatant
Mouse anti-IVa2 (6C9, 3H7, 2B9, 9F4, 3F3)	hybridoma supernatant
Goat anti-IVa2	serum
Mouse anti-FLAG	purified antibody

3.2 Methods

3.2.1 Non-denaturing and denaturing protein electrophoresis

For blue-native electrophoresis, Coomassie blue G250 (B0770, SIGMA) was used to eliminate the effect of protein charges on mobility. Samples containing loading buffer were incubated for 10 minutes prior to loading in the wells. For denaturing electrophoresis, the loading buffer contained 2% SDS, 1% β-mercaptoethanol, 10% glycerol, 50mM Tris-HCl pH 6.8, and the incubation was carried out at 95ºC, while for native-PAGE, the loading buffer contained Tris-HCl 200mM pH 6.8, glycerol 40%, Coomassie Brilliant Blue G 0.4% (p/v) and the incubation took place at 4ºC.

Acrylamide gels (both native and denaturing) were run in a minigel BioRad electrophoresis system. Different acrylamide percentages were used in the home-made gels (indicated in "Results"), while gradient gels were 4-20% Mini-PROTEAN TGX Precast gels (#456-1096) from BioRad.

Molecular weight markers used were #161-0374 from BioRad for denaturing electrophoresis and #17044501 GE Healthcare for non-denaturing electrophoresis.

3.2.2 Sequential native and denaturing PAGE of disrupted virions

Viral disruption products in sample buffer (Tris 12.5 mM, SDS 4%, glycerol 20%, Bromophenol Blue 0.02% up to 100 ml with H_2O, pH 6.8) were electrophoresed in a 1

mm thick native polyacrylamide gel (5%) under constant voltage (70 V) until the tracking dye reached the bottom of the gel.

Bands were excised from the native gel where Coomassie G signal was observed or alternatively the complete lane was cut into pieces of 2mm, including the stacking gel and the well bottom.

The excised pieces were boiled (95ºC, 10 minutes) in the presence of denaturing buffer (containing Tris 12.5 mM, SDS 4%, Glycerol 20%, Bromophenol blue 0.02% and 1% β-mercaptoethanol) and then loaded in a 0.75 mm thick SDS containing gel in the same orientation they had in the native one. SDS-PAGE was performed at 100 V in minigels of 10% or 15% acrylamide.

3.2.3 Silver staining

The following protocol was used for mini-gel silver staining:

1.- After electrophoresis, the gels were fixed in 20 ml ethanol, 5 ml acetic acid and distilled water up to 50 ml for at least 30 minutes.

2.- Gels were sensitized by soaking for 30 minutes in 15 ml ethanol, 2 ml of sodium thiosulfate (5% w/v), 3.4 g of sodium acetate and water up to 50 ml.

3.- Gels were rinsed three times in water, for 3 minutes for each wash.

4.- Silver nitrate 0.25% (w/v) for 20 minutes was used to stain the gels.

5.- Gels were rinsed twice for 30 seconds for each wash in distilled water.

6.- Gels were transferred into the developer solution (6.25 g of sodium carbonate, 50 µl of formaldehyde, up to 250 ml with distilled water)

7.- When the adequate degree of staining was achieved, gels were transferred to the stop solution (40mM EDTA-Na2*2H2O) for at least 30 minutes.

8.- Gels were washed in distilled water (at least, twice, for 5 minutes for each wash).

All gel manipulations were performed using powder-free, nitrile gloves to avoid contaminations.

3.2.4 Western Blot

Proteins were transferred from the gels to nitrocellulose (Cat.162-0115, BioRad) on a Bio-Rad semidry transfer apparatus (#170-3940 BioRad) for 40 minutes at 15 V, blocked 1 hour at room temperature in 5% skimmed powdered milk in Tris buffer saline (NaCl 0.09% (w/v), Tween 20 0.01% (v/v), Tris-HCl 0.1M, pH 7.5. The membrane was then probed overnight at 4°C with the primary antibody. After this incubation, the membrane was washed three times in TBS-T and probed for 1 h at room temperature with the appropriate horseradish peroxidase (HRP)-conjugated secondary antibody. The signal was detected using ECL Plus (GE Healthcare).

3.2.5 Far Western blotting

The following protocol was used to detect protein-protein interactions by far western blot:

1.- After SDS-PAGE, the proteins were transferred to a nitrocellulose membrane by semidry electro blotting (#170-3940 BioRad), 15 V, 40 minutes .

2.- The membrane was washed three times in TBS-T, 10%glycerol and 5mM 2-mercaptoethanol.

3.- Overnight incubation at 4ºC in TBS-T, 10% glycerol and 5mM 2-mercaptoethanol. In this step SDS was removed and the re-folding of the proteins in the nitrocellulose was assisted.

4.- Membrane was blocked with a first step of washing in 0.05% Tween20 in PBS for two hours at room temperature with gentle agitation and a blocking step with 1g BSA in 100ml PBS; at room temperature with gentle agitation.

5.- The membrane was rinsed with 100ml PBS.

6.- The membrane with the probe protein (4 µg/ml in TBS-T 0.05% skimmed powdered milk) was incubated overnight, 4ºC, with gentle agitation.

7.- The membrane was washed five times in TBS-T.

8.- The membrane was incubated with the primary antibody (mAb anti-FLAG (SIGMA, #F1804) 1:10000 in TBS-T 0.05% skimmed powdered milk) o.n. at 4ºC with gentle agitation.

9.- The membrane was washed three times in TBS-T.

10.- The membrane was incubated with the secondary antibody (mAb anti-mouse horseradish peroxidase (*#NA931V*, Amersham Biosciences) diluted 1:10000 in TTBS 0.05% skimmed powdered milk) for one hour at room temperature, gentle agitation.

11.- The membrane was washed three times in TBS-T.

12.- Protein detection was performed with Enhanced ChemiLuminescence method. (LiteAblot, #EMP010004).

3.2.6 Epitope mapping of anti-IVa2 antibodies

Epitope mapping was done in collaboration with the Protein Tools service (Leonor Kremer) and Proteomics facility (Fernando Roncal) at CNB. Using the so-called SPOT synthesis (Frank and Overwin, 1996), the amino acid (aa) sequence of Ad5 IVa2 was synthesized as short overlapping peptides on a cellulose membrane. The peptides remain covalently bound to the surface of the insoluble membrane, which is used as in the case of immunoblots to determine the epitope of the antibody.

Two different membranes were used, containing 12 aa IVa2 peptides overlapping the next either 3 or 2 aa.

Five monoclonal antibodies (named 2B9, 6C9, 3H7, 3F3 and 9F4) provided by our collaborator Prof. Jane Flint and one polyclonal antibody (Christensen et al., 2008) were tested on the membranes. For most of the monoclonal antibodies, comparing the signal from two membranes, allowed to enclose the epitope in a more accurate way.

The protocols is detailed bellow:

1.- Blocking the membrane in TBS 5% skimmed powdered milk for 4 hours.

2.- Testing the unespecific binding of the peroxidase conjugated antibody, diluted 1:10000, 2 hours shaking at room temperature. The membrane is washed three times in TBS-T and unespecific binding is detected with Enhanced ChemiLuminescence method. (LiteAblot, #EMP010004).

3.- The membrane is washed three times in TBS-T.

4.- Diluted primary antibody is added and incubated o.n. at 4 ºC.

5.- The membrane is washed three times in TBS-T.

6.- Peroxidase conjugated antibody is added and incubated for 2 hours .

7.- The membrane is washed three times in TBS-T and binding is detected with ECL.

8.- To reuse the membrane, wash 3 times with 8M urea in PBS, pH 7, 1% SDS 0.5% β-mercaptoethanol and again 3 times with Acetic acid, EtOH and H2O in a proportion 10:50:40, all at 40ºC and shacking. Repeat steps 6 and 7 to test the correct stripping of the membrane.

3.2.7 Sample preparation for electron microscopy

For negative staining EM, several dilutions of the sample were prepared in all cases. A drop of 5 µL of the sample was incubated on glow discharged collodion/carbon coated grids for 5 minutes to allow sample adsorption. Excess fluid was removed by touching on the edge of the grid with a piece of Whatman paper, without allowing it to become completely dry (blotting step). Then the grid was either washed with the sample buffer (and subsequently blotted) or directly incubated with the staining agent, 2% uranyl acetate, for 45 sec. After staining, the grids were blotted and air dried on a filter paper in a Petri dish.

3.2.8 Sample preparation for cryo-electron microscopy

Virus samples were dialyzed for 1 hour at 4ºC against phosphate-buffered saline, applied to freshly carbon-coated Quantifoil R2/4 300 mesh Cu/ Rh grids and vitrified in liquid ethane using a Leica CPC plunger.

3.2.9 Negative staining immunoelectron microscopy

1. Virus adsorption, by floating the grid on a 3-5 µL drop of the sample during 5 minutes onto a glow discharged collodion/carbon coated Ni grid.
2. The grid was blotted and washed by floating on a drop of TBS (Tris-base 10mM, HCl up to pH 8.2, 150mM NaCl).
3. The grid was blotted and blocked with TBG (TBS+0.1% BSA+1%gelatin, pH8.2) for 15 minutes.
4. After a new blotting, the grid was incubated with primary antibody at different dilutions (in TBS/1%BSA) for 50 minutes.

5. The grid was blotted and washed three times with TBG, 10 minutes for each wash.
6. After a new blotting, the grid was incubated with antibody-Au 10 nm, diluted to 15% in TBS/1%BSA for 30 minutes.
7. The grid was washed three times with TBG, and three more times with TBS, 5 minutes for each wash.
8. The grid was negatively stained with uranyl acetate 2%, 45 seconds.

3.2.10 Crosslinking of IVa2 recombinant protein

Fresh SIGMA EM grade 25% glutaraldehyde stock was first diluted in water, then adjusted to the final concentration in the protein solution. The reaction mixture was incubated for 10 minutes at 25 ºC in a thermo-mixer with slow mixing rate. To stop the reaction, 2M NH_4Cl was added to its final concentration of 200 mM and incubated for 10 minutes at room temperature.

3.2.11 EM image acquisition for structural analysis

Grids were examined in either a JEOL JEM 1230 at 100Kv (for negative staining) or a Tecnai F20 transmission electron microscope at 200kV (for cryoEM). IVa2 and SnAdV-1 micrographs were taken at low electron dose conditions. CryoEM images were recorded on Kodak SO-163 film under low-dose conditions at a nominal magnification of 50000x (with defocus values from 1.2 to 3.5 µm) and digitized in a Zeiss Photoscan TD scanner scanner using a step size of 14 µm. IVa2 images were recorded on Kodak SO-163 film under low-dose conditions at a nominal magnification of 60000x and digitized in a Zeiss Photoscan TD scanner scanner using a step size of 14 µm.

3.2.12 EM image processing

All image processing tasks were performed using the software package XMIPP (Scheres et al, 2008), except for determination of micrograph contrast transfer function (CTF) parameters, which was done with CTFFIND. To reduce computational demands, IVa2 scanned micrographs were downsampled by a factor of 3 giving a pixel size of 3.5

Å. Without downsampling, SnAdV micrographs had a final pixel size of 2.8 Å. 2D alignment and classification of IVa2 images was performed using maximum-likelihood based algorithms in Fourier space (MLF2D) (Scheres et al., 2007). The 3D reconstruction of IVa2 ring was performed using the standard EMAN procedure (http://blake.bcm.edu/emanwiki/EMAN/) for generation of a C5 model (startcsym) and refinement. The 3D reconstruction of SnAdV was performed using projection matching. As initial 3D reference, an Ad5GL map low pass filtered to 15Å resolution was used. The final datasets included 1432 (IVa2) and 3715 (SnAdV-1).

3.2.13 Homology modelling

Homology modeling of hexon and penton base of SnAdV-1 was carried out by Juan Carlos Sánchez, at the CNB Sequence Analysis and Structure prediction facility (http://pdg.cnb.csic.es/bioservice_es.html).

Sequence similarity between SnAdV-1 and Ad5 was statistically significant for hexon, penton, fiber, IIIa, VIII, VII, Mu, IVa and terminal protein. However, there were crystal structures available for being used as templates in homology modeling only for hexon and penton. The modelling was done with SWISS-MODEL (http://swissmodel.expasy.org/).

3.2.14 Fitting of SnAdV-1 and difference mapping

The homology models of four hexon trimmers and one penton base molecule were fitted into the SnAdV-1 maps using VEDA (http://mem.ibs.fr/VEDA/), with icosahedral symmetry enforced. Difference maps revealing those capsid components other than the hexon and penton base were calculated by subtracting this map from the cryo-EM reconstruction. Surface rendering figures were created with UCSF Chimera, using the Hide Dust tool to remove small unconnected blobs from the difference maps. The electrostatic potential of a hexon trimer was calculated with the PyMOL APBS plug-in and visualized with Chimera.

Fitting and difference mapping of SnAdV-1 was carried out by Dr. Carmen San Martin.

3.2.15 Modeling the structure of IVa2

To create a 3D structure prediction of IVa2. The sequence of the AdV5 protein was submitted to the RaptorX web server (http://raptorx.uchicago.edu/).

The alignment uses a profile-entropy scoring method, taking in consideration the number of non-redundant homologs available for the target sequence and template structure, assessing the quality of information content in sequence profiles.

The model obtained was used to perform a fitting into the 3D-reconstruction of IVa2 ring-shape oligomer with VEDA (http://mem.ibs.fr/VEDA/) resulting in a cross-correlation index of 91.3.

3.2.16 Viral amplification

3.2.16.1 Propagation of AdGL5 in HEK 293 cells

Cell propagation and viral infection

HEK 293 cells were propagated in Dulbecco's modified Eagle's high glucose medium (DMEM) supplemented with 10 % foetal bovine serum (FBS) -Biological Industries # 04-001-1A-, penicillin, streptomycin and glutamine (all cell culture reagents were obtained from SIGMA) and maintained at 37ºC in a humidified incubator with 5% CO2. Cells were seeded in p100 tissue culture dishes at a density of 2.9 E+06 cells in 10 ml of the medium (passage 1:5). When the cell monolayers reached about 70% confluence, virus was thoroughly mixed with fresh media and added to the cells at a multiplicity of infection (MOI) of 10 viral particles per cell. The cells were collected when substantial cytopathic effect was observed, 48 hours after infection.

Infected 293 cells from 100 p100 tissue culture plates were collected and centrifuged in a Heraeus 1.0R megafuge for 10 min at 800 rpm, 4ºC. The cells were then resuspended in 35 ml of 10mM Tris-Cl pH 8.1 and lysed by four freeze-thaw cycles. Cell lysates were clarified to remove cellular debris by centrifugation in a Heraeus 1.0R megafuge at 3000 rpm for 60 min at 4ºC.

Virus purification

For a double CsCl ultracentrifugation, the supernatant was layered onto a discontinuous gradient of 1.2 g/ml, 1.45g/ml CsCl in Tris-HCl 10mM pH 8.1 and

centrifuged at 20,000 rpm for 120 min at 4ºC in a Beckman Optima L-100 XP ultracentrifuge using a Beckman SW28 swinging bucket rotor. The low density and high density virus bands from each tube were collected, pooled, mixed with Tris-HCl 10 mM pH 8.1, and centrifuged overnight at 20,000 rpm and 4°C in a Beckman SW40Ti swinging bucket rotor. The virus band from each tube was collected and pooled. The final virus pool was then transferred into Econo-Pac 10 DG disposable chromathography columns (Cat. #732-2010, BioRad) with molecular weight cutoff of 6,000 daltons for buffer exchange. The virus titer (in viral particles/ml) was determined by absorbance as detailed in section 3.2.17. Purified virus was stored at -80ºC after adding 10% glycerol.

3.2.16.2 Propagation of LAdV in IgH2 cells

Cell propagation and viral infection

IgH2 cells were propagated in DMEM supplemented with 10 % FBS penicillin, streptomycin and AANE and maintained at 37ºC or 28ºC in a humidified incubator with 5% CO2. Cells were seeded in 10-cm tissue culture dishes with passages 1:3. When the cell monolayers reached about 70% confluence, virus infected supernatant was added to the cells. The infection was carried out at 28ºC. The cells were collected when substantial cytopathic effect was observed, from 3 to 5 days post-infection.

Infected IgH2 cells from 100-200 p100 tissue culture plates were collected and centrifuged in a Heraeus 1.0R megafuge for 10 min at 800 rpm, 4ºC. The cells were then resuspended in 35 ml of 10 mM Tris-Cl pH 8.1 and lysed by four freeze-thaw cycles. Cell lysates were clarified to remove cellular debris by centrifugation in a Heraeus 1.0R megafuge at 3000 rpm for 60 min at 4ºC.

Virus purification

As Ad5GL and LAdV viral particles present similar density, the same purification protocol was used in all cases.

3.2.16.3 Propagation of SnAdV in VH2 and IgH2 cells

VH2 cells were propagated in DMEM supplemented with 10 % FBS, penicillin and streptomycin and maintained at 37ºC or 28ºC in a humidified incubator with 5% CO2. Cells were seeded in 10-cm tissue culture dishes with subcultures 1:3. When the cell

monolayers reached about 70% confluency, virus infected supernatant was added to the cells. The infection was carried out at 28ºC. The cells were collected when substantial cytopathic effect was observed, from 5 to 10 days post-infection.

Infected VH2 cells from 200 p100 tissue culture plates were collected and centrifuged in a Heraeus 1.0R megafuge for 10 min at 800 rpm, 4ºC. The cells were then resuspended in 35ml of 10 mM Tris-Cl pH 8.1 and lysed by four freeze-thaw cycles. Cell lysates were clarified to remove cellular debris by centrifugation in a Heraeus 1.0R megafuge at 3000 rpm for 60 min at 4ºC.

When the IgH2 cell line was also used to propagate SnAdV, the procedure described for LAdV was followed.

Virus purification

As Ad5GL and SnAdV viral particles present similar density, the same purification protocol was used in all cases.

3.2.17 Quantification of physical viral particles

The number of purified viral particles was determined by measuring the absorbance at 260 nm of the sample diluted 1:50 in PBS and after treatment with 1% SDS for 10 minutes at room temperature. Blank sample was PBS suplemented with 1% SDS. Measurements were taken in a NanoDrop 1000 (Thermo Scientific). Determination of the viral concentration in the sample was made as follows:

(OD reading) x (50) x (1E+12) = viral particles/ ml (Maizel et al, 1968)

3.2.18 Quantification of infectious viral particles

The end-point dilution assay was used to measure virus titer. Serial dilutions of a virus stock were prepared and inoculated onto replicate cell cultures, in 96 well plastic plates. The number of cell cultures that are infected is then determined for each virus dilution, by looking for cytopathic effect.

For purified virus, an initial 1E-07 dilution is made, making serial dilutions 1:5 in the following wells, up to 2.56E-13. For culture supernatant, an initial 1E-04 dilution has been chosen, making 1:5 serial dilutions in the following wells, up to 5.12E-11.

After 1 hour of incubation, 150µL of infection medium was added to each well. After 10 days of infection, the highest dilution presenting cytopathic effect was used in the following formula:

(Highest dilution with CPE x initial dilution)/infection volume = infective units/µL (i.u./µL)

3.2.19 Sequential disruption of virions

This protocol (based on Prage et al., 1970) allows obtaining samples enriched on different viral components (vertices, facets of viral capsid, and cores). Capsid disassembly is due to hypo-tonic dialysis followed by centrifugation and freezing-thawing cycles, as follows:

1. Dialysis against 0.005 M Tris-maleate buffer pH 6.3, 1 mM EDTA at 4ºC, 24 hours.
2. Centrifugation 20200 g/ 60 minutes, 4ºC.
3. Sediment redissolved in 0.01M Tris-HAc buffer pH 8.0 and kept at 25ºC for 3 hours.
4. Centrifugation 20200 g/60 minutes.
5. Sediment redissolved in 0.01 M glycine 0.001M Tris Hcl buffer pH 7.2, 0.01% Triton X-100 and frozen and thawed 20 times with liquid nitrogen and 37ºC, respectively.
6. Centrifugation 20200 g/60 minutes.
7. Sediment resuspended.

3.2.20 NanoHPLC-ESI-MS/MS of high resolution Triple TOF

Mass Spectrometry assays were carried out by the CNB Proteomics Facility. (Alberto Paradela for purified virus analysis and Rosana Navajas for recombinant IVa2 preparations).

Proteins and viruses in solution were subject to precipitation, reduction and carbamidomethylation of cysteines and trypsin digestions. The resulting tryptic peptides were separated in a chromatographic system and detected with mass spectrum, obtaining fragmentation spectra MC/MS. The proteins were identified

automatically using the program Mascot which correlated the experimental mass spectra against theoretical mass spectra from adenovirus proteins from data base Swissprot for IVa2, NCBI for SnAdV-1 and a local data base in the case of the novel adenovirus LAdV. A double search with taxonomic restriction to Viruses and Animal was performed to detect contaminants from eukaryotic cells used to produce the recombinant IVa2. Only peptides with scores higher than 45 were accepted.

3.2.21 MALDI-TOF-TOF

Peptide Mass Finger printing MS-MS by MALDI TOF TOF assays for electrophoresed protein bands identification were carried out by Silvia Juárez at the CNB Proteomics Facility.

After trypsinization of the samples, they are loaded in the mass spectrum MALDI-TOF-TOF. The result is a spectrum with a group of masses (m/z) corresponding to the characteristic tryptic peptides of the proteins present in the sample. The proteins were identified automatically by the computer program Mascot which correlated the experimental mass spectra against theoretical mass spectra from adenovirus proteins from a local data base containing the sequenced proteins of the novel adenovirus LAdV. The result is a list of candidates statistically validated with a score for a p-value of 0.05.

Results

4 Results

4.1 IVa2 protein

4.1.1 Locatization of IVa2 within the viral particle

The requirement of the IVa2 protein for DNA packaging (Ostapchuk, Almond, and Hearing, 2011) suggests that it would occupy a location in the virus similar to that of other packaging ATPases. Viral packaging motors comprise structures that are situated at a single vertex of the icosahedron, and act as the site of entry of the genome into the capsid by their association with enzymatic functions that translocate the DNA. Locating IVa2 in a single vertex of the capsid could relate this protein with its putative function as DNA translocase. If adenovirus had a portal complex similar to those from bacteriophages, and IVa2 was part of that structure, it would be expected to be in a external position in one of the vertices.

4.1.1.1 Immunogold labelling

IVa2 was reported to occupy a single vertex of the icosahedron on the basis of immunogold labeling technique during the course of this thesis (Christensen et al., 2008). The idea of labeling a special vertex of adenovirus made us to consider the possibility of taking advantage of the antibody density to align cryo EM images of the viral particles without using icosahedral symmetry to reveal the non-icosahedral structural features, including the portal vertex. Based on this idea, immunogold labeling experiments were performed to define antibody binding conditions to capsids.

To determine the location of IVa2 in capsids, we examined purified mature viruses using immunogold labeling and electron microscopy. Viral capsids adsorbed to EM grids (Section 3.2.7) were probed with five mAb raised against purified IVa2-FLAG, or a goat polyclonal antiserum against purified IVa2-GST. Positive control experiments were performed with a virus displaying the FLAG tag on the capsid surface and an anti-FLAG antibody, while negative control experiments consisted of Ad5GL probed with anti-FLAG antibody.

4.1.1.1.1 Monoclonal antibodies

Initially, a battery of five mAb provided by our collaborator Prof. Jane Flint was used to locate IVa2 within the viral capsid.

A first checking of the grids indicated that the labeled particles were little. Based on this fact and because of the presence of some labelled particles in the negative control, double blind quantification of the label was performed for all the anti-IVa2 mAb antibodies and for the negative controls. The percentages of labeled particles were very low, as shown in **Figure 15-A and 15-B**.

In any purified adenovirus sample, it is possible to find a few broken or damaged capsids. Results from immunogold labelling were therefore divided into two classes: label on intact viral particles, and label on broken particles. This division was based on the initial qualitative observation that broken particles seemed to present more gold labels than intact ones (**Figure 15-C and 15-D**). It has to be considered that even when the capsid looks intact, a small damage might be present in the virus, so the low rates of label in intact particles should not be considered as detection of external protein.

This result indicated that IVa2 protein is not accesible from the outside of the capsid, or that the accesible sites of the protein are not recognised by none of the five tested antibodies. It also ruled out the possibility to use the tested mabs in 3DEM studies of virus-antibody complexes.

A

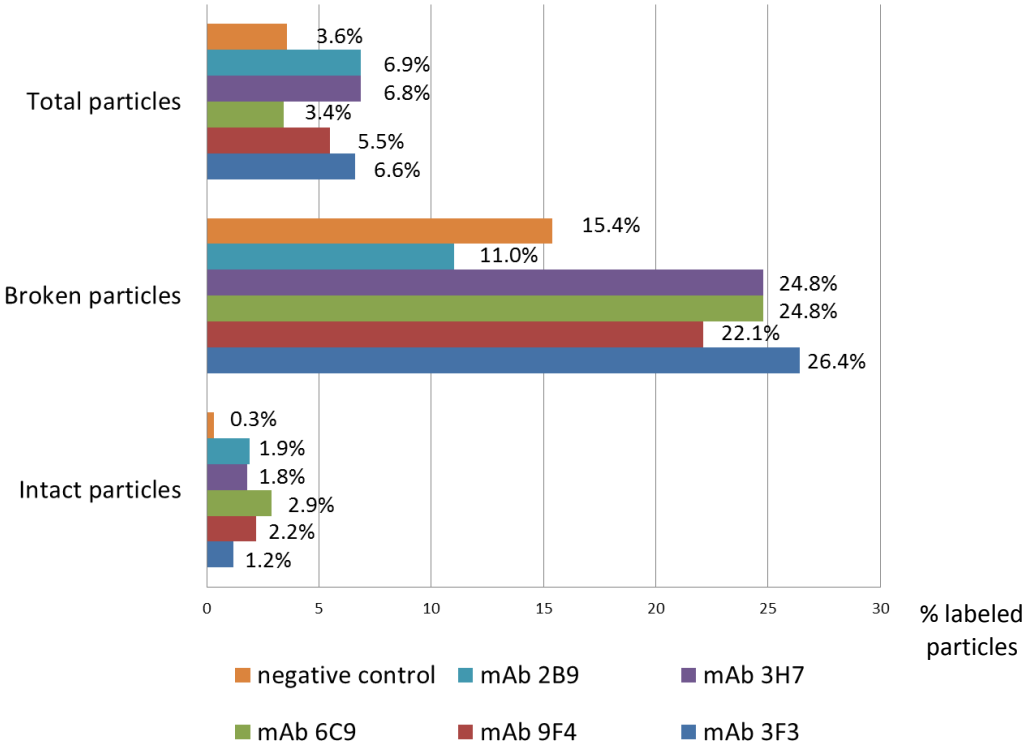

B

	mAb 3F3	mAb 3H7	mAb 9F4	mAb 2B9	mAb 6C9	Negative control
Intact labelled particles	5 (406)	11 (503)	10 (345)	7 (397)	8 (414)	2 (680)
Broken labelled particles	29 (110)	34 (154)	13 (74)	28 (113)	9 (82)	29 (186)

C D

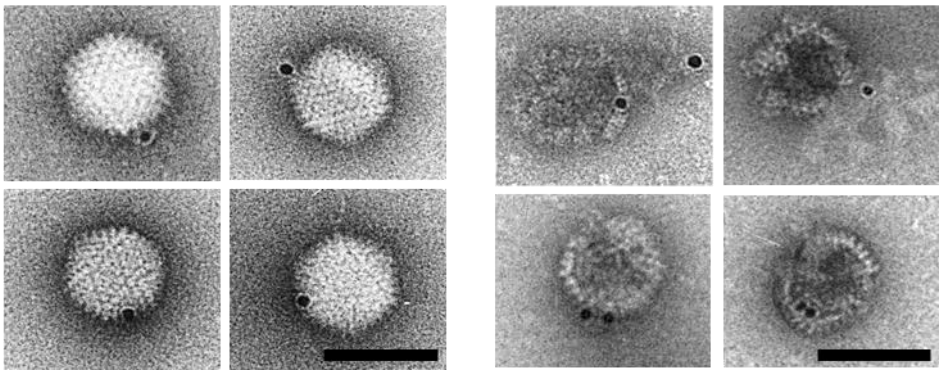

Figure 15.- Immunogold labeling of viral particles with a battery of 5 different mAb anti-IVa2 (1:20). As negative control, a primary antibody anti-flag (1:25) was used (Amersham). (A) Percentage of labeled particles respect to the total particles of each class. (B) Number of labeled particles and total counted particles by double blind. (C) Intact and (D) damaged Ad5GL labeled particles with anti-IVa2 antibody. Scale bars represent 100 nm.

4.1.1.1.2 Polyclonal antibody

At this point of the project, a report locating IVa2 at one viral vertex in 19% of the particles was published (Christensen et al., 2008). Hence, the antibody used in this publication seemed a better candidate to perform the 3DEM reconstruction of the virus-AB complex. An aliquote of anti-IVa2 was obtained from Prof. Michael Imperiale. The antibody was a serum anti IVa2 from goat.

When the serum was tested with immunoEM and the results quantified as for the mab, the results published in (Christensen et al., 2008) were reproduced with 17% of labeled particles. However, when analyzing again the previous data considering broken and intact particle classes, the results of testing for immunoEM the polyclonal antibody showed a behavior similar to that of the monoclonal antibodies (**Figure 16**). While over 40% of damaged particles were labeled, gold was only observed in 7% of intact particles, indicating that IVa2 protein is not easily accessible from the outside of the viral capsid.

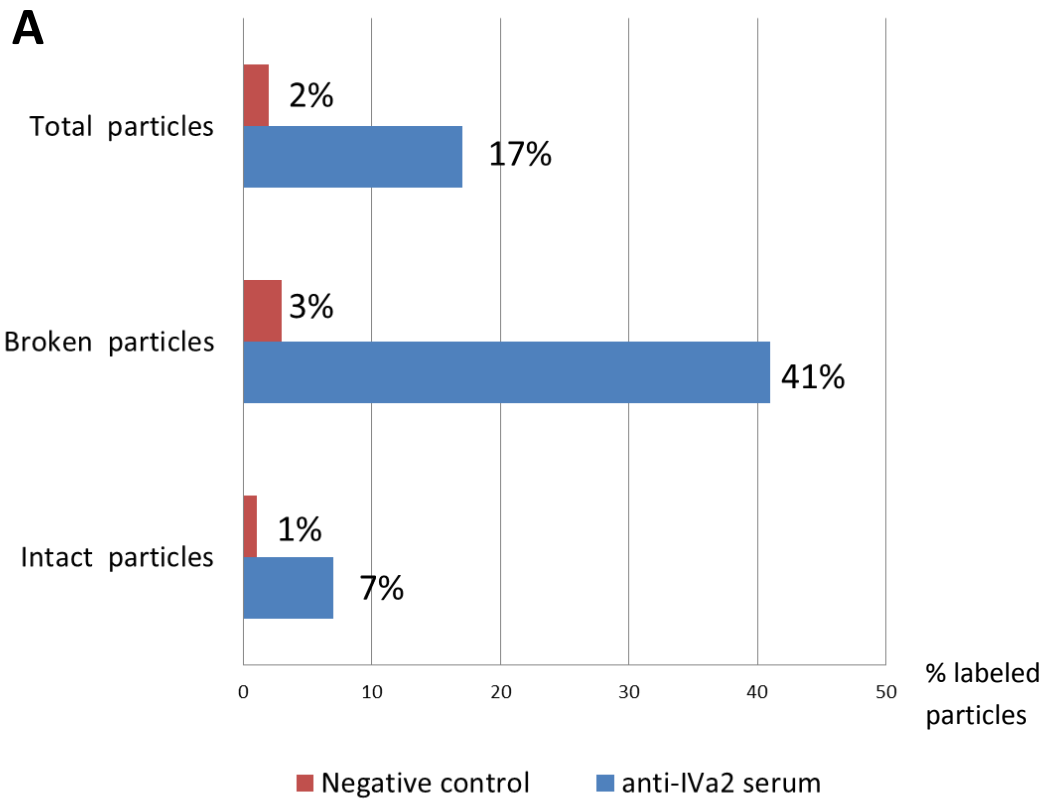

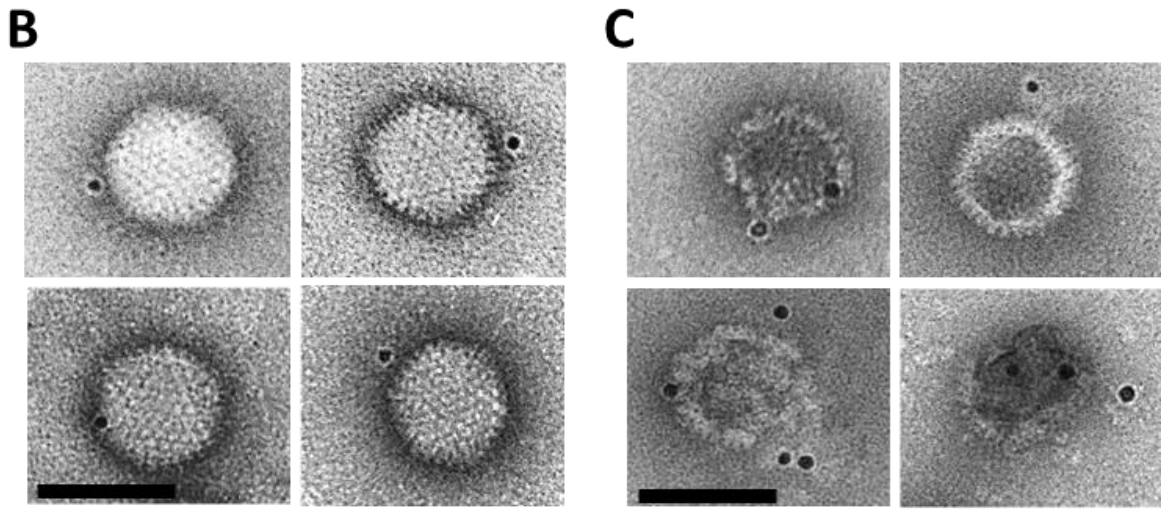

Figure 16.- Immunogold labeling of viral particles with a polyclonal antibody (1:20). (A) Percentages of total, broken and intact labeled particles respect to the total of particles of each class. Total particles counted= 851, number of experiments= 5. (B) Intact and (C) damaged Ad5GL labeled particles with anti-IVa2 antibody. Scale bars represent 100 nm.

4.1.1.2 Antibody characterization

The low label obtained in immuno EM experiments, particularly with mAbs raised the possibility that all epitopes correspond to a specific part of the polypeptide chain that was masked in the virion. To further understand the poor IVa2 accesibility to the antibodies, epitope mapping of mAb and the polyclonal serum was performed.

Determination of the Ig isotype by ELISA, revealed that all five mAbs have an IgG1 heavy chain. Localization and length of the recognized epitopes from this five monoclonal antibodies, named after their clones: 3F3, 3H7, 9F4, 2B9 and 6C9, was addressed by systematically scanning through the entire IVa2 sequence in two membranes using an overlapping peptide strategy with an offset of two or three amino acids, respectively.

The reaction patterns of the tested mAbs were limited to small areas of the sequence, as expected (**Figure 18-A**). In some cases (3H7 and 6C9) the epitope was localized in a more accurate way thanks to the comparison of signal from the two membranes containing the IVa2 sequence with overlapping peptides on 3 or 2 aa (**Figure 17**). As expected, the polyclonal antibody showed an extensive coverage of the

sequence (**Figure 18-C**). In both cases, the corresponding secondary antibody (anti-mouse or anti-goat) alone was also tested to rule out unspecific binding.

Figure 17.- Accurate definition of mAb epitope by the use of two membranes with different overlapping. The result from membrane 1 was confronted to that from membrane 2. Spot intensities were qualitatively represented by a certain number of crosses (higher intensity is equal to higher number of crosses). As an example, in membrane 1 for mab 6C9, the difference of signal between spot 1 and 2 indicates that residues "EAL" do not contribute in the binding of the antibody. On the other hand, membrane 2 shows that residues "GLM" are not needed for mAb binding neither. From this signal comparison, the epitope for this antibody was established to be "QWCYLHPRD".

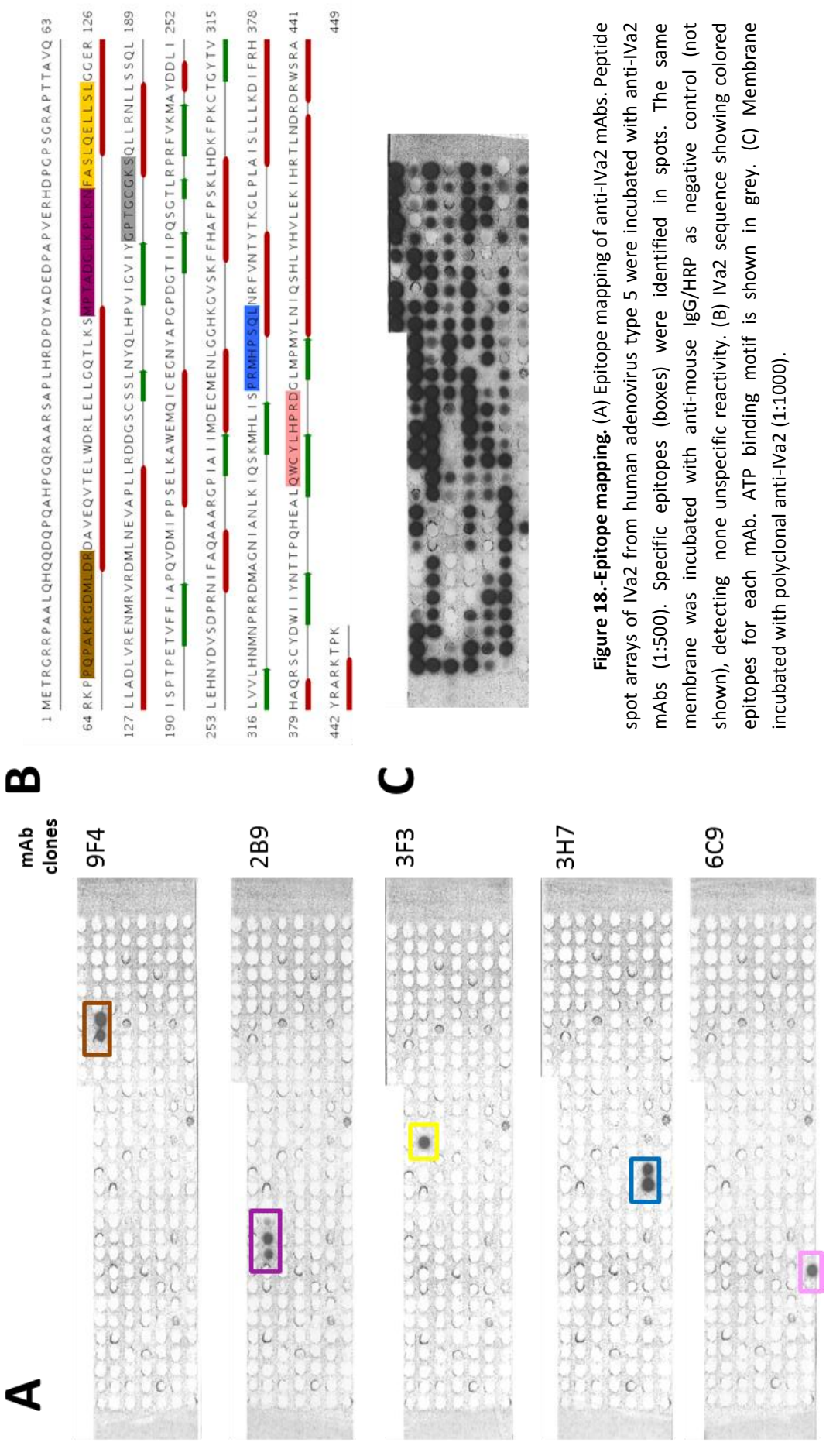

Figure 18.-Epitope mapping. (A) Epitope mapping of anti-IVa2 mAbs. Peptide spot arrays of IVa2 from human adenovirus type 5 were incubated with anti-IVa2 mAbs (1:500). Specific epitopes (boxes) were identified in spots. The same membrane was incubated with anti-mouse IgG/HRP as negative control (not shown), detecting none unspecific reactivity. (B) IVa2 sequence showing colored epitopes for each mAb. ATP binding motif is shown in grey. (C) Membrane incubated with polyclonal anti-IVa2 (1:1000).

Taken together, these results indicate that not only a small region of the protein, but most of it is recognised by the Abs used. Therefore IVa2 is not exposed on the viral particles, but somehow masked by other proteins when the virus is intact.

4.1.1.3 Controlled proteolysis of viral particles

To obtain alternative evidence on protein IVa2 accessibility in intact capsids, controlled proteolysis assays of viral particles were carried out. As a control, an external (penton base) and an internal (polypeptide V) proteins were followed. IVa2 has an estimated copy number 6.3 ± 1.5 (Christensen et al., 2008) and its size (50 kDa) is close to polypeptide V (42kDa), with a copy number 157±1 (van Oostrum and Burnett, 1985). To be able to distinguish IVa2 from V in a 4-20% PA gel, proteins were detected with antibodies in sequential WB analysis. Penton base (63 kDa a copy number 60) (van Oostrum and Burnett, 1985) can be visualized by silver staining.

Two different proteases (proteinase K and trypsin) were used. Intact and disassembled virions (10E+11 vp) were incubated at 4ºC in the presence of 0.625 µg/ml proteinase K (**Figure 19**). In the setting up of the experiment, proteinase K showed to be too processive at 37ºC and at 25ºC. Protease concentration was also adjusted from higher amounts which also resulted in extensive proteolysis even at the shortest time. Viral intact and disassembled capsids (10E+10vp) were also incubated at 37ºC in presence of 25 µg/ml trypsin (**Figure 20**).

Increasing proteolysis times were analyzed by silver staining and consecutive WB in the same nitrocellulose. As shown in figures 19 and 20, by the time penton base was completely processed, the internal protein V was still unaltered and remained so until the end of the experiments. The same intact appearance was observed for IVa2 protein. Results from two different proteases (proteinase K and trypsin) showed how an external protein was proteolyzed while an internal protein and IVa2 protein did not show apparent cleavages.

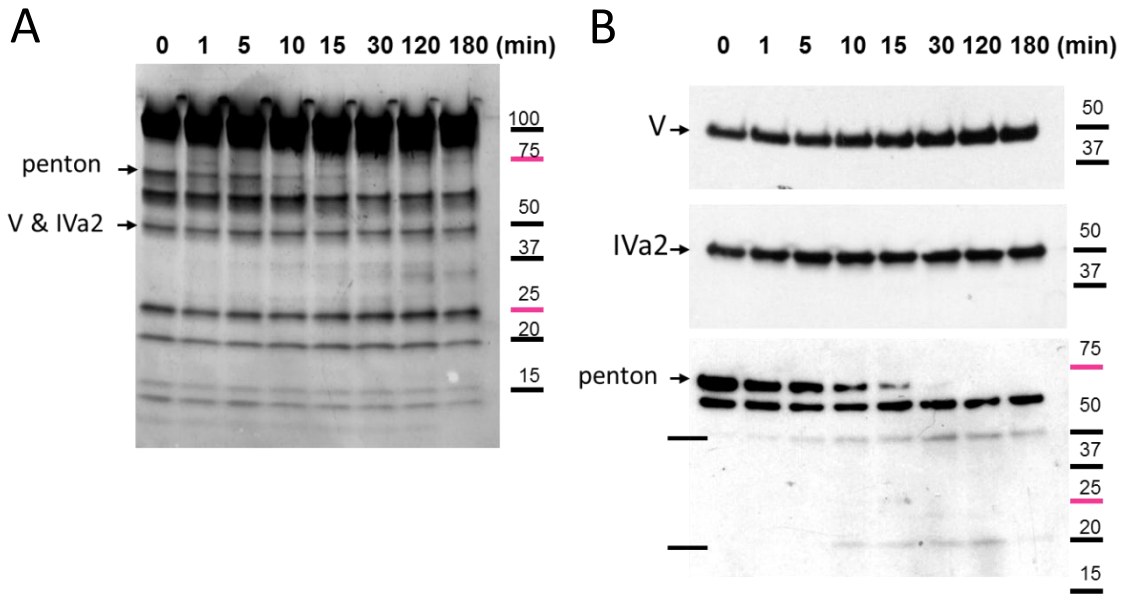

Figure 19.- Proteinase K. (A) Silver stained SDS-PAGE and (B) immunoblot showing Ad5GL proteins treated during increasing proteolytic times with proteinase K. The same blot was probed sequentially for the proteins indicated in the figure (anti-V diluted 1:500, anti IVa2 diluted 1:500, anti penton base diluted 1:2000).

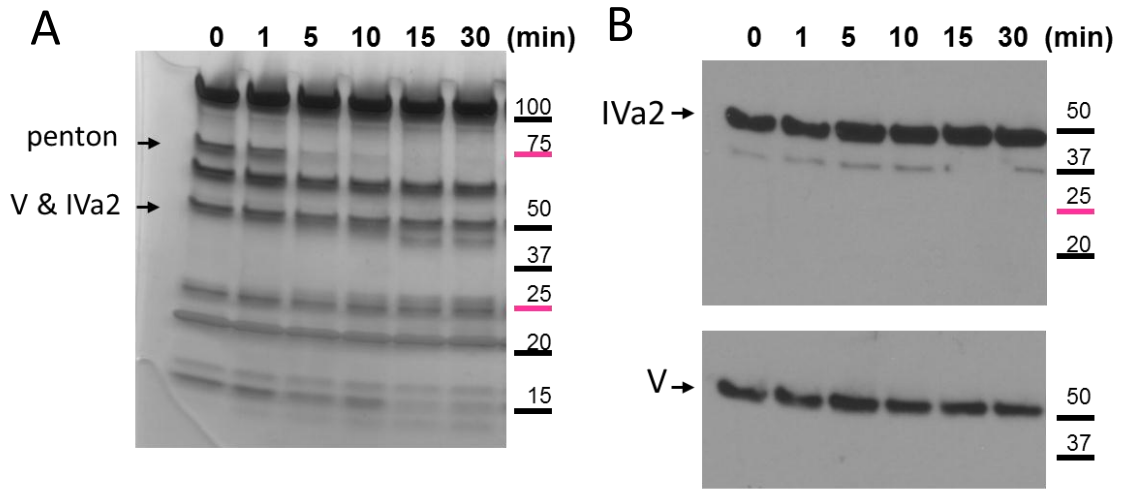

Figure 20.- Trypsin. (A) Silver stained SDS-PAGE and (B) immunoblots showing Ad5GL proteins treated during the indicated increasing proteolytic times with trypsin (anti-V diluted 1:500, anti IVa2 diluted 1:500).

Using ExPASy PeptideCutter was verified that all three proteins had sequence cleaving motives for both proteases (**Table 3**), but a control of protease activity in folded protein conformation was still needed. Broken capsids were used for this purpose. In this way, protease accessibility to the internal proteins is possible. An initial

method for disrupting virus by heating capsids at 48ºC for three minutes (based on previous works, (Perez-Berna et al., 2009)) was ruled out due to the presence of proteolysis in the capsids without external protease treatment. This could happen due to auto-proteolytic activity of viral proteins, or by the viral protease activity on new accessible viral proteins enhanced with temperature. An alternative disruption method chosen for this activity control was the one described in section 3.2.19, based on sequential dialysis against hypotonic buffer, room temperature incubation, and freezing and thawing cycles in the presence of detergent. Disassembled capsids treated with either proteinase K or trypsin showed a clear proteolysis of proteins V and IVa2 by both external proteases (**Figure 21**).

Name of enzyme	Target protein	No. Of cleavages	Positions of cleavage sites
Proteinase K	Iva2	192	2 3 9 10 11 20 26 27 30 32 38 39 41 44 46 47 57 59 60 61 62 70 76 80 81 82 84 85 86 87 88 91 92 93 94 97 98 103 104 107 110 113 114 116 118 119 120 122 125 127 128 129 131 132 134 138 142 144 145 146 148 149 158 160 162 165 166 168 169 170 173 180 181 184 185 189 190 193 195 196 197 198 199 200 201 204 207 211 212 214 215 216 219 221 224 225 231 232 233 238 239 243 244 247 248 251 252 253 254 257 259 265 266 267 269 270 271 275 276 277 278 281 284 286 292 295 296 298 299 303 307 311 313 314 315 316 317 318 319 329 332 333 335 337 343 344 353 356 357 359 360 361 364 366 367 368 370 371 372 375 376 380 385 387 388 389 390 392 393 397 398 399 401 403 404 410 414 415 417 421 422 424 425 426 428 431 432 438 441 442 444 447
	V	179	6 8 9 11 13 14 15 17 18 19 25 26 29 34 37 47 48 51 52 53 54 55 57 58 59 64 66 71 74 75 79 80 81 82 83 84 87 90 92 93 96 97 99 100 101 104 106 107 108 110 112 114 116 117 118 119 127 128 129 131 133 137 140 143 144 145 148 149 151 152 153 156 157 161 164 168 169 171 172 174 176 182 183 185 186 187 190 191 192 195 196 198 199 201 204 207 208 211 213 215 216 218 220 222 223 226 228 229 230 231 232 233 236 237 239 242 243 245 246 247 249 250 251 253 254 255 256 257 258 261 263 264 265 267 270 272 274 276 286 288 289 291 292 293 295 296 297 298 302 303 305 308 311 312 313 319 320 321 325 326 327 329 339 340 341 343 345 348 349 351 355 356 357 358 360 361 363 367 368
Trypsin	Iva2	51	4 6 25 28 34 48 56 64 71 72 78 90 99 111 126 133 137 139 150 177 182 213 242 245 263 272 290 294 302 306 309 325 326 336 340 347 355 362 373 377 382 407 427 430 435 437 440 443 445 446 449
	V	58	3 4 5 7 23 24 32 33 35 36 38 39 40 41 42 61 63 67 69 70 72 73 88 91 94 95 113 121 122 124 158 159 162 163 178 179 181 188 200 205 260 273 278 281 284 285 309 316 318 322 324 330 336 346 347 350 354 362

Table. 3.- ExPASy PeptideCutter prediction of potential cleavage sites cleaved by external proteases (proteinase K and trypsin) in sequences of adenoviral proteins IVa2 (Uniprot P03271) and V (Uniprot P24938).

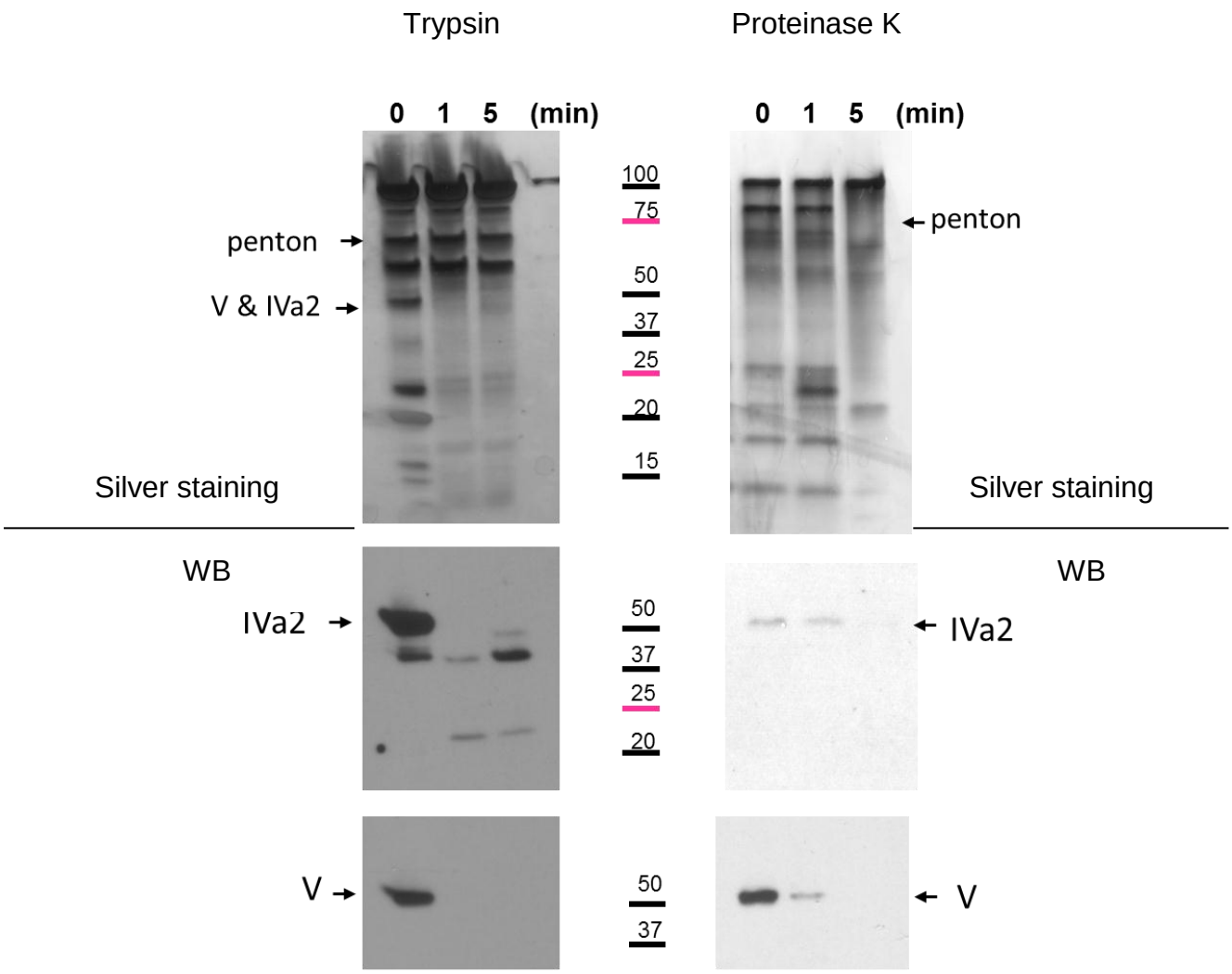

Figure 21.- Proteases effect on disassembled capsids. Silver stained SDS-PAGE and immunoblot showing disassembled Ad5GL proteins treated during the indicated increasing proteolytic times with trypsin or proteinase K.

Therefore, both the immune EM and the limited proteolysis assays indicate an internal location for IVa2 in the virion.

4.1.1.4 Detection of IVa2 in viral disruption products

To further investigate the location of IVa2 within the virion, disrupted virus products were analyzed by sequential native and denaturing electrophoresis. This technique could give information on proteins interacting with IVa2 (neighbours) or on the oligomeric state of IVa2 in the virion. Ad5GL was disrupted by heating at 50ºC at different times and disruption products were analyzed in a 5% native gel (**Figure 22-A**). A reproducible band pattern was observed for fragments entering the gel. Time of heat treatment was finally set at 30 minutes, since longer incubations did not yield different

band composition. Disrupted viruses were visualized by EM (**Figure 22-B**), detecting viral fragments of different sizes, some of them too large to enter the native gel.

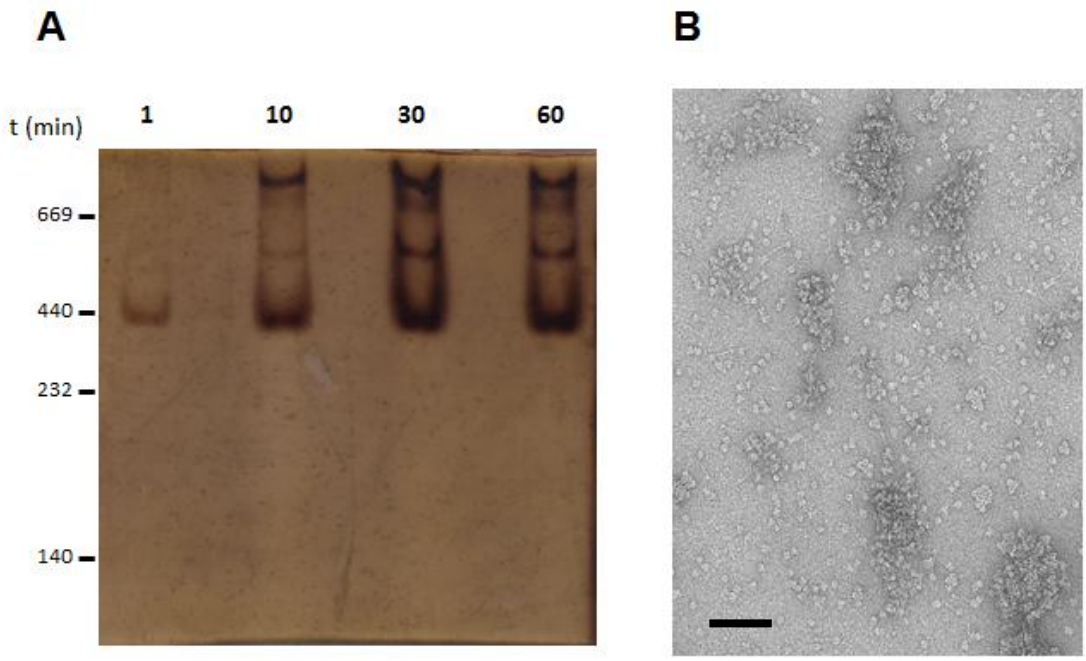

Figure 22.- Heat disrupted capsids. (A) Different fragment sizes from disassembled viruses (3E+12 vp/well) are analyzed by silver stained native PAGE. Increasing the heating time longer than 30 minutes did not produce a change in band pattern. (B) EM visualization of disassembled viruses after treatment of 50ºC for 30 minutes.

The regions in the native gel corresponding to the 6 bands visible by silver staining (**Figure 23-A**) were excised, loaded onto a 15% PA gel and electrophoresed under denaturing conditions. Denaturing gels were analyzed by either silver staining (**Figure 23-B**) or WB with a mAb against IVa2 (**Figure 23-C**). IVa2 protein was detected in bands 2 and 5. Band 2 has an apparent low molecular weight (higher than 66 but lower than 140 kDa). It is interesting the fact that the major component of this fraction is protein VII. The interaction between these two proteins has previously been shown by co-immunoprecipitation experiments from infected cells (Zhang and Arcos, 2005). Other proteins present in Band 2 are: IIIa (or fiber), V, VIII and IX. A weaker signal for

IVa2 was also detected in a higher molecular weight band (band 5), containing majoritary penton base and IIIa or fiber, proteins localized in the viral vertex.

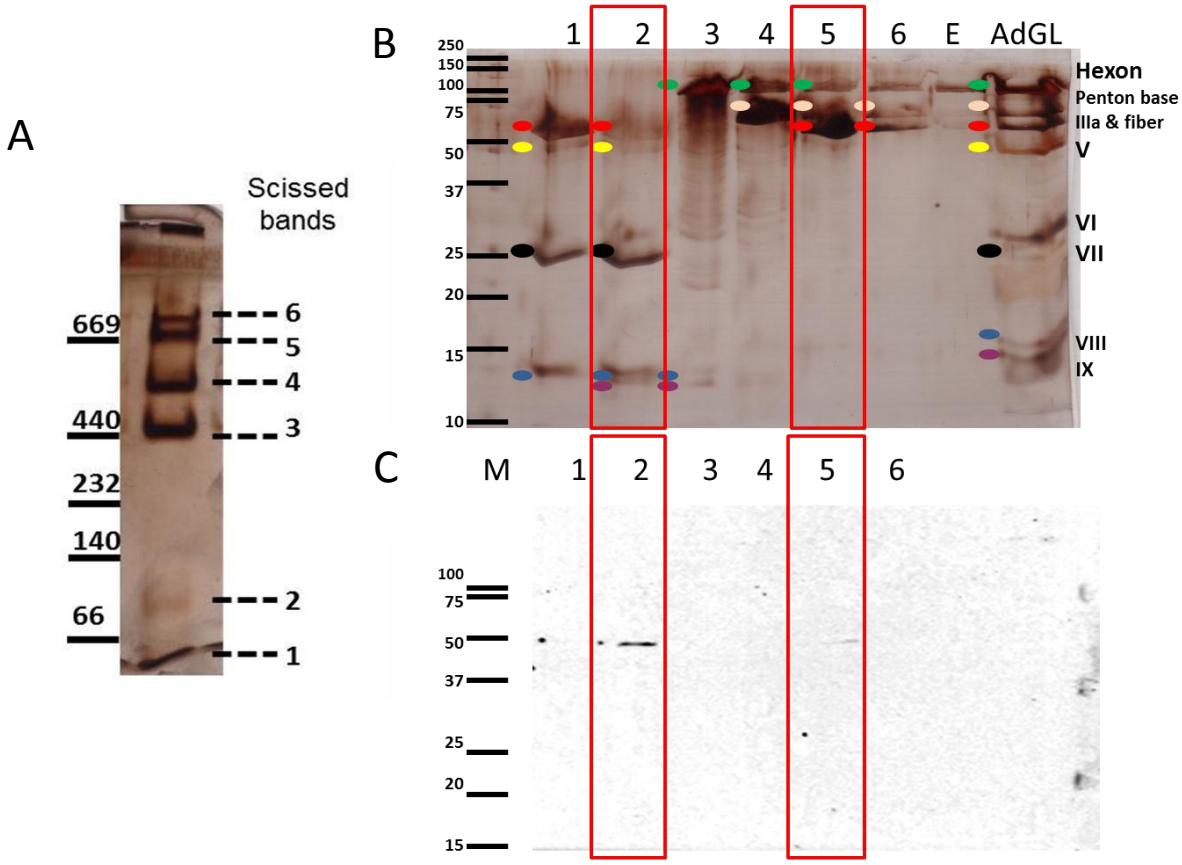

Figure 23.- Detection of IVa2 in disrupted capsids (I). (A) Native electrophoresis of disassembled virus followed by (B) SDS-PAGE and (C) immunoblot probed with mAb anti-IVa2 (3H7) of the separated viral fragments.

To analyze the possible presence of IVa2 in other fragments not detected by silver staining in the native gel, the whole lane was excised and the total of 18 gel pieces were loaded in a denaturing gel. Weak signal for IVa2 was found in the same bands described above. However, the largest IVa2 content was observed in the well (**Figure 24**).

This indicates that the majority of IVa2 proteins remains in fragments too large to enter the 5% PA gel. A smaller quantity is released from the virus in the company of core or vertex proteins, suggesting an internal position close to the vertex.

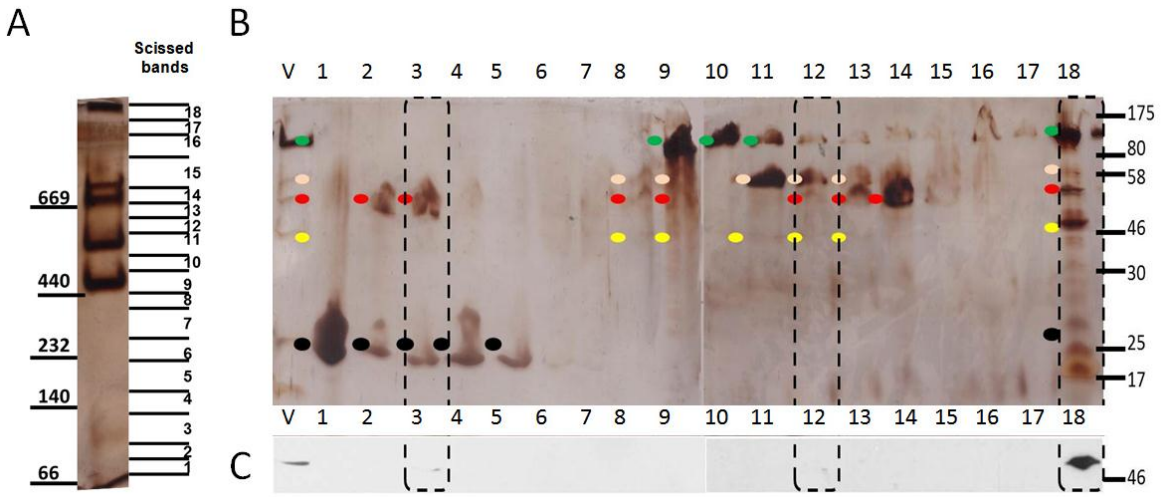

Figure 24.- Detection of IVa2 in disrupted capsids (II). (A) Native electrophoresis of disassembled virus followed by (B) SDS-PAGE and (C) immunoblot probed with mAb anti-IVa2 (3H7) of the separated viral fragments. "V" indicates a control lane with 10E+09 vp.

4.1.1.5 Protein-protein interaction: Far Western Blot (FWB)

Examining the interaction of IVa2 with other viral proteins is an alternative way to determine its position within the viral capsid. For this analysis, the technique of FWB was used.

Ad5GL, Ad5GLflagIIIa (an Ad5GL variant with a FLAG tag at the N-terminal of polypeptide IIIa) and bacteriophage T7 as a negative control were electrophoresed in denaturing conditions and probed with recombinant IVa2 with a FLAG tag at the C-terminus, followed by detection with mouse anti-FLAG antibody and the anti-mouse peroxidase conjugated antibody, as described in Materials and Methods, section 3.2.5 (**Figure 25**). The anti-FLAG antibody was previously tested on the nitrocellulose in the absence of recombinant IVa2 protein to rule out nonspecific binding.

A clear single band appeared in the Ad5GL lane, at a MW of 50kDa approximately. The same band is present in the Ad5GLflagIIIa lane, together with the expected extra-band at the MW of protein IIIa (which contains the FLAG-tag). The negative controls using no recombinant IVa2 probe or bacteriophage T7 capsids showed no signal at all. The signal at 50 kDa could be due to IVa2-IVa2 binding, however there is another viral protein falling in a similar MW range in a SDS-PAGE: protein V(41.5 kDa).

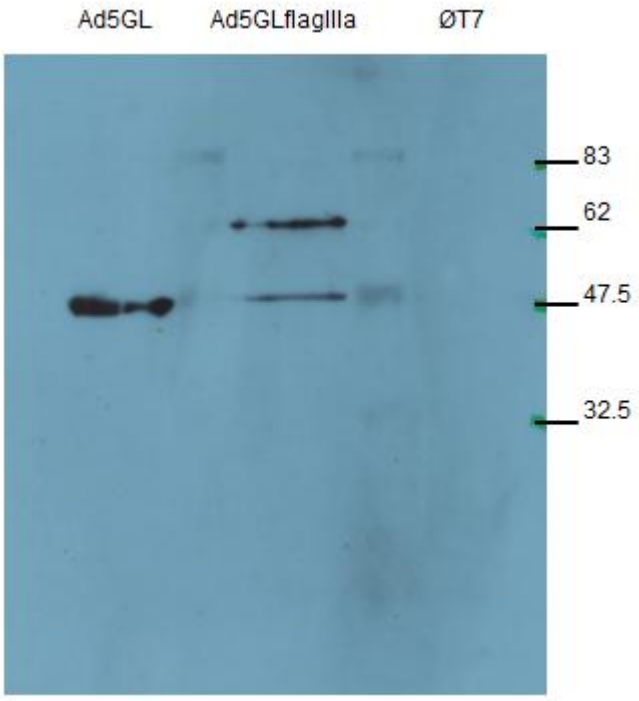

.

Figure 25.- Analysis of IVa2 interactions with other viral proteins by FWB (I) Equal amounts of Ad5GL, Ad5GLflagIIIa and bacteriophage T7 were electrophoresed, transferred and probed with the recombinant protein IVa2-FLAG, followed by detection with mouse anti-FLAG and anti-mouse peroxidase. Ad5GL shows a band around 50 kDa, while Ad5GLflagIIIa shows an additional band corresponding to the expected MW of protein IIIa carrying a FLAG tag. MW marker (6-175 kDa) from New England BioLabs, P7708S.

To determine if the signal detected corresponds to a IVa2-IVa2 or a IVa2-V interaction, the isoelectric points (IP) of proteins IVa2 and V were considered to separate them in a 2D SDS-PAGE. IVa2 has an IP of 8.9, while V is even more basic, with an IP of 10.3. Therefore, an Immobilline DryStrip gel pH 6-11 (Healthcare) was used for the first dimension, followed by SDS-PAGE to separate the viral proteins by size. This

electrophoresis was the starting point for a new FWB (**Figure 26**). Signal was detected again at a MW of 50kDa, with an associated IP around 9. Therefore binding to pV is ruled out and the FWB signal can be attributed to IVa2-IVa2 binding. No other interactions were detected with this method.

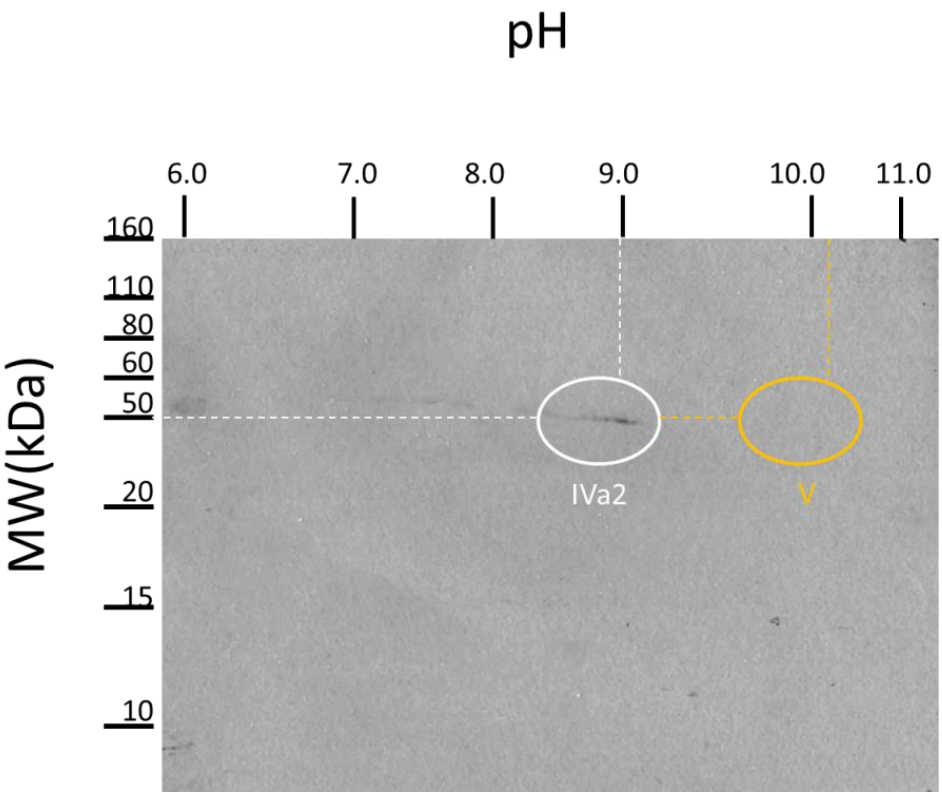

Figure 26.- Analysis of IVa2 interactions with other viral proteins by FWB (II) FWB of a 2D-electrophoresis of AdV5GL in a pH range from 6 to 11, showing a signal (white oval) at 50kDa and a IP close to 9. Expected position for protein V is rounded with a yellow oval.

4.1.2 Oligomeric state of IVa2

Previous studies have established that a dimer of protein IVa2 (DEF-B) binds specifically to an intragenic ML promoter sequence necessary for late phase-specific stimulation of ML transcription (Lutz and Kedinger, 1996). Studies on recombinant IVa2 behavior in solution and in the absence of DNA indicated a monomeric form (Lutz and Kedinger, 1996; Yang, Yang, and Maluf, 2009). EMSA studies (Tyler, Ewing, and Imperiale, 2007) showed binding of several IVa2 monomers to the packaging sequence, but this multiple protein complex on the DNA does not necessary imply protein oligomerization.

However, the FWB experiments (Section 4.1.1.5) showed a self-interaction of IVa2 that could indicate the ability to oligomerize. Oligomerization in a ring is a common feature in packaging motors. Therefore, the oligomeric state of recombinant IVa2 protein was examined.

4.1.2.1 Initial sample characterization: SDS and native electrophoresis

Several recombinant IVa2 preparations with different expression systems have been described in the literature (Lutz and Kedinger, 1996; Tyler, Ewing, and Imperiale, 2007; Yang, Yang, and Maluf, 2009). To study the oligomeric state of IVa2 in solution, the only IVa2 protein with proved ATP binding activity was selected (Ostapchuk and Hearing, 2008). This protein was considered to be a good candidate for structural studies, since activity and structural preservation usually go together. The strep-tagged recombinant IVa2 protein at the C-terminal was initially characterized by SDS PAGE in the absence and presence of glutaraldehyde (**Figure 27-A**). When cross-linker was added, new protein bands appeared, corresponding to multiples of the molecular weight of IVa2. Since the presence of glutaraldehyde might give rise to unspecific protein aggregation, to further assess this oligomeric behavior of protein IVa2, electrophoresis in native conditions using the Blue-native PAGE system was performed. Again, bands of sizes corresponding to multimers of IVa2 were detected (**Figure 27-B**).

From these experiments it can be concluded that the recombinant strep-tagged IVa2 protein is able to form homo-oligomers in solution, but there is not a preferred oligomeric state. The same result was obtained using centrifugation in glycerol gradients, with or without cross-linker (not shown). The largest oligomeric form detected in blue native PAGE could correspond to a 6mer.

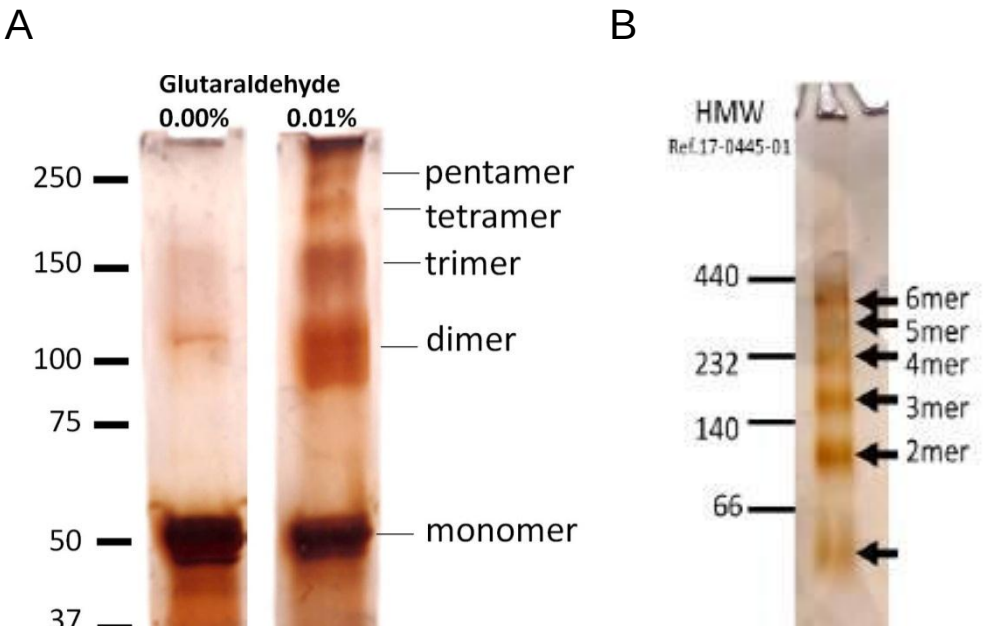

Figure 27.- IVa2 electrophoretic pattern. (A) Discrete bands corresponding to multiples of IVa2 molecular weight appear in SDS-PAGE (10%) when cross-linking with glutaraldehyde. (B) Similar oligomeric bands appear when IVa2 is electrophoresed under native conditions in a 5% polyacrylamide gel. In both cases, the protein loaded was 2 µg per lane.

4.1.2.2 IVa2 visualization by electron microscopy

To further characterize the IVa2 oligomeric forms detected by PAGE, negative staining EM in the presence and absence of glutaraldehyde was carried out (**Figure 28**).

In all cases, the sample presented a heterogeneous aspect, with objects of different shapes and sizes. Nevertheless, in both cases, objects compatible with a ring-like structure were detected.

Further, in the cross-linked sample, particles compatible with top and side views of ring-shaped multimers were observed (**Figure 29**). This finding resulted very interesting, since ring-shaped oligomerization is consistent with the function of IVa2 as DNA translocase.

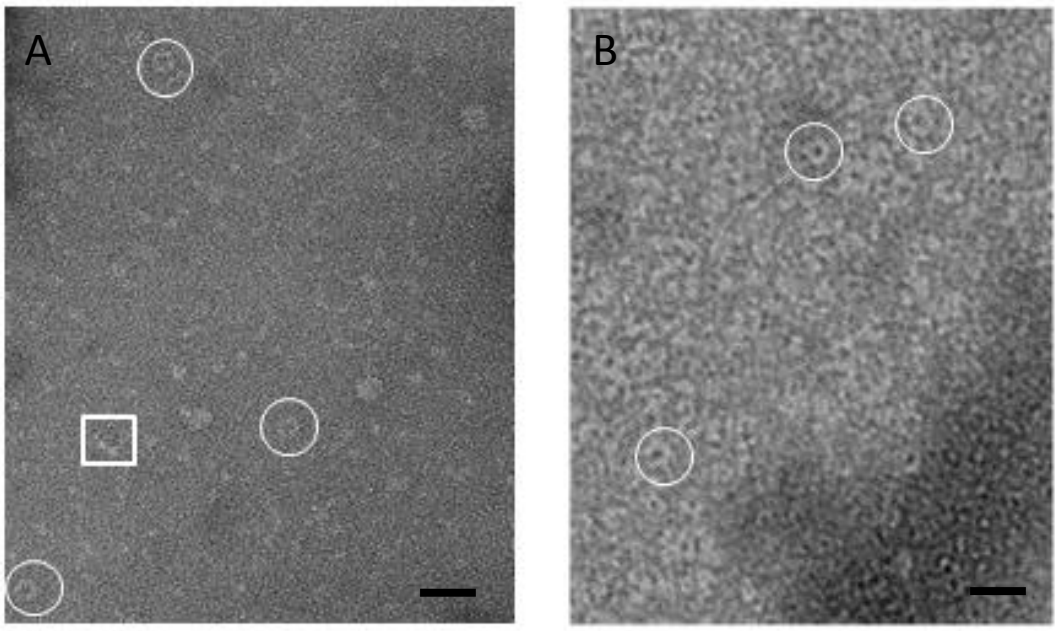

Figure 28.- EM of IVa2 in the presence or absence of crosslinker. (A) Micrograph from cross-linked IVa2 protein reveals top (circles) and side (squares) views of IVa2 oligomers. (B) EM of negatively stained IVa2 in the absence of cross-linkers shows ring-like conformations of the protein. In both cases a heterogeneous proteic background is observed. Scale bars equal to 25nm.

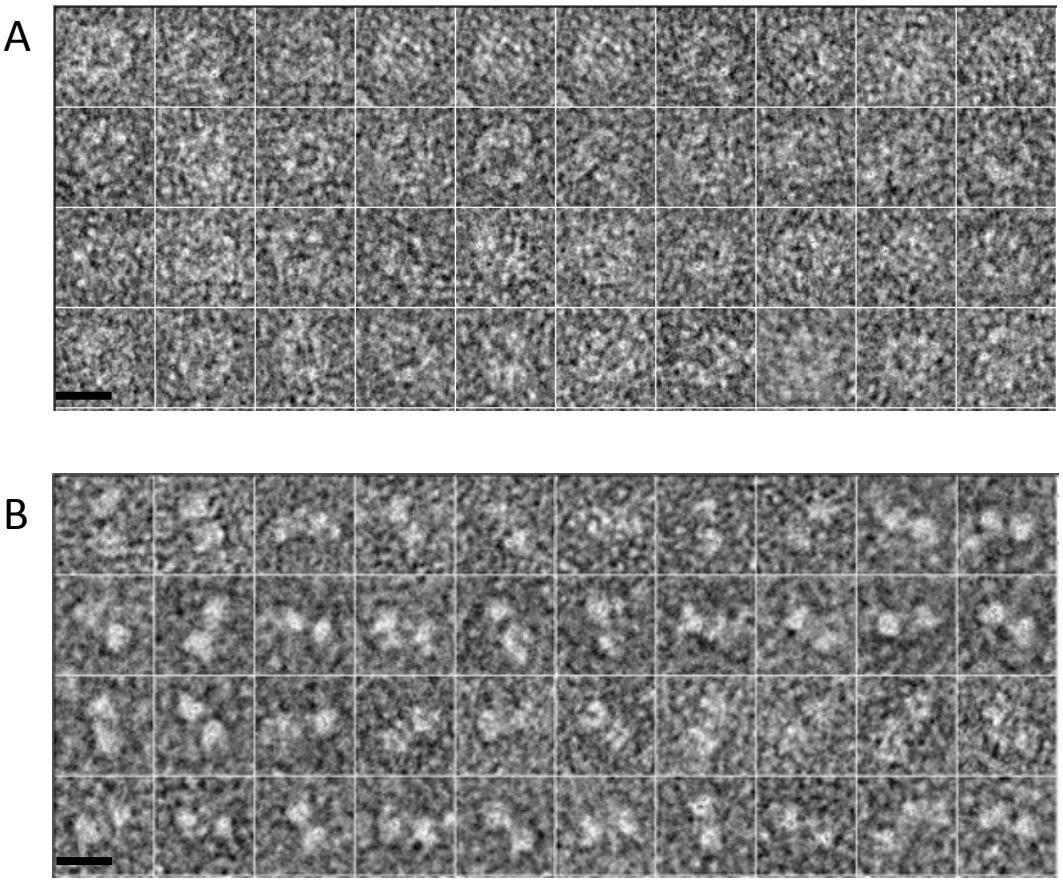

Figure 29.- Particle galleries from cross-linked IVa2 sample. (A) Top views and (B) side views. Scale bar represents 12 nm.

4.1.2.3 *Verification of the absence of ring-like contaminants in recombinant IVa2 protein sample.*

Since ring-shaped particles corresponded only to a minority of the protein observed, the possibility that they were not IVa2 but a contaminant was considered. To evaluate this possibility, two different strep-IVa2 preparations were subjected to mass spectrometry analysis as described in Methods, section 3.2.19.

IVa2 fragmentation MC/MS spectra were identified automatically by the program Mascot (http://www.matrixscience.com) which correlated the experimental mass spectra against theoretical mass spectra from adenovirus proteins (data base: Swissprot). A double search with taxonomic restriction to Viruses and Animal was performed to detect contaminants from eukaryotic cells used to propagate IVa2.

In addition to the expected P03271 (IVa2 from human adenovirus C serotype 5) with a score of 28345 and a coverage of 69% of the sequence, in one of the preparations tested, a possible ring shaped contaminant was detected. Q9V3PO (Peroxiredoxin-1from *Drosophila Melanogaster,* MW=21738) gave a score of 700, and a coverage of 21% of the sequence. This protein belongs to the Cys-1 type peroxireductases. While Cys-2 type peroxireductases have been shown to form rings under certain conditions, there are no data showing ring oligomerization for cys-1 type peroxireductases (Wood et al., 2003). In any case, peroxiredoxin did not appear in the second IVa2 preparation tested, which also contained a minority of ring shaped particles.

4.1.2.4 *Image processing*

No structural data on IVa2 are available. Attempts to crystallize the recombinant protein have failed so far and microscopy studies have not been carried out, since the monomeric form is too small to be subjected to single particle analysis. In this thesis an oligomeric form of IVa2 in solution has been detected for the first time. Although the oligomeric form is minoritary, a first 3D analysis at low resolution can be carried out.

Individual particles were selected from negative staining EM images of crosslinked IVa2 (section 4.1.2.2, figure 28-A) and classified into two families: top views and side views (Figure 29). To analyze structural variability, each family was divided in

ten classes using Maximum Likelihood in the Fourier space in 2 Dimensions (MLF2D)(Scheres et al., 2007). Among the top views, the most populated class contained 42.2% of the particles and presented an appearance of a clear five-fold symmetry ring (**Figure 30-A**). Rotational spectra for each class average were calculated resulting in 70% of particles following five-fold symmetry and 10.1% of particles with a six-fold symmetry (**Figure 30-B**). MLF2D of side views resulted in a major class out of ten, containing 43.5% of the particles (**Figure 30-C**), but all classes looked quite similar with no more variability than the imposed by the negative staining. The assignment of these particles as side views of the ring is based on two facts: the shape and the dimensions of the class average. The shape of the side view (two areas of high density separated by a central area of weaker density) agrees with the expected projection for a ring. In addition, the dimension of the ring diameter is similar to the maximal length of the side view (140Å).

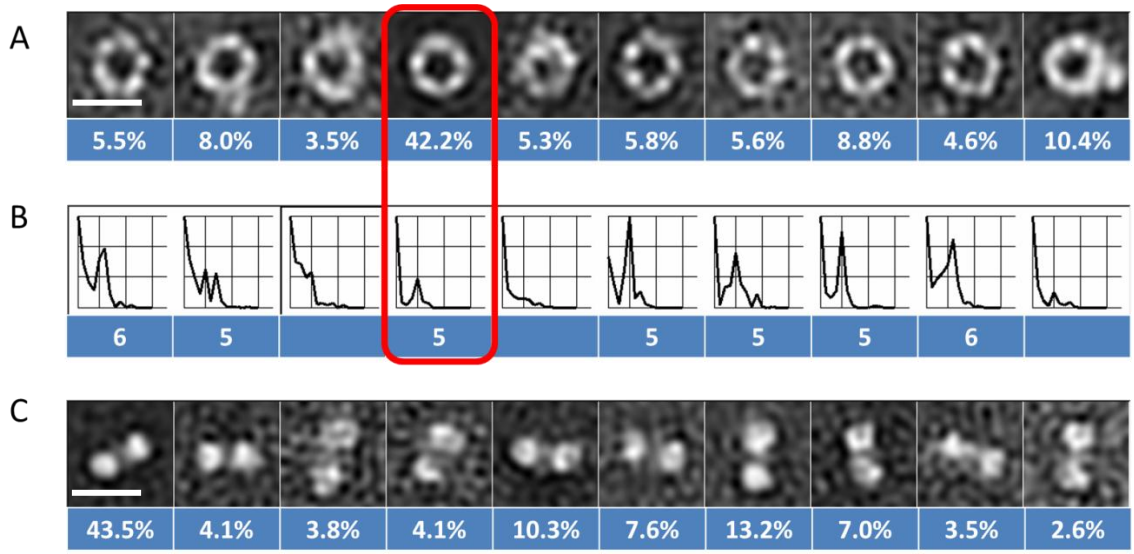

Figure 30.- IVa2 particle classification. (A) Top views classified in ten families using MLF2D. Percentage of particles in each class is indicated below. Total of particles= 964. (B) Rotational spectra for each class average. Symmetry is indicated in the cases the spectra were unequivocal. (C) Side views classified using MLF2D and percentage of particles in each class average. Total of particles = 340. Scale bar represents 12.5 nm.

Using the particles from the major top and side view class averages and imposing 5-fold symmetry, a 3Dmap was calculated with EMAN (http://blake.bcm.edu/emanwiki/EMAN/) (Ludtke, Baldwin, and Chiu, 1999) (**Figure 31**). This low resolution model can give an idea about the general morphological features of the IVa2 oligomer.

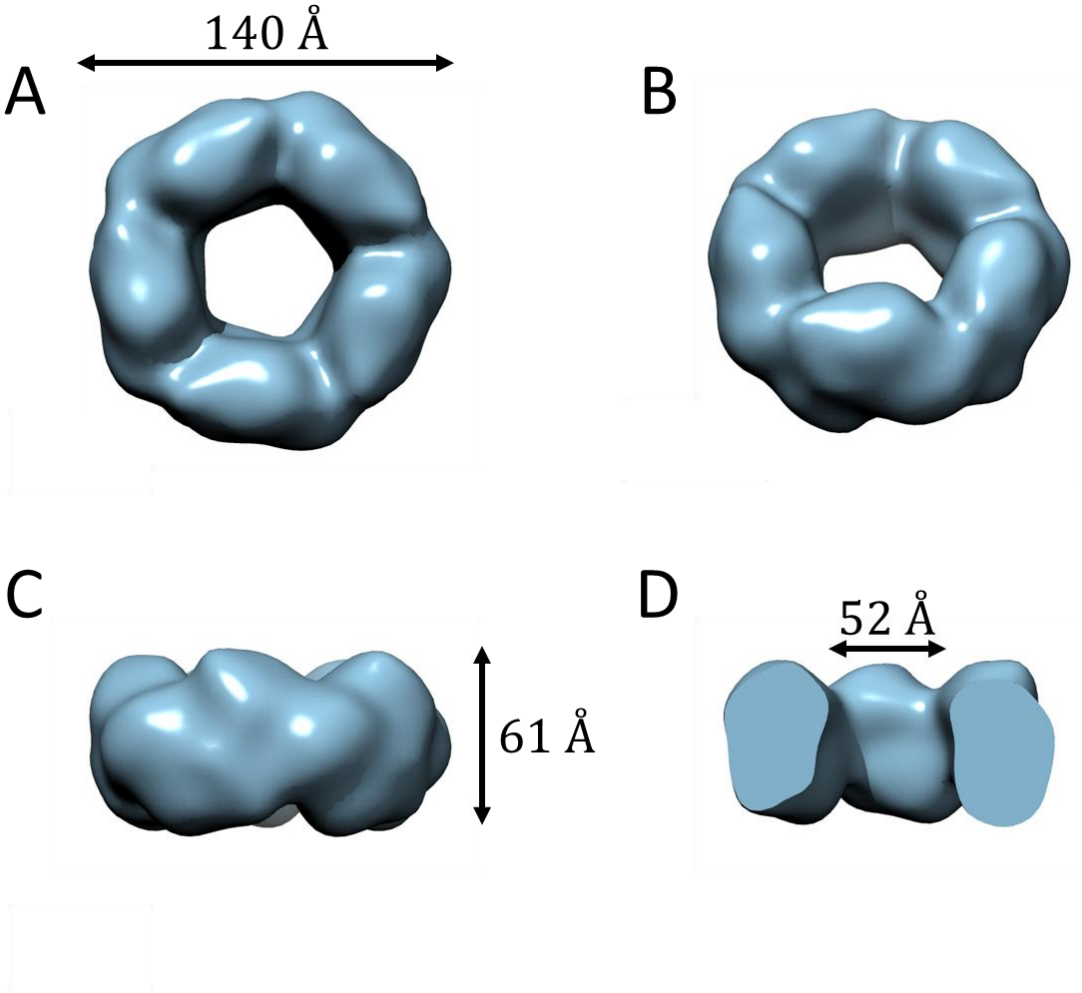

Figure 31.- IVa2 3DEM model. (A) Top, (B) oblique and (C) side views of a 20 Å resolution 3D reconstruction calculated with EMAN, with 5C symmetry imposed. (D) Longitudinal cut showing the central channel.

4.1.2.5 Fitting

As previously indicated, there are no available models of IVa2 to use in validation or interpretation of the 3D-reconstruction of the ring-shaped oligomer. Standard homology modeling is not an option, as there are no close homologous with solved structures. Recently, a new server using remote homology for modeling, Raptor X, has been released (Kallberg et al., 2012). When the Ad5 IVa2 sequence was submitted to

Raptor X, a remote homology model could be constructed using as templates Bacterial L-aspartase beta-decarboxylase and Tyrosine aminotransferase from *Trypanosome cruzi*.

Five copies of the homology model (**Figure 32-A**) were fitted into the oligomeric EM map using VEDA (http://mem.ibs.fr/VEDA/) and imposing C5 symmetry. (**Figure 32-C, 32-D, 32-E, 32-F**).

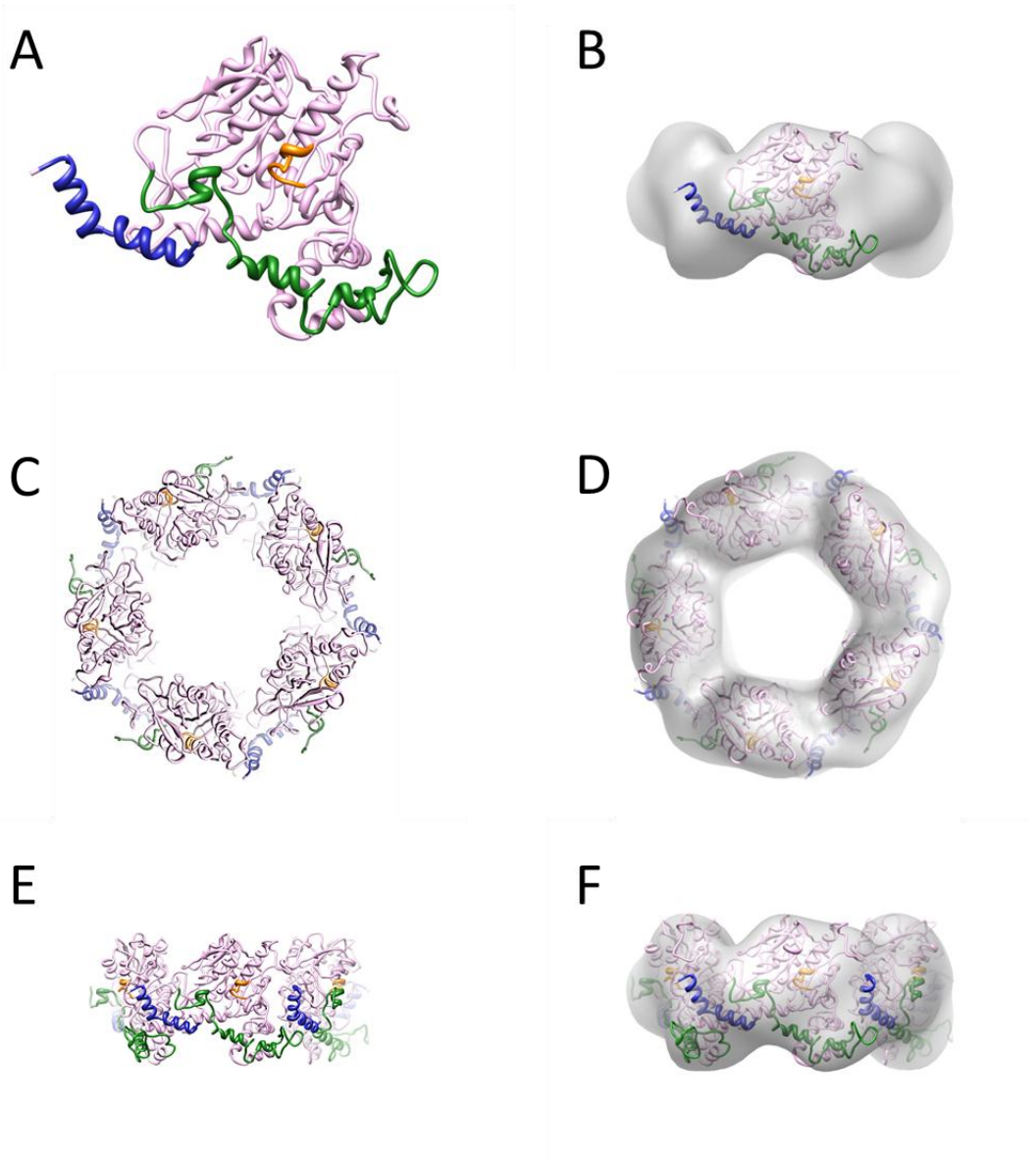

Figure 32.- Fitting of IVa2 model. (A) IVa2 remote homology model obtained with Raptor X. (B) Final fitting of the IVa2 homology model into the 3D EM map, showing only one monomer. (C) and (E) Top view (C) and side view (E) of the predicted 3Dmodel following 5-fold symmetry. (D) and (F) Top view (D) and side view (F) of the fitted 3D model into the EM map. Colour code: orange, Walker box domain (170-179); blue, DNA binding domain (440-449); green, N-terminal domain (1-78).

Several initial positions were tested and refined. The best cross-correlation value (91.3%) was obtained after hand flip of the EM map.

Although the structural data are limited, it is remarkable that the shape and size of the homology model is in excellent agreement with the boundaries imposed by the low-resolution 3DEM map. To investigate if the charge distribution in the model could indicate DNA-binding regions, coulombic surface coloring was used. This representation showed one facet clearly negative and the other mostly positive (**Figure 33**). No predominant positive charge was predicted in the central channel.

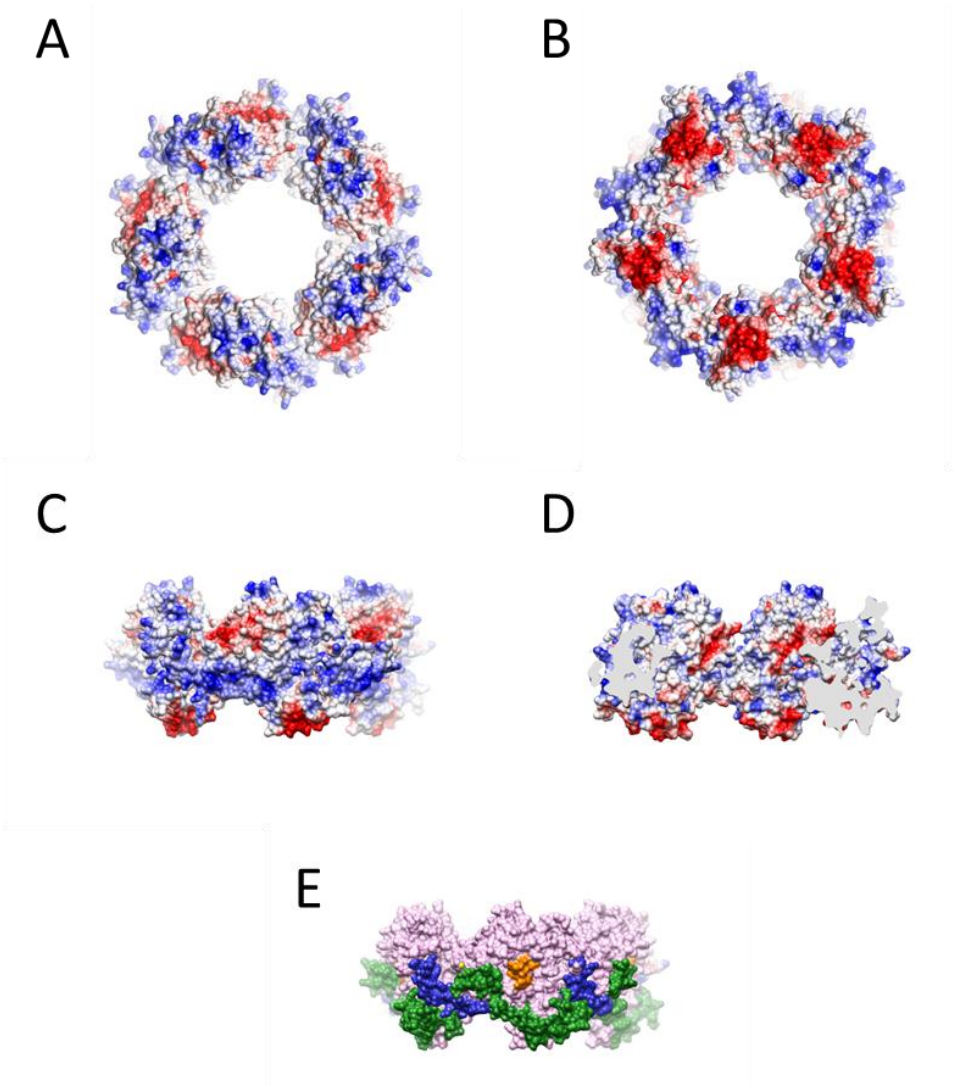

Figure 33.- Coulombic surface of IVa2 5-fold oligomer showing charged areas. (A) and (B) are opposite facets of the oligomers. (C) Side view of the oligomer and (D) is a cut of the ring showing the inner channel. (E) Shows the same surface as in (C) colored by functional motifs as in Figure 32.

4.1.2.6 Truncated IVa2

A truncated form of the IVa2 protein, lacking the first 74 aa, can function *in vivo* to produce infectious adenoviral particles (Pardo-Mateos and Young, 2004). It has been also reported to be a monomer in solution (Yang, Yang, and Maluf, 2009). Because the N-terminal region is predicted to be disordered, it seemed worthwhile to investigate the oligomerization state of this truncated version to see if heterogeneity was reduced.

Truncated IVa2 (trIVa2), was produced by our collaborators at Patrick Hearing laboratory. As the full length IVa2 (flIVa2), it was produced by infecting Sf9 cells with baculovirus containing the IVa2 sequence (75-449) and a Strep Tag II located at the C terminus, which was used to purify the protein in only one step by affinity chromatography.

Native electrophoresis and SDS-PAGE in presence of cross-linker showed the same oligomeric pattern in both flIVa2 and trIVa2 (**Figure 34**). EM of flIVa2 and trIVa2 also showed some ring-shaped particles on a heterogeneous background (**Figure 35**). This result indicates that the N-terminus of the protein is not essential for oligomerization, in agreement with the ability of the truncated protein to function in assembly. The model described in the previous sections would also agree with the dispensability of the N-terminal domain for ring formation. However, the structural heterogeneity was not reduced. All previous studies had shown both flVIa2 and trIVa2 in a monomeric state (Lutz and Kedinger, 1996; Yang, Yang, and Maluf, 2009).

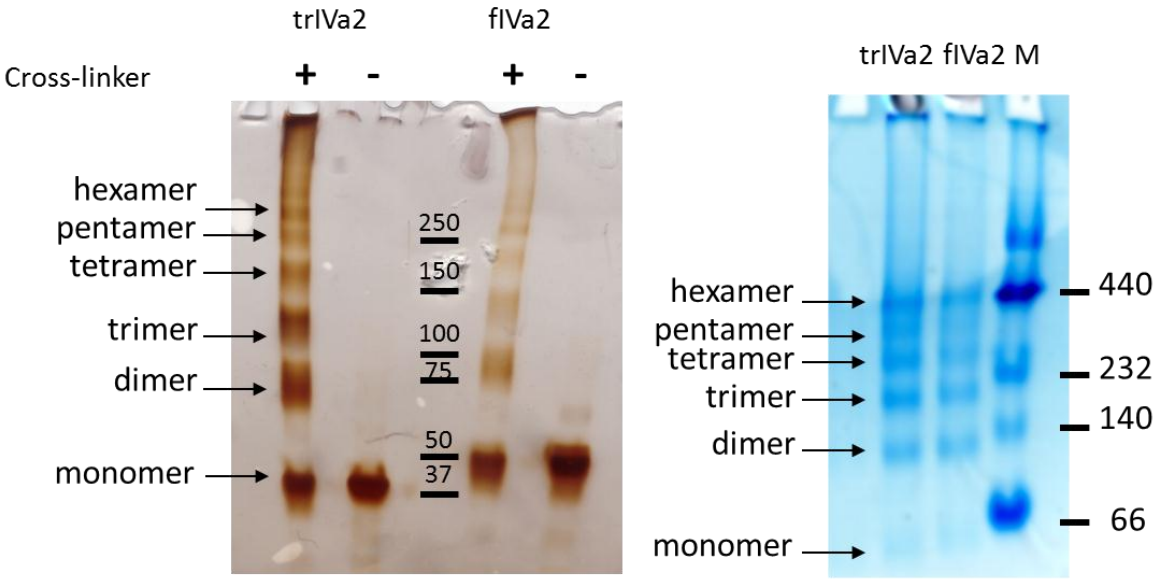

Figure 34.- Oligomerization of flIVa2 and trIVa2. (A) Silver stained SDS-PAGE in a 4-20% Tris-HCl gel shows the same band pattern in flIVa2 and trIVa2 in the presence of 0.01% glutaraldehyde. (B) 5% native-PAGE visualized with Coomassie blue G shows again the same band pattern in the full length and the short form of IVa2.

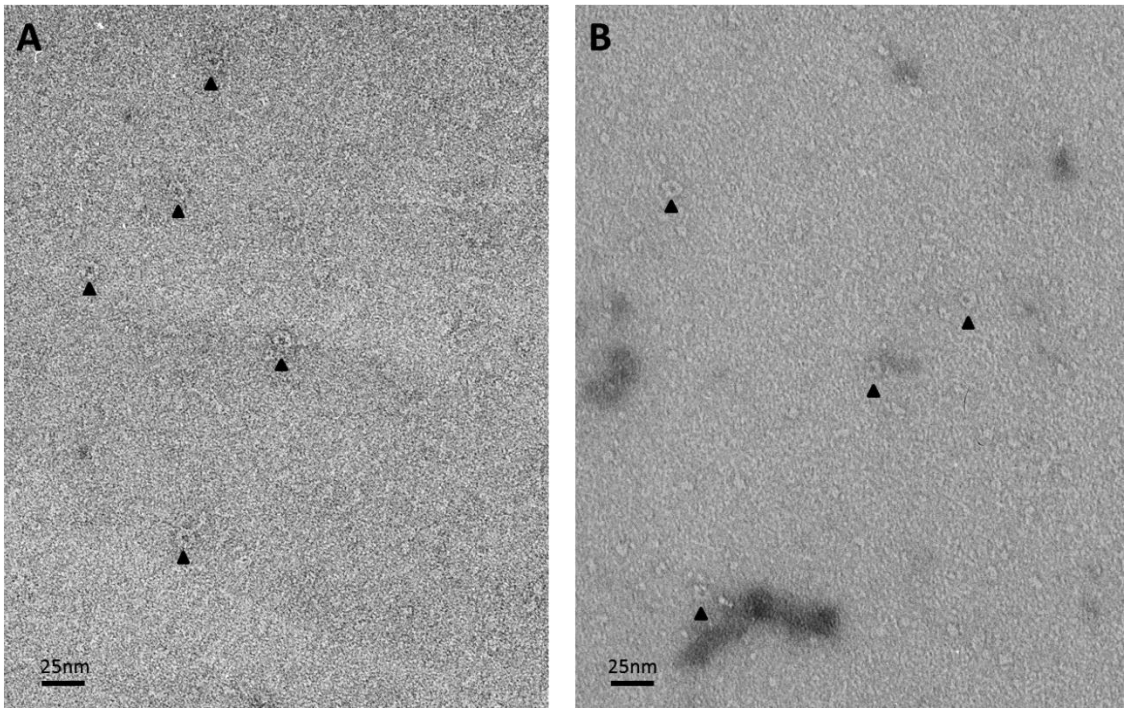

Figure 35.- flIVa2 and trIVa2 negative staining EM micrographs (A) full length IVa2 and (B) truncated IVa2 protein, supplemented with 0.01%glutaraldehyde. Ring-like oligomers are indicated with black triangles. Protein concentration was 15ng/µl in both cases.

4.2 Characterization of reptilian AdVs

4.2.1 Propagation and purification of snake and lizard adenoviruses

There is only one previously solved structure within the Atadenovirus genus, the ovine adenovirus (Pantelic et al., 2008). Structural studies on reptile adenoviruses, also encompassed within the Atadenovirus genus, may provide new structural insights due to their infecting lower vertebrates. They are also interesting due to the clinical applications that these viruses may possess (Introduction, section 1.1).

Initial seeds provided by Dr. Rachel Marschang consisted on supernatants from VH2 and IgH2 infected cells. VH2 had been infected with SnAdV-1 isolated from Boa and IgH2 infection had been made with LAdV isolated from a Mexican beaded lizard, *Heloderma horidum*.

VH2 cell line was initially used to propagate SnAdV-1 and IgH2 to propagate LAdV. In parallel, infection with SnAdV-1 was also tested in the iguana cell line, resulting in higher titers of purified virus than the purification from VH2 cell line. Because of this difference in viral titers, both, LAdV and SnAdV-1 were finally propagated in the cell line IgH2 (**Figure 36**) and purified (**Figure 37**) as described in Material and Methods, section 3.2.15.

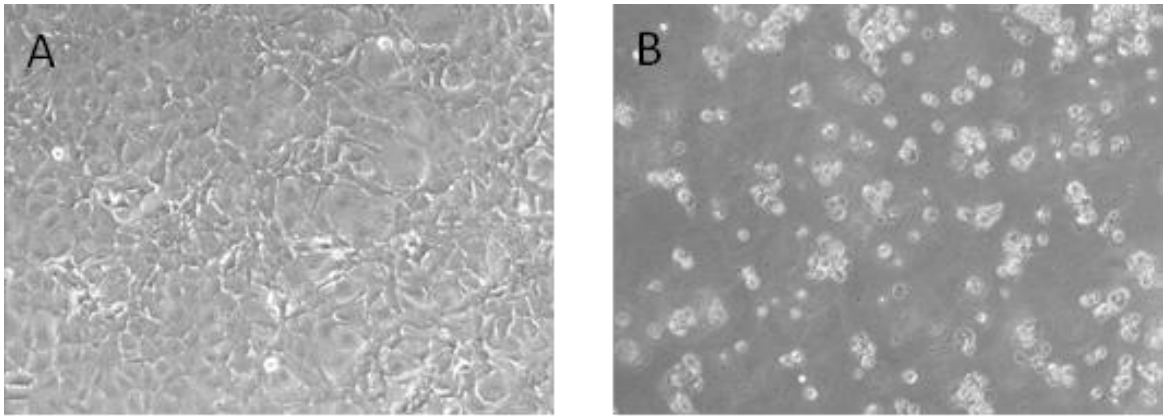

Figure 36.- IgH2 cell line (A) Before infection and (B)after infection, showing cytopathic effect (CPE).

To achieve an optimal viral concentration to carry out cryo-EM studies, the initial virus concentration of 10E+05 particles per milliliter found in the infected culture plates needed to be improved, as well as the purity of the sample. A summary of the titers obtained for each virus in different purifications can be found in **Table 2**.

Virus	Purification_1	Purification_2	Purification_3	Purification_4
SnAdV-1	2.16E+11 vp/ml	3.2E+10 vp/ml	1.2E+11 vp/ml	
LAdV	1.2E+11 vp/ml	5.0E+11 vp/ml	8.6E+11 vp/ml	1.53E+12vp/ml

Table 4.- Viral titers calculated by absorbance of the purified samples.

Therefore, this work shows that reptile AdV can be propagated and purified from cell culture in amounts similar to those of other AdV used as vectors.

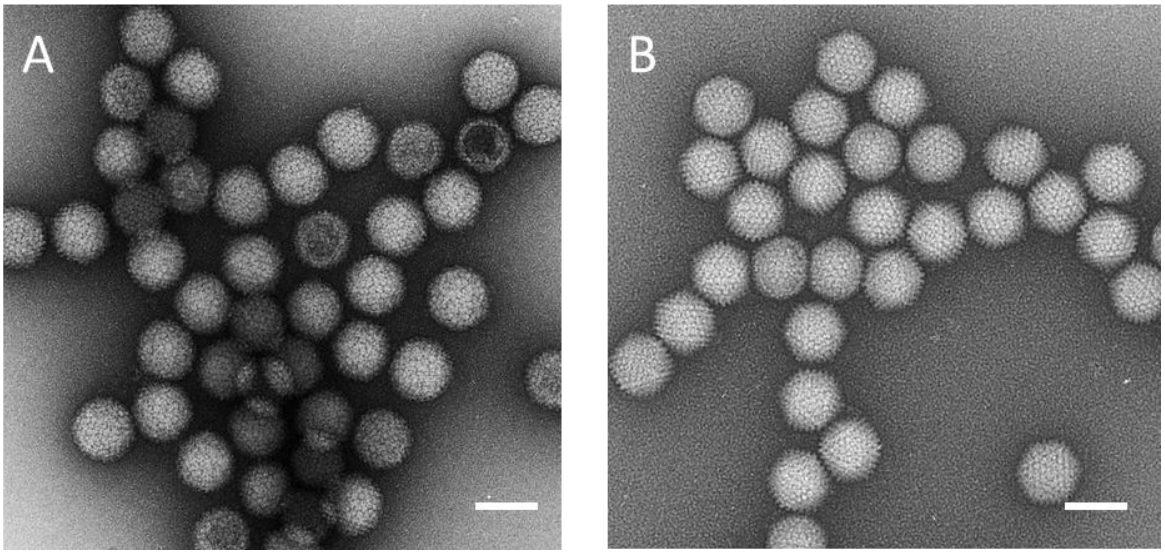

Figure 37.- Double caesium gradient purified adenovirus (A) LAdV and (B) SnAdV-1. Scale bar represents 100 nm.

4.2.2 Molecular composition of purified reptilian AdVs

The genomes of SnAdV-1 and LAdV have been fully sequenced (Farkas, Harrach, and Benko, 2008; Menéndez-Conejero, R., Penzes, J., in preparation). However, there is no experimental confirmation regarding expression and incorporation of the predicted proteins. To analyse this issue, samples of purified virus were subject to NanoHPLC-ESI-MS/MS of high resolution triple TOF as described in Materials and Methods. Tables 3 and 4 summarize the proteins identified for each virus. Proteolysis sites were predicted

with the consensus proteolysis patterns for adenoviral protease, -Yaa-Xaa-Gly-Gly-|-Xaa- and -Yaa-Xaa-Gly-Xaa-|-Gly- (in which Yaa is Met, Ile or Leu, and Xaa is any amino acid).

Protein name	Predicted immature protein MM (Kda)	Proteolysis sites	Predicted proteolyzed protein MM (Kda)	Calculated IP	No. of peptides	Coverage (%)	Mascot score	emPAI
hexon	102217		102217	5,28	425 (355)	51	11388	7,01
pIIIa	67733		67733	6,9	125 (103)	46	3816	5,05
E1B 55K	41398		41398	5,76	62 (54)	42	2474	3,30
pVI	23888	28, 213	**19381**	9,75	68 (50)	47	2174	2,71
penton	50361		50361	5,74	73 (62)	68	2039	6,13
p32K	38233		38233	11,51	83 (55)	30	1652	2,48
fiber *	43793		43793	5,74	29 (26)	28	1353	1,57
pVIII	31264	121, 203	**21870**	6,45	41 (32)	57	1341	6,52
IVa2	50722		50722	6,89	12 (11)	40	684	1,00
pVII	13450		13450	12,23	28 (15)	8	368	0,97
52K	37166		37166	5,57	12 (8)	29	321	0,82
pTP	70213		70213	8,6	8 (6)	10	280	0,38
protease	23154		23154	9,4	8 (7)	25	254	0,71
33K	20275		20275	7,85	9 (6)	41	180	1,92
LH2	15746		15746	9,1	3 (3)	22	103	0,79
100K	76802		76802	5,57	3 (2)	5	73	0,09

Table 5.- Adenoviral proteins detected in the purified SnAdV sample.

* Studies carried out by Dr. Mark J. van Raaij and Abhimanyu K. Singh (CNB-CSIC) have been determined that the snake fiber is a 35 kDa protein instead of the 44 kDa prediction from the NCBInr. Van Raaij's group has amplified and crystallized the SnAdV-1 fiber from a DNA extraction of the purified virus. They observed a much shorter fiber than expected from the data base annotation. Reanalyzing the snake AdV LC-MS/MS data with the experimental fiber sequence from van Raaij's group resulted in a complete match.

Surprisingly, non-structural proteins as 100K and LH2 were also detected.

Protein name	Predicted immature protein MM (Kda)	Proteolysis sites	Predicted proteolyzed protein MM (Kda)	Calculated IP	No. of peptides	Coverage (%)	Mascot score	emPAI
hexon	102040		102040	5,44	394 (391)	73	20915	21,80
pIIIa	66941		66941	5,89	142 (139)	62	7888	17,6
pVI	24075	29, 216	**19871**	9,73	79 (77)	83	4683	9,39
penton	50713		50713	5,75	72 (70)	69	3651	8,64
LH3	41838		41838	6,59	75 (73)	61	3439	6,22
pVIII	30750	122, 173, 204	**23602**	5,78	48 (48)	71	2796	7,64
pVII	15239	24	**12760**	12,23	47 (46)	55	1790	12,8
fiber1	34826		34826	5,15	29 (29)	44	1462	2,57
p32K	40025		40025	11,02	33 (32)	36	1345	4,29
IVa2	48186		48186	8,53	23 (22)	46	1132	1,53
protease	20478		20478	8,75	20 (20)	42	908	3,59
fiber2	45930		45930	5,55	22 (20)	40	750	1,64
52 K	37765		37765	5,56	14 (14)	27	636	1,98
pTP	69780		69780	7,71	10 (10)	15	438	0,44
pX	10080		10080	12,8	10 (10)	17	190	1,42
100K	77178		77178	6,07	3 (3)	8	125	0,13
33K	20321		20321	6,36	4 (4)	17	70	0,85

Table 5.- Adenoviral proteins detected in the purified LAdV sample.

The unpublished LAdV genome, facilitated by our collaborators in Hungary, Dr. Balázs Harrach and Dr. Mària Benkö's lab contained two different genes for fiber. Adenovirus fibers described so far are homo-oligomers, so the presence of two genes was pointing to an adenovirus with two different fibers. The MS/MS analysis revealed that both fiber gene products are expressed and incorporated into the virions.

As in the analysis of SnAdV, with this sample of LAdV non-structural proteins were also detected (100K, 33K).

4.2.3 Stability of human and reptilian adenoviruses

4.2.3.1 Thermostability

Purified viruses were subjected to heat treatment at 37ºC, 45ºC, 50ºC and 60ºC for 5 minutes and their infectivity was compared to that from purified viruses kept on ice prior to infection or to Ad5GL incubated in the same conditions (**Figure 38 and 39**). There is a remarkable difference in the infectivity levels at 45ºC between the studied Atadenovirus (LAdV and SnAdV) and the Mastadenovirus (AdV5GL). When the human adenovirus has almost lost its ability to infect after the 45ºC incubation, the reptilian viruses still conserve some of their infectivity.

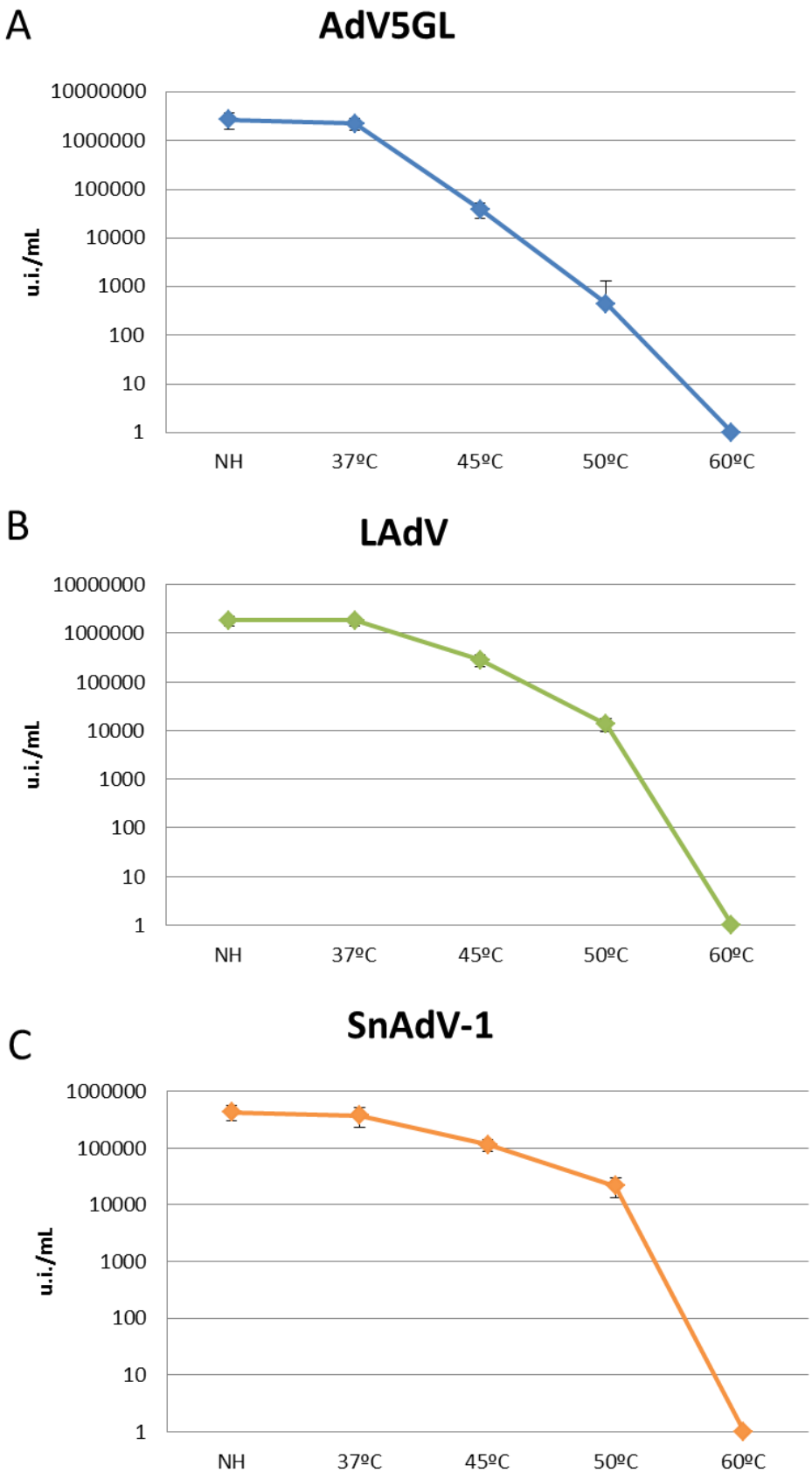

Figure 38.- Thermo-stability. Infectivity of (A) AdV5GL, (B) LAdV and (C) SnAdV-1 after heat treatment**.** NH = No Heated virus. Number of experiments = 3, number of replicates per experiment = 3.

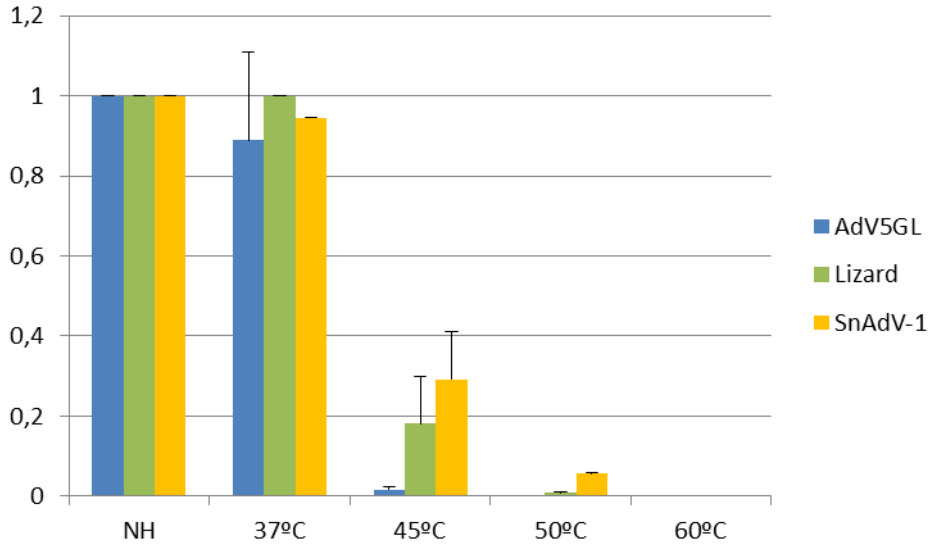

Figure 39.- Comparison of infectivity after heat treatment. Infectivity of Ad5GL, LAdV and SnAdV-1 after treatment for 5 minutes at 37, 45, 50 or 60ºC. Data in figure 39 were normalized dividing for each virus, the i.u. after heat treatment by the u.i of the control sample (NH) , therefore 1 is equal to the original infection capacity.

To relate these infectivity differences with structural changes, virus samples were visualized before and after the heat treatment by negative staining EM (**Figure 40**). In agreement with the infectivity data, human adenovirus at 45ºC presents a background of viral proteins from disassembled viruses. The same sample at 50ºC shows only disassembled viruses and an even more crowded background of isolated viral proteins. In contrast, reptilian viruses conserved the virion morphology at 50ºC and surprisingly, even at 60ºC, when infectivity titer was null, abundant capsids apparently intact were observed.

Figure 40 (next page).- EM of heated viruses. (A) Human (AdV5GL), (B) heloderma (LAdV) and (C) snake adenovirus (SnAdV-1) were subjected to the temperatures indicated on top and visualized by electron microscopy. Scale bar equal to 100 nm.

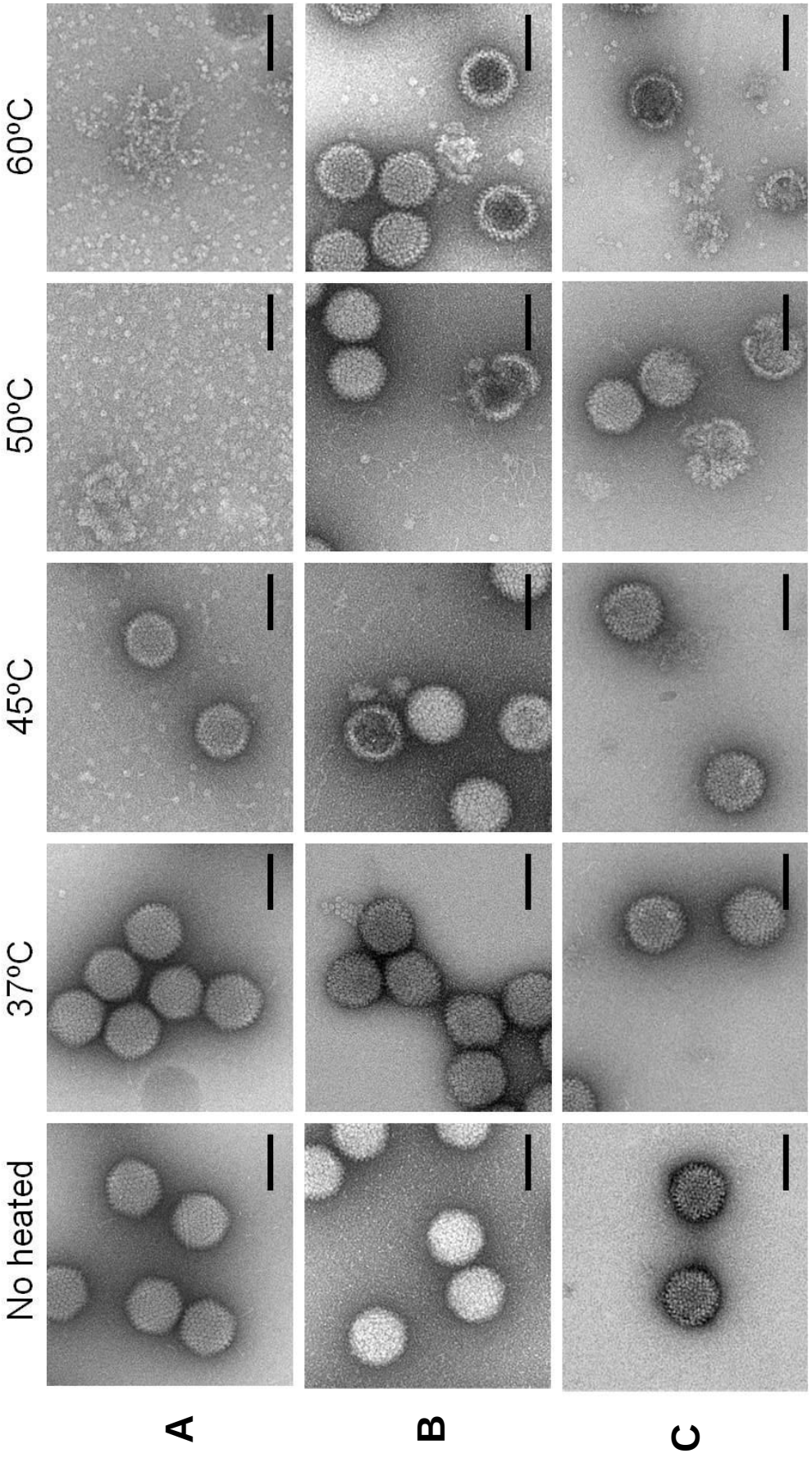
60ºC
50ºC
45ºC
37ºC
No heated
A
B
C

4.2.3.2 Controlled disassembly assays

Capsid disruption pattern in adenovirus is linked to the interactions established by structural proteins in the capsid and between capsid and core. The disrupting protocol described here was used to define the sequential disassembly pattern of human Ad (Prage et al., 1970). In this thesis it is used to investigate differences in the Atadenovirus disassembly pattern that could be originated by the differences in minor coat and core proteins (section 1.3).

Purified virus samples were subjected to a controlled disassembly protocol (Prage and Pettersson, 1971) detailed in figures 42, 43 and 44. Supernatants of each disassembly step and the last resuspended pellet, were analyzed by EM and SDS-PAGE.

4.2.3.2.1 Ad5GL

The Mastadenovirus human adenovirus Ad5GL was subjected to the sequential disassembly protocol as a control (**Figure 41**).

As expected, the first elements to be released were the viral vertices (supernatant A), with the fiber attached to the penton base and the peripentonal hexons. The second and third supernatants (B and C) contained GONs (Groups Of Nine hexons) previously described in the literature (Prage et al., 1970) and some internal proteins. The core (resuspended pellet D) appeared as an amorphous mass of DNA and protein.

4.2.3.2.2 SnAdV

SnAdV-1 (**Figure 42**) did not follow the same rupture pattern observed for Ad5GL. GONs were not detected.

The core stability is another remarkable difference between Ata- and Mastadenovirus. In the case of the Ad5GL, we can only visualize an amorphous mass of DNA and protein while in Atadenovirus the core conserves a rounded shape.

4.2.3.2.3 LAdV

As in SnAdV, LAdV differs from the human adenovirus in the absence of GONs and a compact core structure after disassembly. A feature of particular interest in LAdV is the structure of the vertex.

Figure 43 summarizes the results from LAdV disassembling. Protein assignment was made following different criteria:

*	Hexon, penton, fiber2, fiber1, VI	SDS-PAGE bands from supernatant (A) were excised and analyzed by MALDI-TOF-TOF.
†	p32K, VII	Both protein bands were assigned attending to the MW and the expected abundance. VII has the highest copy number within the adenoviral proteins and p32k is he major protein in the range where falls its MW. VII is the kind of protein that is difficult to detect by MALTI-TOF-TOF: it is a small protein containing an abundance of tryptic cleavage sites (Expasy Peptide Cutter shows 33 sites); consequently, the majority of tryptic peptides expected from protein VII have such low masses that they overlap with ions produced from the matrix during MALDI-TOF-TOF analysis.
‡	LH3	It has been previously reported that LH3 holds the outer capsid of the virus together in OAdV (Pantelic et al., 2008). Comparison of EM and SDS-PAGE from supernatant (B)and (C) shows how big pieces of capsid correlate with a band-pattern presenting the assumed LH3 protein and how in a band-pattern lacking this LH3, the capsid appears disaggregated into individual hexons.
•	pIIIa	This band was assigned by the expected MW.

There are two bands bellow 10 kDa, which might correspond to the non-assigned proteins pX and pVIII. pX, as protein VII, presents the limitation of small size and high number of tryptic peptides, hindering the protein detection by mass-spectroscopy. On the other hand, pVIII has an expected MW of 23602 Da, which do not fit with the extra-band present in the virus before disassembling treatment and the resuspended pellet.

SDS-PAGE of supernatant (A), containing the viral vertices showed the two gene products assigned as fibers. In the same lane of the SDS-PAGE, the rest of the bands were detected by MALDI-TOF-TOF as penton base, hexon and protein VI. Surprisingly, the EM of the sample showed viral vertexes with three fibers, instead the two expected. This finding will be described in section 4.2.4.

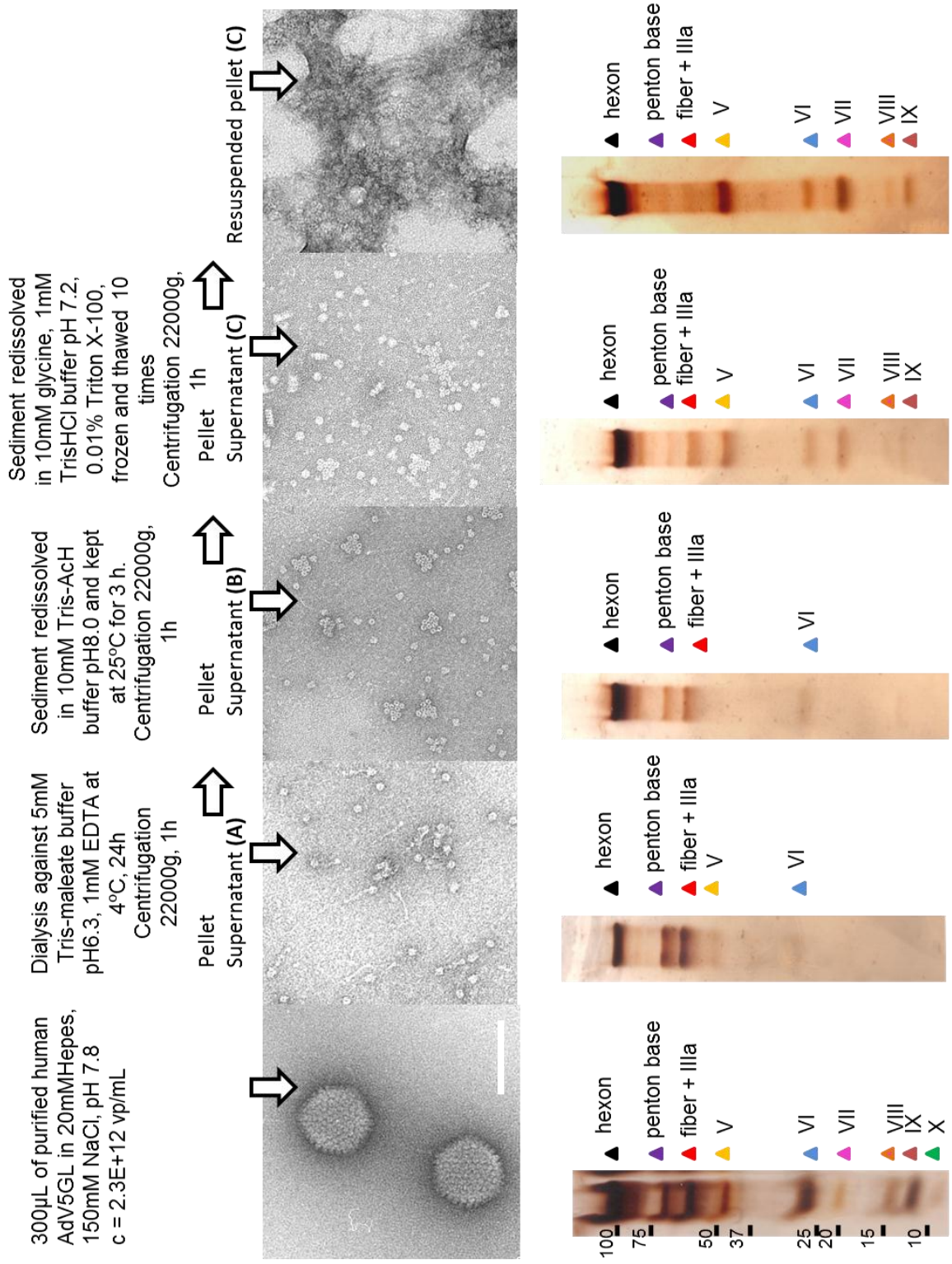

Figure 41.- Sequential disassembly of human adenovirus. Purified Ad5GL was sequentially disassembled and each step of the process was analyzed by EM and SDS-PAGE. Scale bar represents 100 nm.

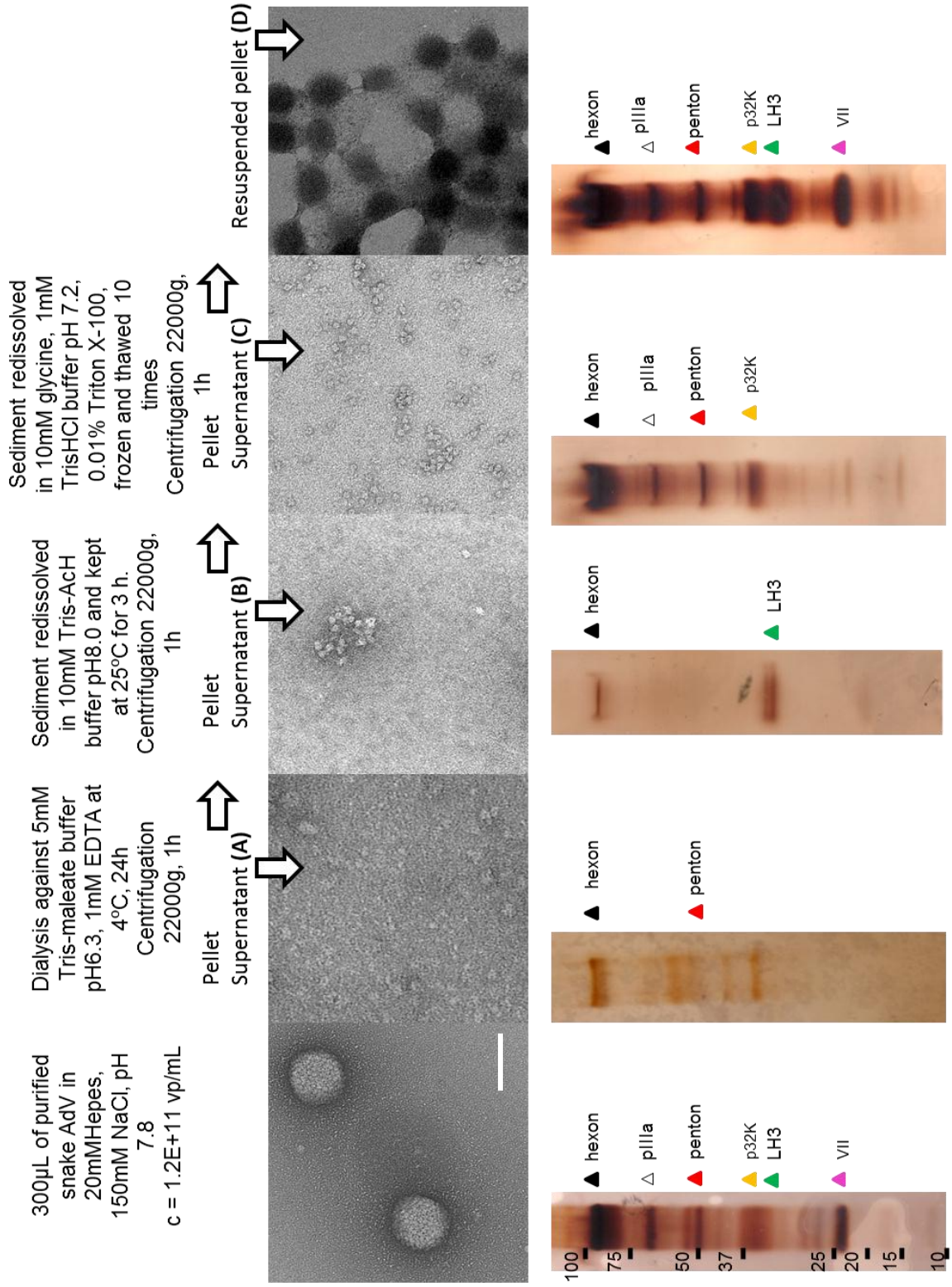

Figure 42 .- Sequential disassembly of SnAdV-1. Purified SnAdV-1 was sequentially disassembled and each step of the process was analyzed by EM and SDS-PAGE. Scale bar represents 100 nm.

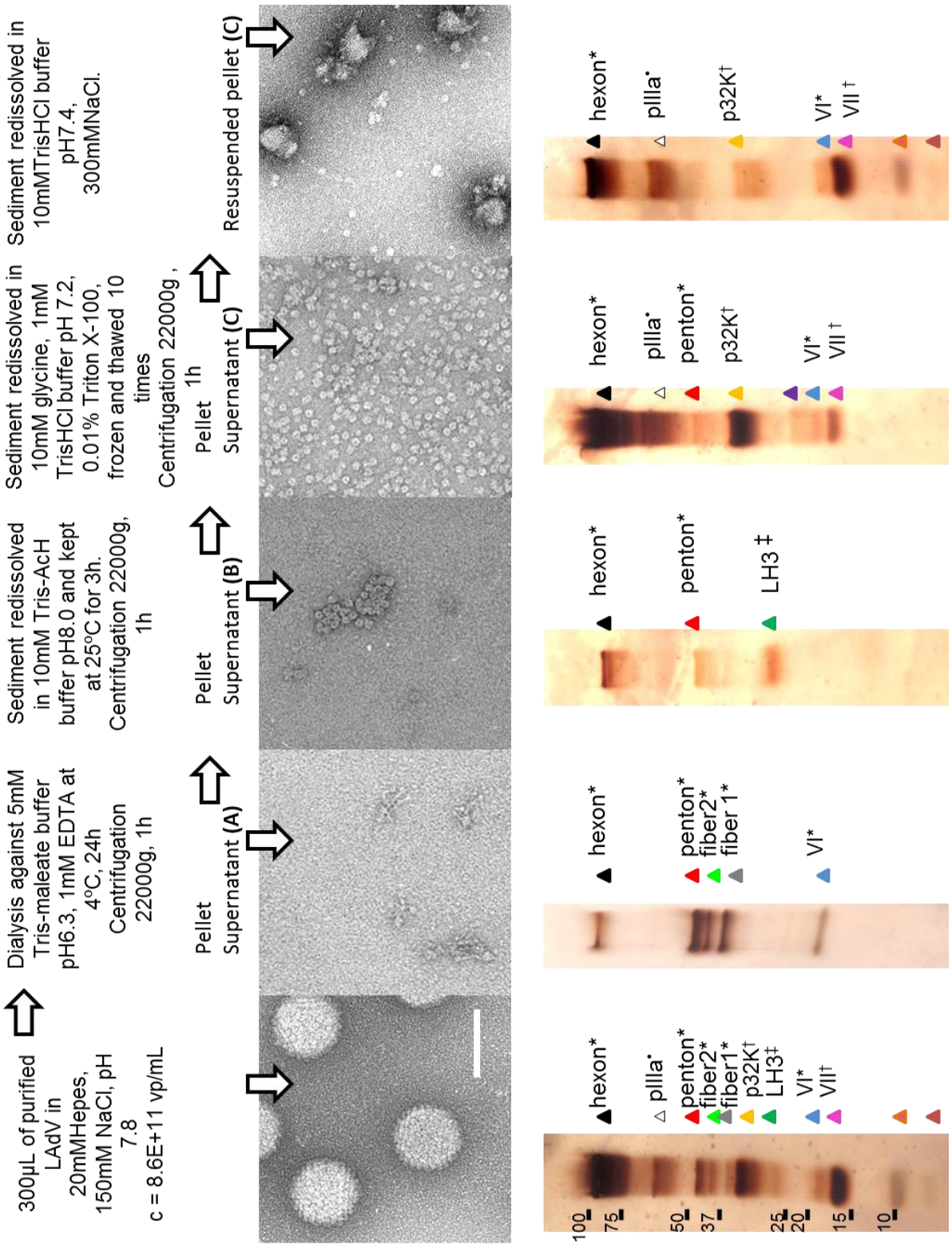

Figure 43 .- Disassembled LAdV. Purified LAdV was sequentially disassembled and each step of the process was analyzed by EM and SDS-PAGE. Scale bar represents 100 nm.

4.2.4 EM of LAdV vertex enriched sample.

From the disassembly protocol described in section 4.2.3.2.3, the vertex-enriched supernatant was visualized by EM to analyze the conformation adopted by the two different fiber proteins (**Figure 45**). Surprisingly, most of the vertex complexes observed showed three fibers, instead the two expected. There is no previous reference of any adenovirus with three fibers per penton, that even more surprisingly originate from only two different genes.

Interestingly, fibers without any associated penton base were also detected (**Figure 44**). These images of three fibers bound together without presence of penton base, suggest a structural arrangement in which fibers interact with each other by their N-terminal tails.

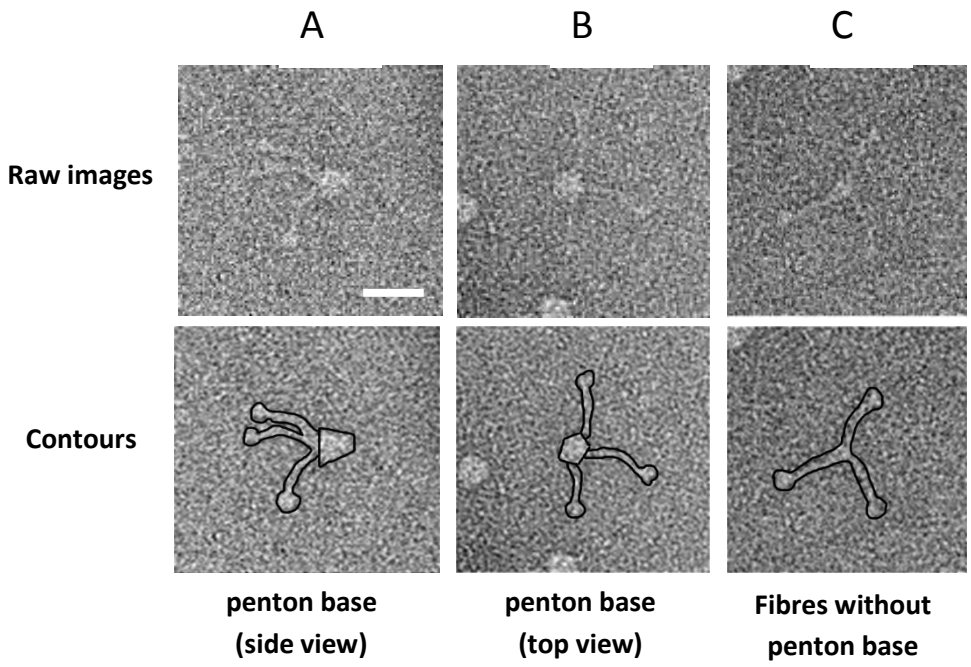

Figure 44.- LAdV pentons and fibers (I) Three LAdV fibers can be found attached to the penton base (A,B) as well as alone (C). Scale bar represents 20nm.

Quantification of the different kinds of complexes observed indicated that most of the fibers were attached in a group of three to the penton base (85%). Only in 10% of the fibers were attached to the penton base as a group of two. All the fibers without

penton base attached (5% of the total complexes) were bound together in groups of three.

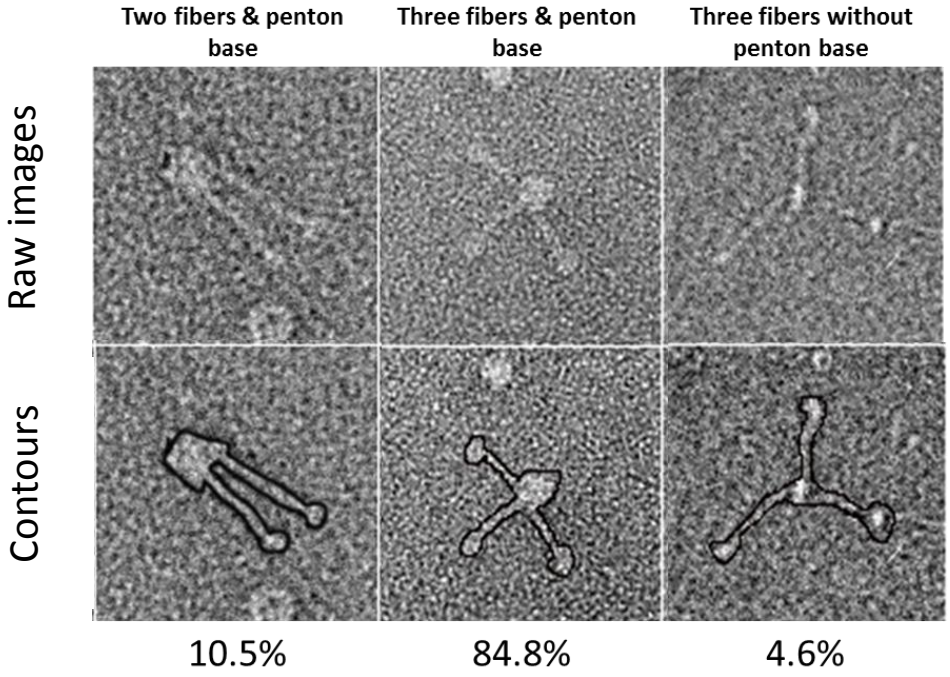

Figure 45.- LAdV penton and fibers (II) Representative images of LAdV vertex complexes and frequencies of appearance in the sample. Total number of counted images: 455

4.2.5 Three dimensional structure of SnAdV-1

4.2.5.1 Calculation of the SnAdV-1 3D map from cryoEM images

A 3D map of SnAdV-1 was generated from an initial set of 3990 images of purified virions, extracted from 111 micrographs. 3990 particles were included in the final density map, which had a resolution of 12.5 Å and 15Å according to the FSC 0.3 and 0.5 criterion, respectively (**Figure 46**).

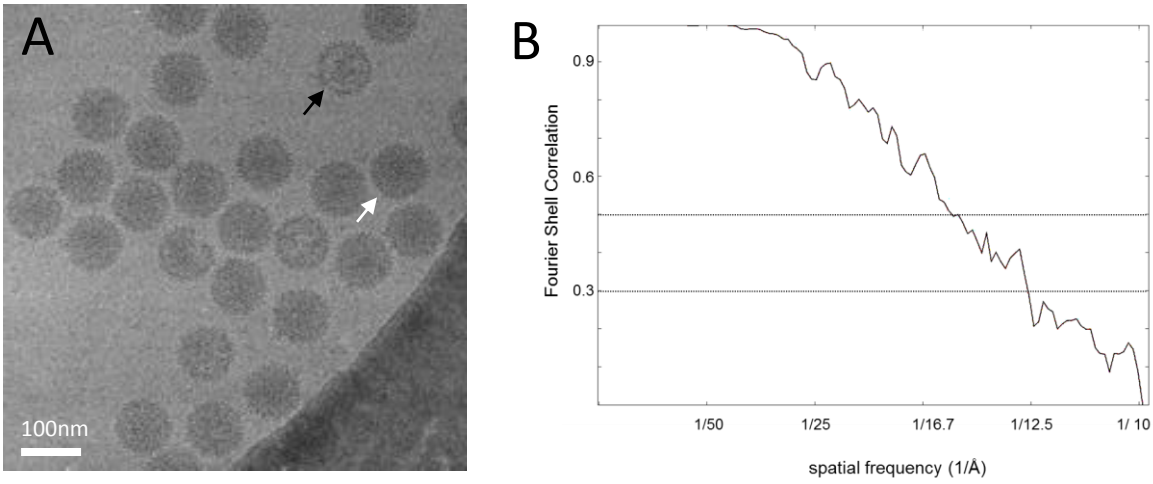

Figure 46.- CryoEM of SnAdV-1. (A) Field showing intact (white arrow) and empty particles (black arrow). (B) Fourier Shell Correlation curve for the 3D map of SnAdV-1.

SnAdV-1 is an icosahedral virus similar in size (around 940 Å of diameter), triangulation number (pseudo T=25) (**Figure 47-A**) and fiber composition (one fiber per vertex) than the human adenovirus.

Comparing the structures of the reconstructed volume of SnAdV-1 and the volume from human adenovirus (Ad5GL), clear differences can be observed at the resolution achieved. Central sections of the volume showed extra masses in SnAdV-1 located in the all internal hexon cavities and beneath the viral capsid, extending into the interior of the particle (**Figure 47-B and 47-C**). The outside of the capsid presents very distinct surface protrusions (**Figure 47**). Two of these extra densities were assigned to Atadenovirus-specific proteins in the only previous structural study of *Atadenoviruses* (OAdV) (Pantelic et al., 2008). The knobs were assigned to the protein LH3 and the internal density to the p32K.

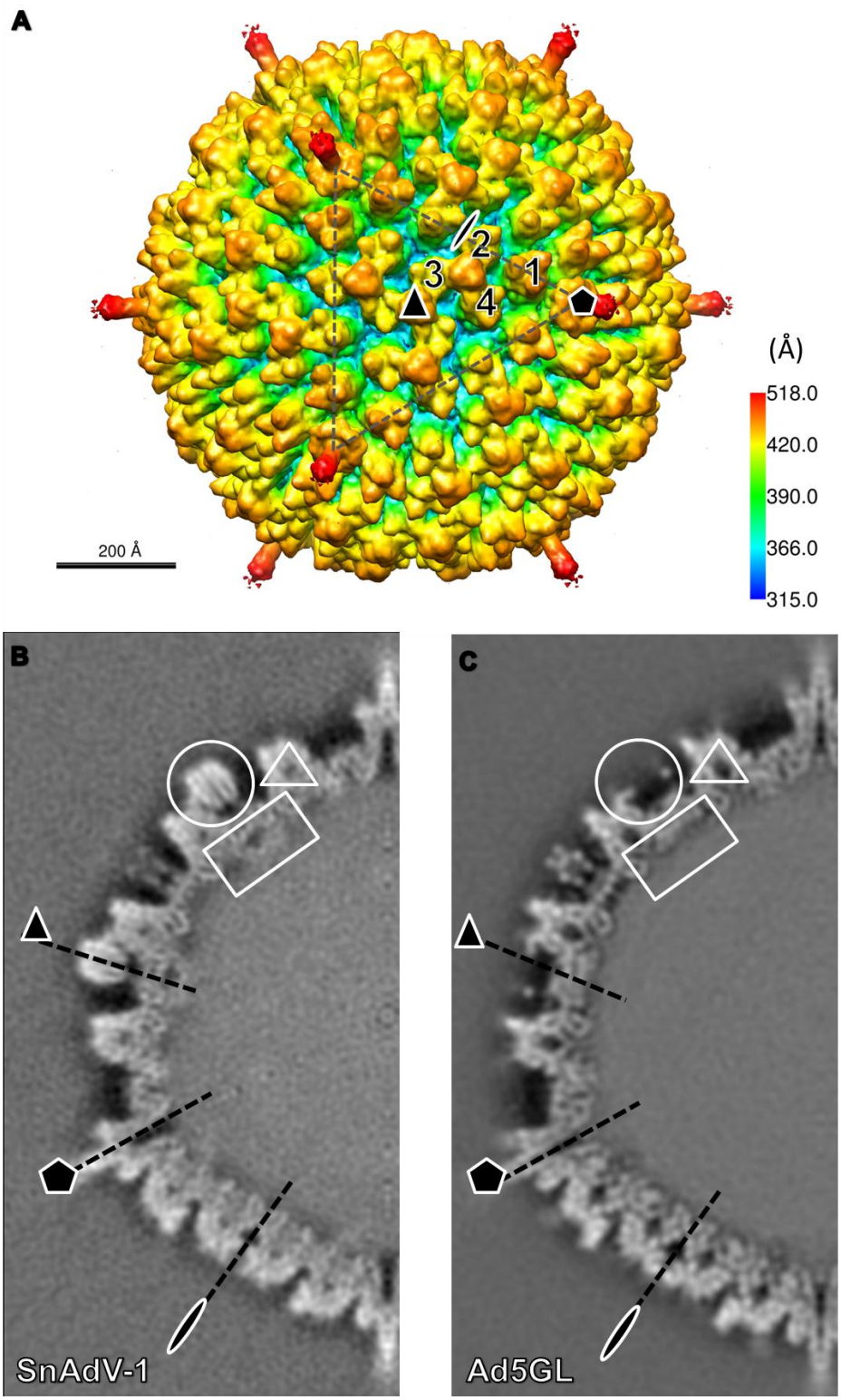

Figure 47.- Comparison of the three-dimensional EM maps from SnAdV-1 and human Ad5GL. (A) Surface rendering of the SnAdV-1 capsid colored by radius as seen along the three fold axis. The triangle represents a facet of the icosahedron, the black shapes indicate the symmetry axes (pentagon for the 5-fold axis oval for the 2-fold axis and triangle for the 3-fold axis). The four independent hexon trimers are labeled 1-4. Hexon 1 and its symmetry mates form the peripentonal ring, and hexon trimers 2-4 form the GON. (B and C) Details of central sections of the (B) SnAdV-1 and (C) Ad5GL maps. Higher density is shown in white. White circles, rectangles and triangles highlight the major differences between SnAdV-1 and Ad5GL.

4.2.5.2 Homology modelingog SnAdV-1hexon and penton

The absence of crystal structures to fit into the 3DEM reconstruction was overcome by homology modeling of the major proteins of the capsid, hexon and penton base. By superposition of both models (**figure 48**) on their corresponding Ad5 templates, it was observed that SnAdV-1 proteins presented shorter loops in the region of the molecules that lies on the exterior of the virion, in particular in the region occupied by the RGD loop in Ad5 pdb and some loops containing hypervariable regions in hexon. In human adenovirus, this region is involved in the tropism and the uptake of the virus by interaction with cell receptors. This kind of differences in the part of the capsid exposed to the host environments for the snake and the human AdV can be originated from the different molecular interactions that both virus need to develop to complete their propagation cycle.

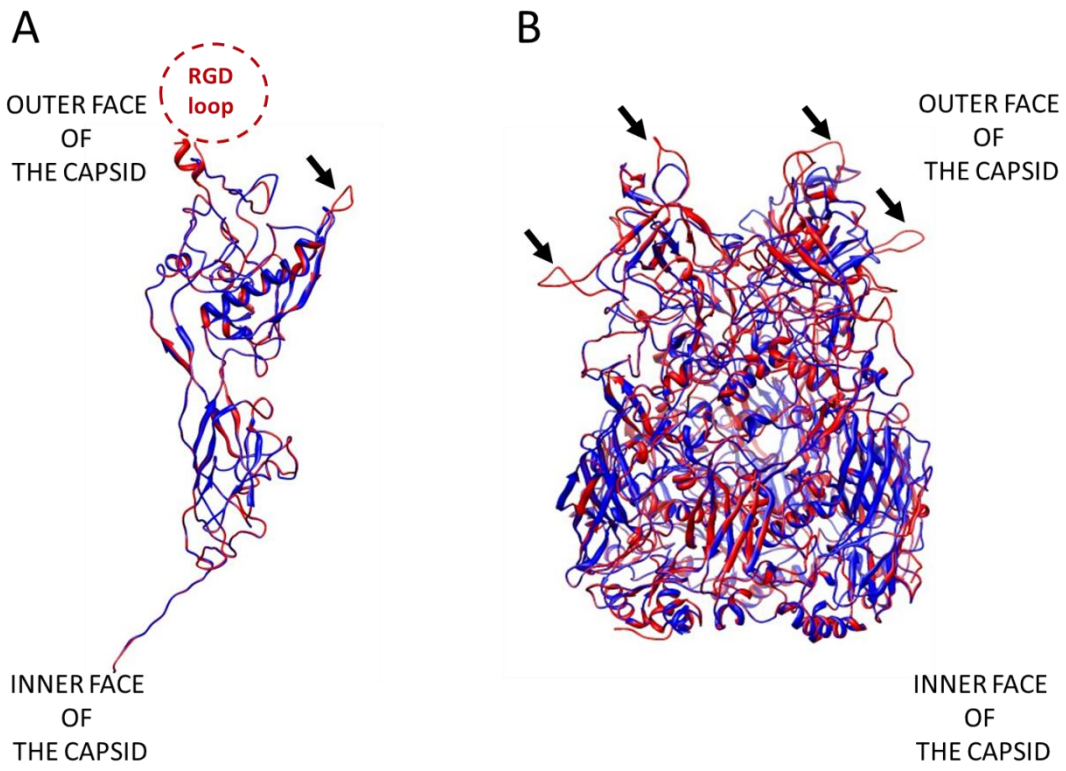

Figure 48.- Superposition of Ad5 hexon and penton atomic structures to their respective homology models for SnAdV-1. (A) Side view of penton base monomer. (B) Side view of hexon trimer. Red color corresponds to human adenovirus Ad5 and blue color is for SnAdV-1. Black arrows signal different sized loops.

The hexon and penton homology models were fitted into the SnAdV-1 3Dmap to generate a pseudo-atomic model of the capsid that could be then subtracted from the map to reveal the minor coat proteins.

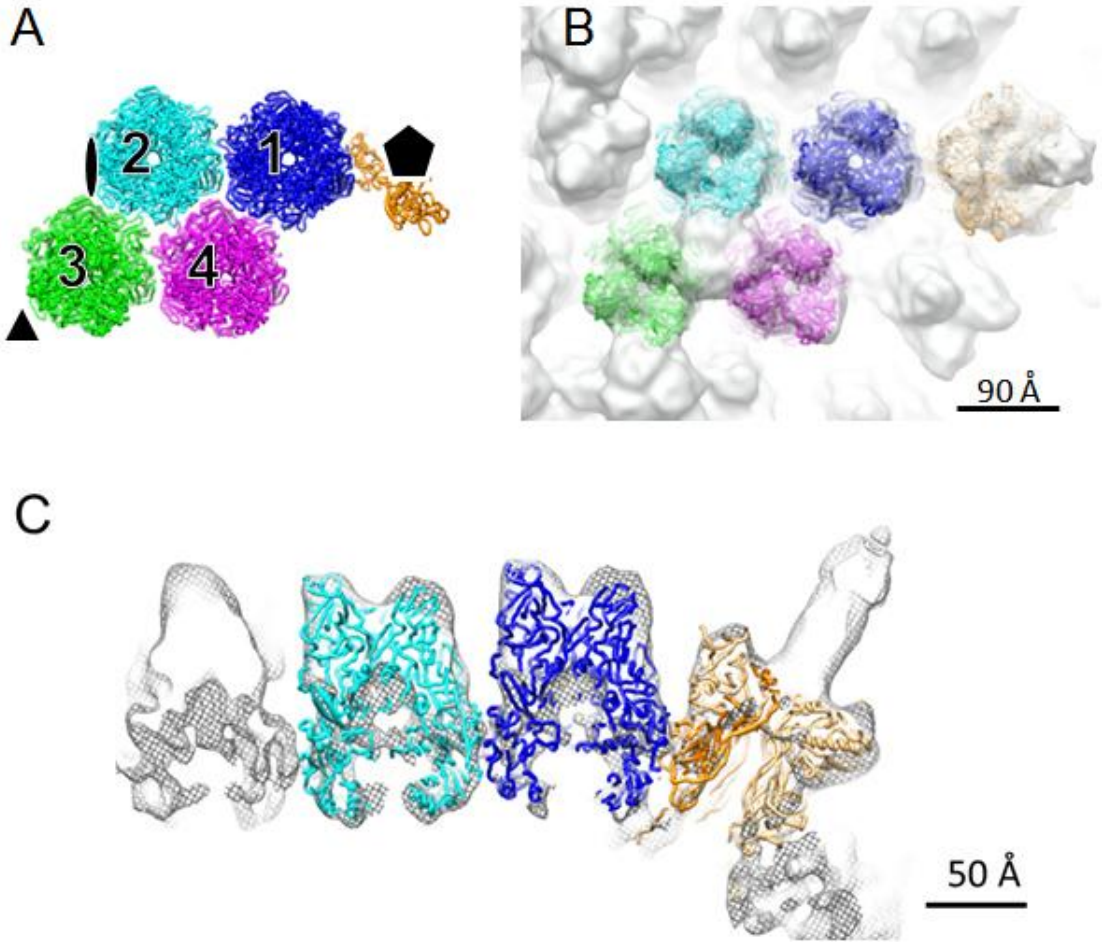

Figure 49.- Fitting of the hexon and penton models into the 3D map of SnAdV-1. (A) Ribbon representation showing the SnAdV-1 AU model. The four hexon trimers have been labeled as in Figure 48-A and are depicted in different colors to facilitate interpretation. One penton base monomer is shown in orange. Black filled symbols indicate the 5-fold (pentagon), 3-fold (triangle) and the 2-fold (oval) icosahedral symmetry axes. (B) Detail of the 3DEM map showing the good correspondence between the cryo-EM density (semitransparent surface) and the docked AU. In this case the penton base pentamer is shown. (C) Side view of the fitting. The EM map is rendered at 1σ level.

4.2.5.3 Difference mapping

The difference map between the SnAdV-1 cryo-EM map and the map obtained from homology models of hexon and penton base proteins lead to the observation of additional densities originated by other capsid components, mainly minor capsid proteins (**Figure 50**).

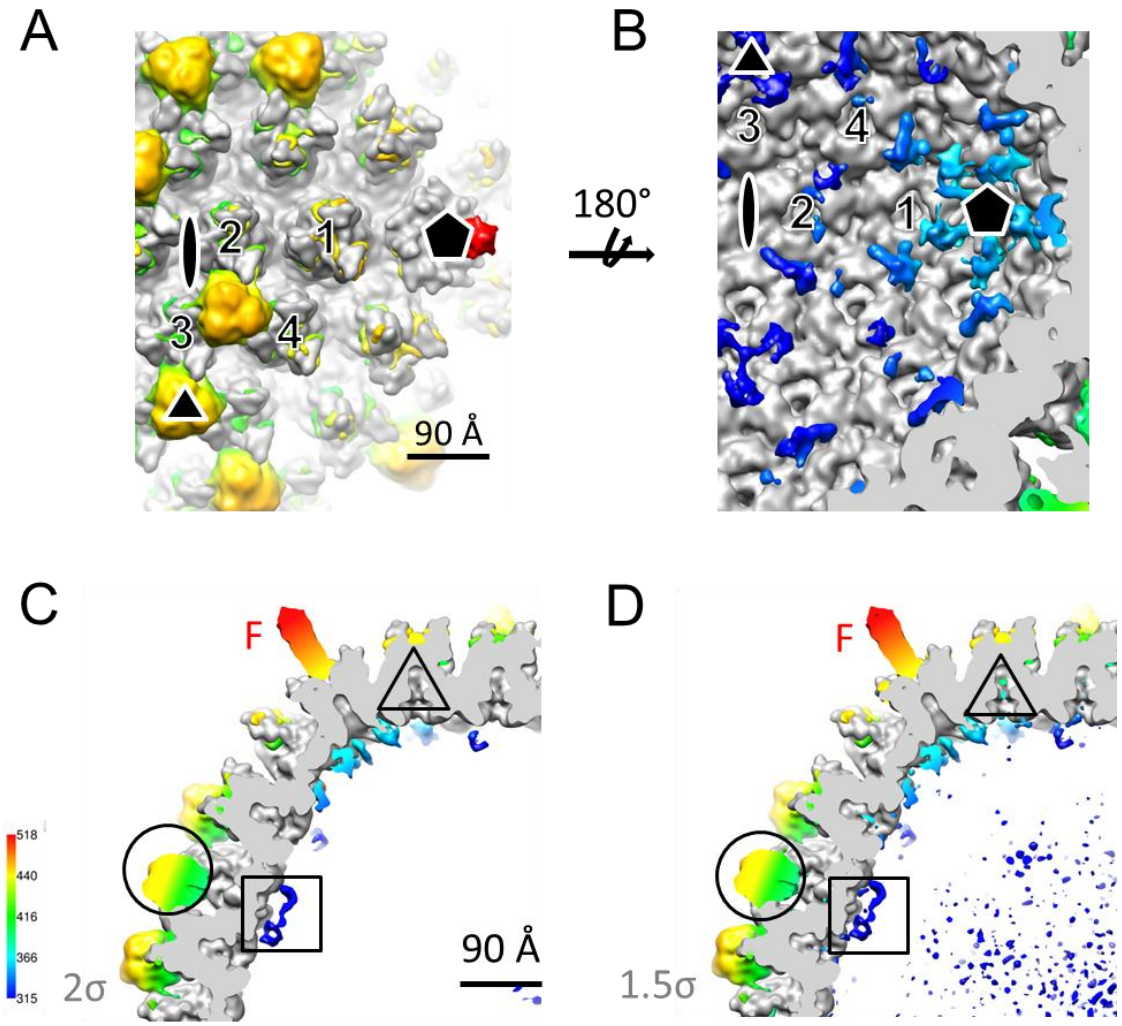

Figure 50.- Difference mapping of SnAdV-1. (A) Two fold view of the outside of the capsid. (B)Two fold view of the inside of the capsid. (C&D) A section across the capsid. The density map calculated from the pseudo- atomic model is in gray. The difference map is shown radially colored according to the scale shown at the left (in Å). The difference map is rendered at 2σ level except in panel D (1.5σ.) The circle, square and triangle highlight the main differences observed between SnAdV-1 and ad5 as in Figure 48. The icosahedral symmetry axes are indicated as in Figure 50. "F" indicates the reconstructed fiber segment.

Some of the extra-volumes observed in SnAdV-1 are absent in the human adenovirus Ad5GL. The major differences are outlined in figure 50-C and D.

Differences on the outer capsid surface

On the outside of the capsid (**Figure 50-A**) the most noticeable differences corresponded to the "knobs" (circle in Figure 50-C) and a first segment of the fiber (F); additionally, there are small differences in the top of the hexons. These differences may

indicate a conformation of the flexible hexon loops different from that given by the homology model.

In *Mastadenoviruses*, the N-terminal domain of minor protein IX is located at the icosahedral 3-fold symmetry axes, stabilizing groups of nine hexons (GONs). IX is absent in *Atadenoviruses* and replaced by LH3 protein, which has been assigned to the outer knobs (Pantelic et al., 2008). The knobs have 3-fold symmetry, suggesting protein trimerization, and interact with the hexon towers, in contrast with protein IX, whose monomers interact at a more basal position between the hexons.

Observation of the knob density at the 3DEM resolution was reminiscent of fold based on beta-sheet elements. Secondary structure prediction of the SnAdV-1 LH3 sequence (JalView, http://www.jalview.org/) (**Figure 51**) indicated a large predominance of beta-sheet secondary structure elements.

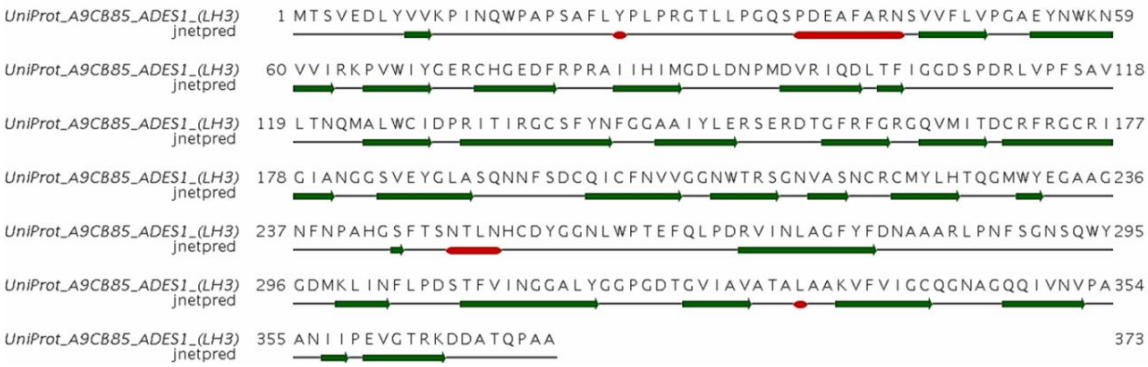

Figure 51.- Secondary structure prediction of SnAdV-1 LH3 protein.

The LH3 sequence was submitted to the RaptorX server for remote homology modeling. Interestingly, the best two candidates for modeling templates fold as left handed beta-helices. These templates are: inulin fructotransferase (PDB ID=2INU) (Jung et al., 2007) and the preneck appendage protein of bacteriophage phi 29 (PDB ID=3GQ7) (Xiang et al., 2009) (**Figure 52**). Both form trimers, have a common function related to the oligosaccarides hydrolysis and, most interestingly, the phi 29 protein is involved in host attachment. The β-helix fold is common in bacteriophage spike-tails, appearing also in phage P22 (REF). Evaluation of the LH3 sequence by the BetaWrap server (Bradley et al., 2001), specialized in predicting β-helix score (-18.59), close to that

given for phage tailspike proteins (-21.24 for P22 tailspike, -20.37 for phi29 appeandage).

Three copies of the remote homology LH3 model fit nicely into the EM-density for the SnAdV-1 3 fold knobs and reproduce the observed cavities parallel to the knob 3 fold axis (**Figures 53 and 54**).

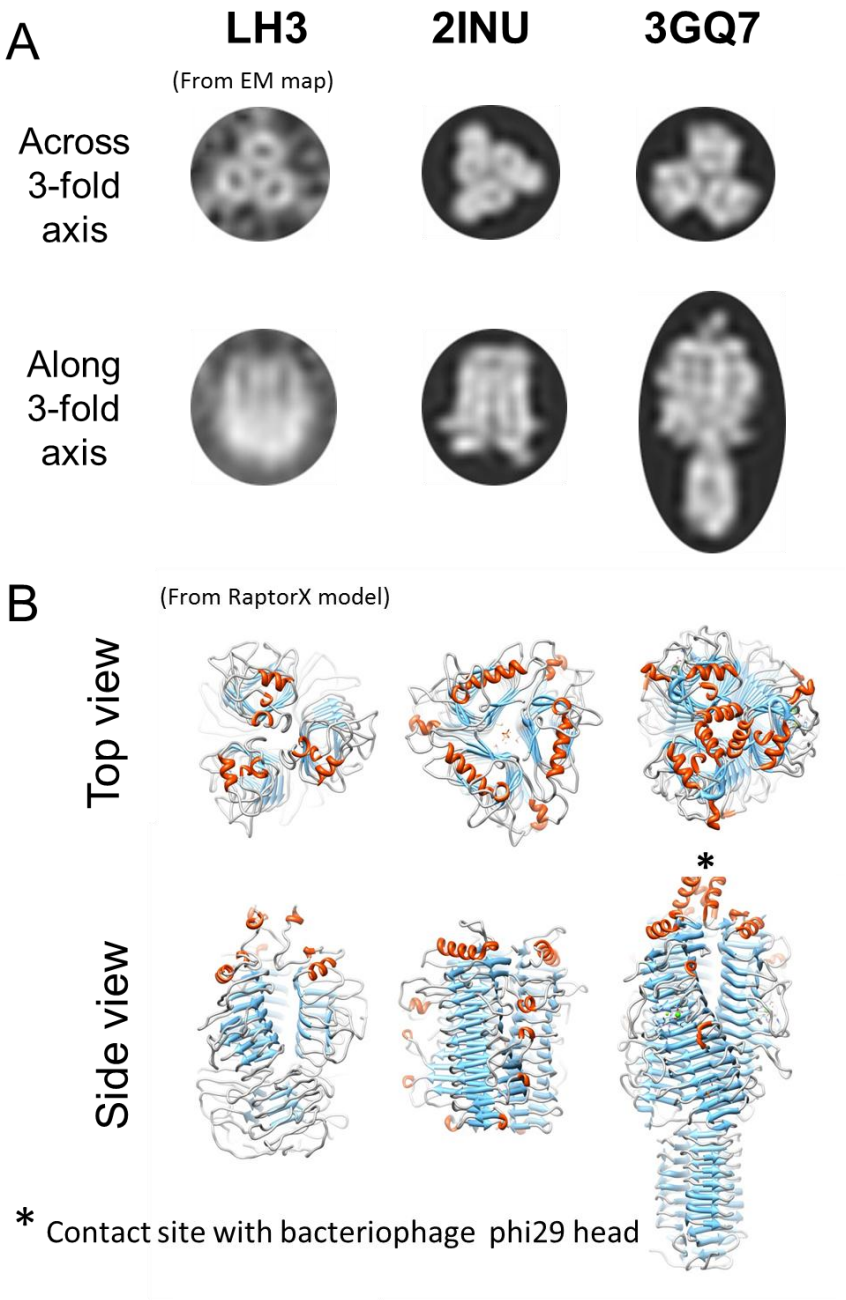

Figure 52.- Comparison of LH3 knobs, inulin fructotransferase and preneck appendage protein of bacteriophage phi 29 structures. (A) Sections of density maps rendered at 12.5 Å resolution. Top row: sections across the trimeric 3 fold axis. Bottom: sections parallel to the 3-fold axis. (B) Top and side views of the atomic structure models of the three proteins. Density maps for 2INU and 3GQ7 were generated at the same pixel size and resolution than the SnAdV-1 EM map for comparison.

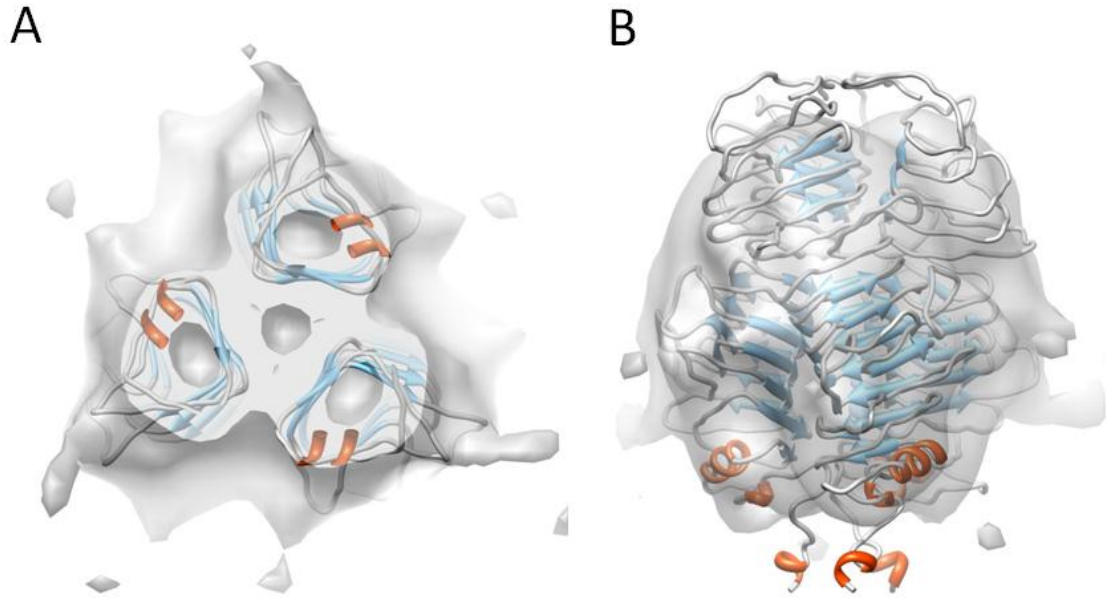

Figure 53.- Docking the remote homology model of LH3 into the EM density of one SnAdV-1 knob. (A) Cutout across the icosahedral 3-fold axis. (B) Side view.

These results suggest that the LH3 may be involved in host attachment in *Atadenovirus,* using a strategy involving host cell surface saccharides similar to that of bacteriophages.

Differences on the inner capsid surface

To interpret densities for internal minor coat proteins, the atomic structures of human AdV polypeptides IIIa and VIII were fitted into the SnAdV-1 difference-map. In the vertex region, at a threshold of 2σ (**Figure 54)**, it was observed that only the body domain of protein VIII fitted into the density present at the locations for this protein in the peripentonal ring, while the IIIa protein had a good fitting only for the N-terminal domain (GOS glue). Several unassigned extra densities appear in the 3DEM map.

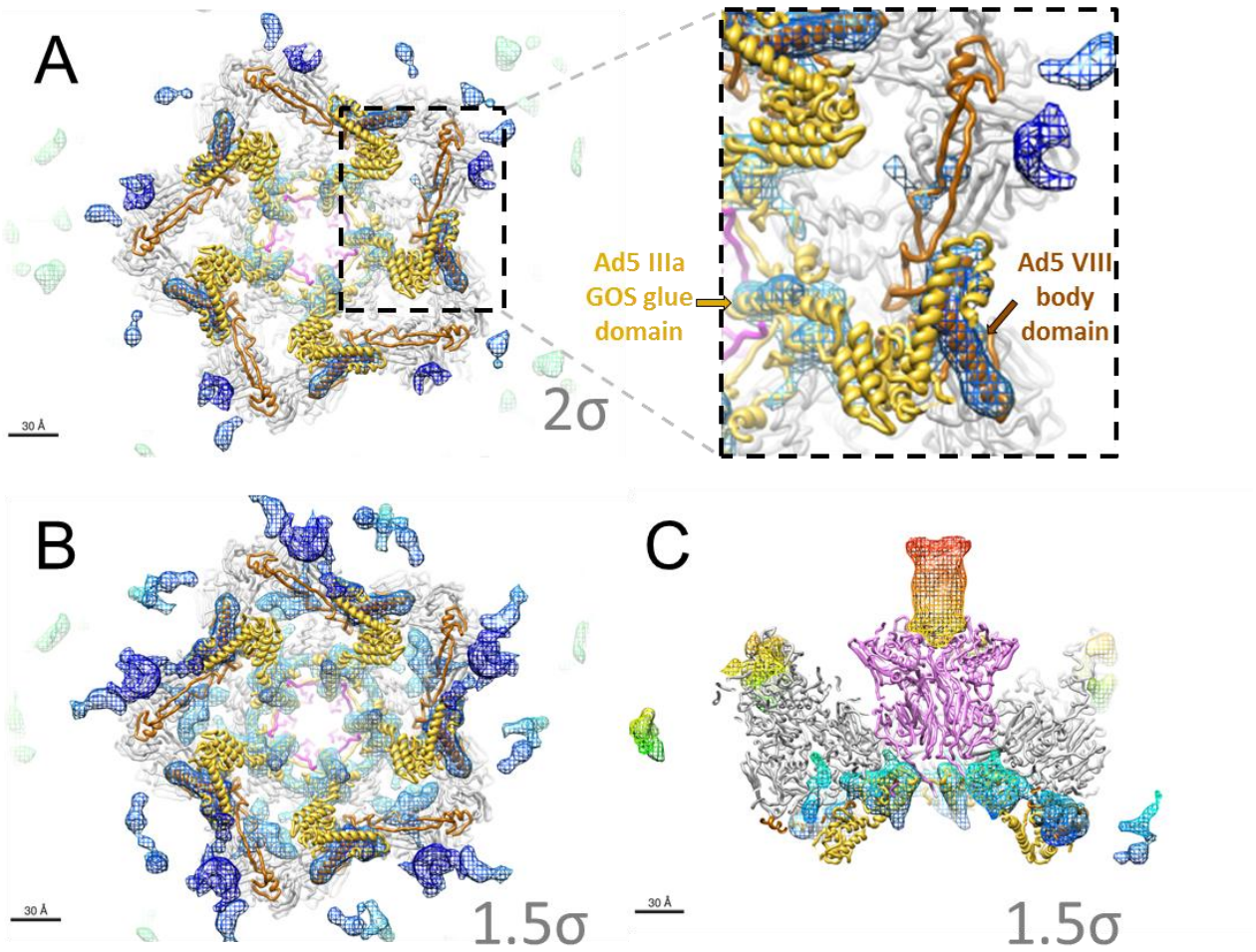

Figure 54.- Difference map at the 5-fold region of the SnAdV-1 EM map. The EM difference map is shown at a threshold of 2 σ (A) and 1.5 σ (B and C). Atomic models of human AdV protein VIII (brown) and IIIa (yellow) are docked into the volume with Chimera. Penton base is colored in purple and peripentonal hexons are represented in grey. The difference map is colored by radius as in figure 51. (C) Shows a transversal cut across the penton.

In the region close to the 3-fold axis of symmetry (**Figure 56**, black asterisk), it is again observed how only the body domain of Ad5 VIII protein fits into the corresponding density in the SnAdV-1 difference map. Lowering the contour level of the difference map to 1.5 σ did not result in density for the rest of VIII or IIIa either. This indicates that in SnAdV-1 polypeptides VIII and IIIa are less ordered than in human Ad5.

At the center of the icosahedral facet, a large triskelion-like density, which is absent in Ad5, appears. In the OAdV reconstruction, this density was assigned to the p32K

protein (Pantelic et al., 2008). Protein p32K is predicted to have a majoritarian secondary structure in α-helix (**Figure 55**).

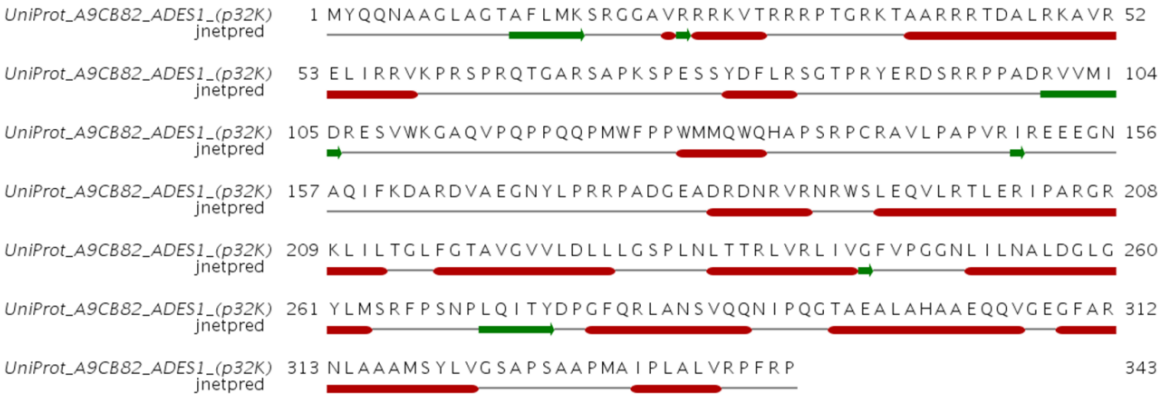

Figure 55.- Secondary structure prediction of SnAdV-1 p32k protein.

When the sequence of p32K was submitted to the RaptorX server, the model obtained was too large to fit in a single arm of the triskelion, even when contoured at 1.5 σ. In **figure 56**, a single helix of the p32K model (residues 200 to 235) is fitted into each arm of the triskelion-like feature. This indicates that either most of p32k is disordered or it is not forming a trimer as suggested by the density shape and its location at the icosahedral 3-fold.

When decreasing the difference map threshold to 1.5 σ, new densities appeared at the 3-fold local axes (in the center of the AU) (**Figure 56-B**, white asterisk). These features do not appear in the human adenovirus.

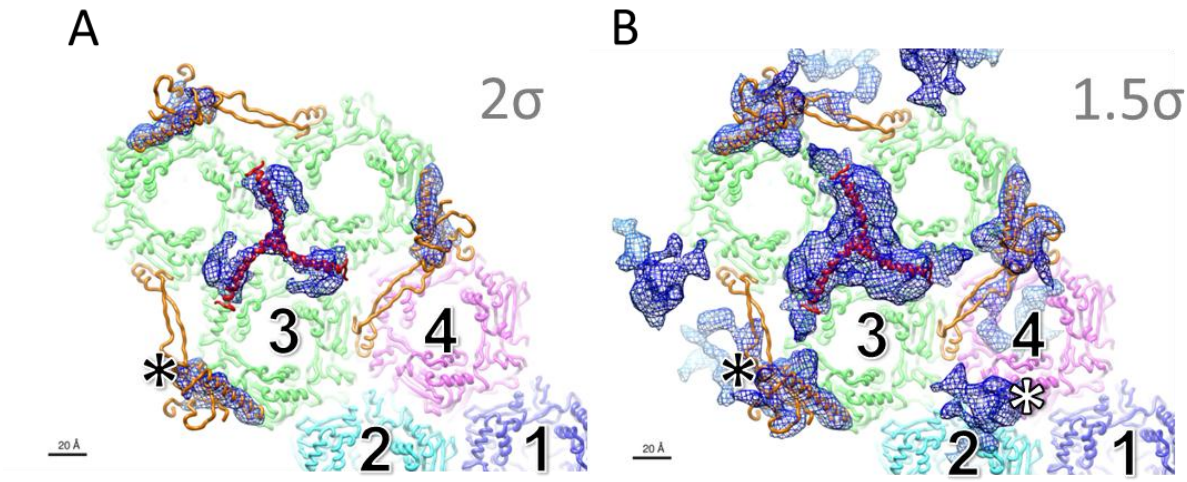

Figure 56.- Difference map at the 3-fold region.. EM volumes are shown at a threshold of 2 σ (A) and 1.5 σ. (B) Atomic models of protein VIII (brown) and a segment of protein p32K (red helix) are docked into the volume with Chimera. Hexons in the AU are numbered from 1 to 4. Black asterisks are for body domain of Ad5 VIII and white asterisk is for the unassigned extra density at the three-fold local axes.

Interestingly, these densities continue towards the hexon internal cavity (**Figure 57**).

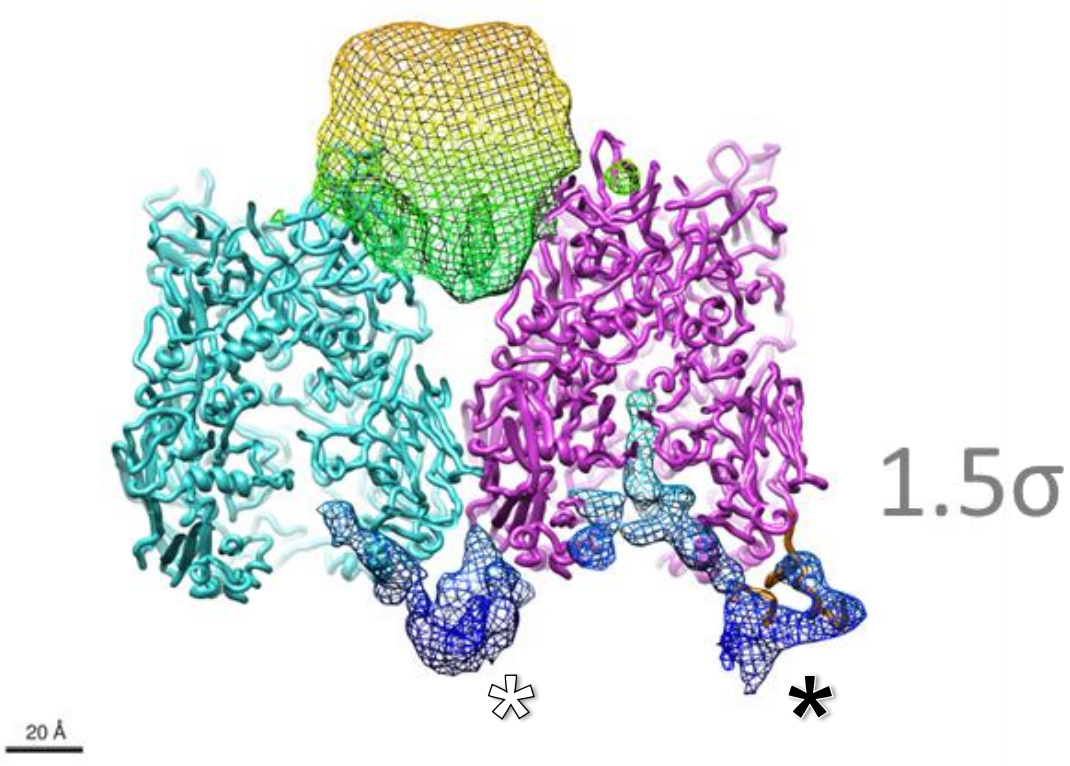

Figure 57.- Side view of the difference map at a threshold of 1.5σ. Violet color corresponds to the hexon 1 of the AU and cyan color corresponds to the hexon 2.

Similarly, at the 1.5σ threshold the density for polypeptide VIII body domain connects to density regions that do not occupy the location of VIII in human AdV, but instead enter the hexon cavities (black asterisks in Figures 56 and 57). In human AdV, densities in the inner cavity of the hexon trimer have been assigned to polypeptide VI (Liu et al., 2010). These densities are very weak, almost at noise level in the mature virion, but appear stronger in the human AdV immature particle (Perez-Berna et al., 2009). Therefore, the extra densities observed in SnAdV-1 connecting the hexon cavity to the inner capsid surface may correspond to polypeptide VI, indicating a more ordered conformation for this protein in *Atadenoviruses* than in *Mastadenoviruses*.

Discussion

5 Discussion

5.1 IVa2: oligomeric state, location and implications for viral DNA packaging

IVa2 has been suggested to be the motor protein for DNA packaging in adenovirus. This putative role is supported by the existence of ATPase conserved motifs in the sequence and the ATP binding activity of the protein (Ostapchuk and Hearing, 2008), the requirement of IVa2 for DNA packaging (Ostapchuk, Almond, and Hearing, 2011), its low copy number (6.3 ± 1.5) (Christensen et al., 2008) and its specific recognition of the packaging sequence (Zhang and Imperiale, 2000).

If IVa2 was conforming a packaging motor machine similar to those found in bacteriophage, an oligomeric ring-like form of this protein would be expected at a single vertex of the capsid. (Morais et al., 2008; Sun et al., 2008).

There are two previously published works addressing oligomerization of IVa2. The first one showed that a IVa2 protein dimer binds specifically to an intragenic ML promoter sequence (Lutz and Kedinger, 1996) and that in the absence of DNA, IVa2 is detected as a monomeric form. This monomeric form was detected by combined EMSA and glycerol gradient experiments. IVa2 protein purified to homogeneity from Ad5-infected HeLa cells was used to perform the experiments. The protein was loaded on glycerol gradients and the fractions were analyzed by EMSA with a 48 bp labeled probe. DNA migration was detected only for fractions corresponding to the monomeric form of IVa2, indicating that all the IVa2 protein was present as monomer in solution. Oligomerization of IVa2 cannot be ruled out under the conditions used in (Luzt and Kedinger, 1996), since direct observation of the distribution of the protein along the glycerol gradient was not performed. The second analysis about the oligomerization state of IVa2 was made with a recombinant N-terminally truncated IVa2 (Yang, Yang, and Maluf, 2009). This truncated form of IVa2 had previously been shown to function *in vivo* to produce infectious adenoviral particles (Pardo-Mateos and Young, 2004). The monomeric form in solution of this trIVa2 was established by sedimentation velocity assays. Two relevant differences with the material used in this thesis are that in (Pardo-Mateos and Young, 2004) the recombinant protein was produced in *E.coli*, therefore

lacking putative post-translational modifications, and purified by denaturation-renaturation, which could affect proper folding.

In this thesis, an oligomeric form of IVa2 protein *in vitro* has been reported for the first time. The evidence supporting oligomerization includes protein-protein interaction by FWB, migration patterns in native electrophoresis or crosslinking followed by denaturing electrophoresis, and visualization of ring-like structures by EM. A truncated IVa2 protein has been reported to be a monomer in solution by Yang and co-workers (Yang, Yang, and Maluf, 2009). A IVa2 protein carrying the same truncation has been used in this thesis. trIVa2 showed the same oligomeric pattern than full length IVa2 in electrophoresis experiments and similar ring-like particles when observed by EM. Could oligomerization be dependent on concentration? In (Pardo-Mateos and Young, 2004), at concentrations up to 6.7 μM, only monomers were detected. Here, protein concentrations from 10 μM (for electrophoresis) down to 1 μM (for EM) have all given data consistent with a range of oligomeric species up to a 6 mer. Therefore, protein concentration does not seem to be the main factor. The recombinant IVa2 protein used in this thesis has been produced in insect cells (Sf9 cell line) and purified in one step by affinity chromatography by adding a Strep-tag to the C-terminus of the sequence (both in the full and the truncated forms) and in addition to the *in vivo* function by production of infectious adenoviral particles, the ATP binding activity was detected by our collaborators (Ostapchuk and Hearing, 2008), suggesting that the purified protein is properly folded. It must be noted, however, that a well defined oligomer could not be produced, and that a clear IVa2 oligomeric form was not detected in virion disruption products (Section 4.1.1.4). This implies that oligomerization may be only achieved in the context of the intact capsid, or that it is transient and only required for a part of the IVa2 roles during assembly. One additional possibility is that the Strep tag has properties mimicking those of other capsid components helping in IVa2 oligomerization. This phenomenon has previously been observed in other viral systems (Saugar et al., 2005).

In bacteriophages of the order *Caudovirales*, the packaging motor proteins (named terminases) are generally located on the outside of the particle, bound to the capsid in a transient manner. After DNA packaging, this structure disassembles from the virion. In

contrast, adenoviral IVa2 protein is detected both in the empty and the full capsids (Gustin and Imperiale, 1998; Winter and D'Halluin, 1991).

Previously, localization of IVa2 was reported at a single vertex of the icosahedron (Christensen et al., 2008) based on immunoEM experiments. The evidence reported in this thesis is consistent with the location of IVa2 protein close to the viral vertex, in a position not accessible from the outside of the capsid. This result indicates another difference with Caudovirales packaging motors.

Other dsDNA viruses not belonging to the Caudovirales may have packaging machines that are not exposed to the outside of the capsid. Cryo-EM tomography studies have indicated that Herpes simplex virus (HSV) capsids have a single vertex occupied by a portal that is situated just inside the capsid shell, beneath one of the pentameric vertices (Rochat et al., 2011) (**Figure 58-A)**. *Paramecium bursaria Chlorella* virus-1 (PBCV-1) also presents a specialized vertex with a large protruding spike. Inside this vertex, a five-fold feature that may correspond to a portal structure located at the inside of the capsid has been described (Cherrier et al., 2009; Yamada, Onimatsu, and Van Etten, 2006) (**Figure 58-B**). Interestingly, PBCV-1 belongs to the same structural lineage of AdV, including dsDNA viruses with major coat proteins based on the double jelly-roll fold perpendicular to the capsid surface (Benson et al., 2004)

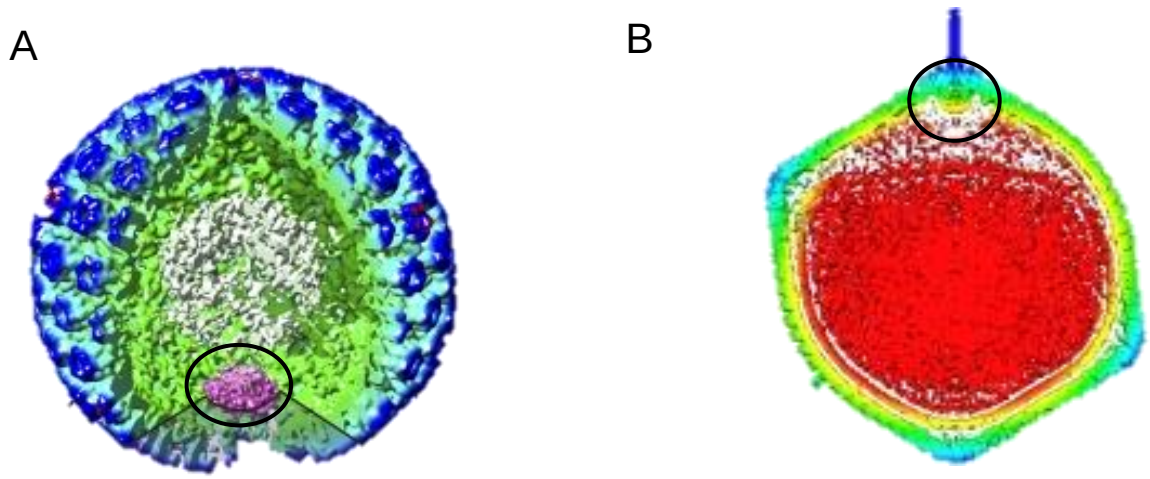

Figure 58.- Internal viral portal structures. Portal structures are circled in the (A) cryo-electron tomography map of the HSV-1 B capsid without symmetry enforcement (Rochat et al., 2011) and (B) the 5-fold-averaged cryoEM structure of PBCV-1 viewed down a quasi-2-fold axis (radially colored central cross-section). (Cherrier et al., 2009; Yamada, Onimatsu, and Van Etten, 2006)

How could the AdV packaging motor work? A unique feature of adenovirus is that the histone-like protein VII, is bound to the viral DNA before it is packaged (Brown and Weber, 1980; Chatterjee, Vayda, and Flint, 1986a; Chatterjee, Yang, and Flint, 1986; Dery et al., 1985; Weber and Philipson, 1984). This DNA-protein complex forms a filament thicker in the immature than in the mature virion, due to the proteolytic process suffered by pVII during maturation (Perez-Berna et al., 2009). The diameter of the channel in the 3DEM map of IVa2 is large enough to allow passage of naked dsDNA or of the mature DNA-protein complex, but it is not large enough to allow passage of the viral genome in complex with the immature core proteins (**Figure 59**).

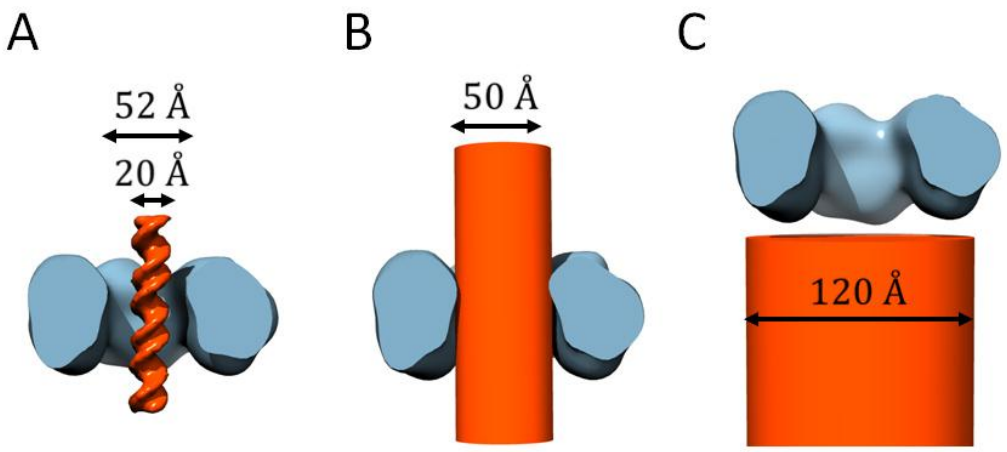

Figure 59.- Dimensions of IVa2 channel and dsDNA naked and in complex with AdV core proteins . IVa2 channel size compared to (A) naked DNA, (B) mature virus DNA-core protein complex and (C) immature virus DNA-core protein complex(Perez-Berna et al., 2009).

Facing the lack of structural studies on any part of IVa2 and hence, the absence of models to contrast the 3DEM reconstruction presented in this thesis, docking of a remote homology model for IVa2 was used. The fitting showed a remarkable agreement between the model and the five-fold symmetric 3DEM map.

Although this model is tentative, due to the limitations of the structural analogous, it is worthwhile to consider its possible implications as a start point for future experimental work.

The model would predict that the DNA binding motif of IVa2 is not in the channel but in the outer region of the ring. A combined mechanism of DNA capture and DNA

translocation might explain this putative location of the DNA binding domain. In some bacteriophage, two different ring-like structures (minor and major terminase) are in charge of the DNA capture (minor terminase, holding the DNA binding motif at the outside of the ring) and DNA capsid intake aided by ATP hydrolysis (major terminase) (Zhao et al., 2010). If the prediction for DNA binding motif in the outside of IVa2 were right, an activity of genome capture by PS recognition on the outside of the ring might also be performed by IVa2 protein during AdV packaging. Given the dimensions of the channel, it is more difficult to reconcile the data with translocation of the DNA-core protein complex unless its conformation during packaging is not the same as in the immature virus.

In summary, with the results obtained in this thesis, a model for the organization of the IVa2 protein within the viral capsid can be proposed, where a pentameric ring like structure would be located on the inner capsid surface, beneath one vertex (**Figure 60**), and the genome would be tethered to the capsid by wrapping of the PS region around the periphery of the ring.

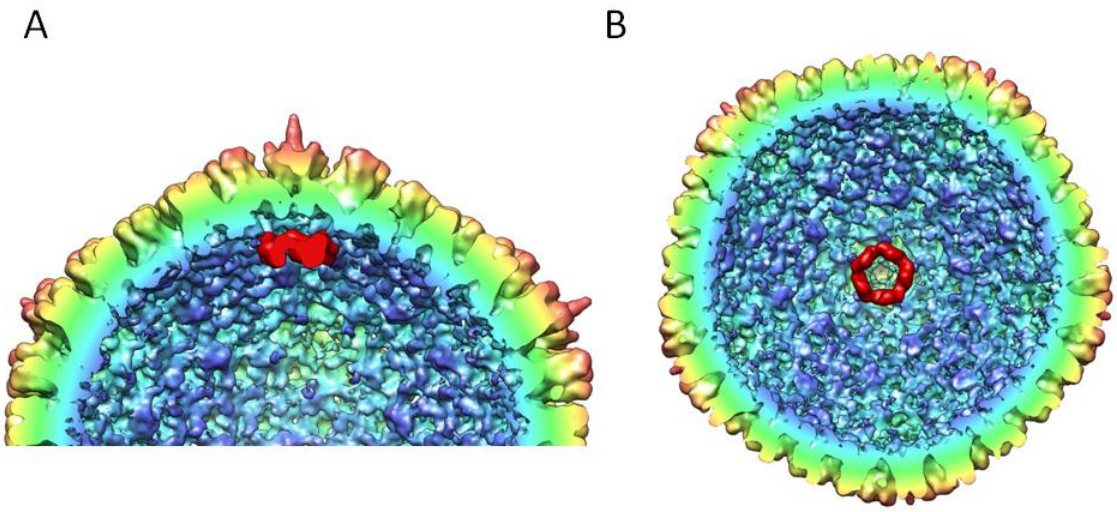

Figure 60.- Proposed model for organization and localization of IVa2 within the viral particle. The IVa2 3DEM map is shown in red beneath one vertex of a 3DEM map of Ad5GL, colored by radius. (A) Cutout across the capsid as seen from a 3-fold orientation, and (B) from a 5-fold orientation.

5.2 Future directions for IVa2 researching

Increasing the number of particles for the 3DEM model is mandatory to validate the model. Due to the low rate of ring-like particles per micrograph (an average of 20) this task is not straight forward. Structural heterogeneity of the recombinant IVa2 sample is an additional disadvantage to perform the 3DEM reconstruction of the oligomeric form of the protein. In native-PAGE experiments there was no predominant oligomeric form, and EM images confirmed this lack of homogeneity. To assist the formation and to increase the stability of the ring-like structure detected, other viral proteins might be needed. IVa2 protein can form complexes on the packaging sequence with another viral protein, L4 22K (Ewing et al., 2007), and this protein is also essential for DNA packaging (Wu, Orozco, and Hearing, 2012). This interaction makes L4 22K a good candidate to take part of the adenoviral DNA packaging structure, and might help to stabilize the ring-like conformation of IVa2. Alternatively, the ring like structure may be required to form only transiently during assembly.

In relation to the localization of IVa2 within the viral particle, different techniques might help to assess the proposed model. IVa2 antibody-viral vertex complex could allow reconstruction of the special vertex without blurring it due to the icosahedral symmetry application; however, the inaccessibility of IVa2 to antibodies in intact particles makes this approach useless. A different way to label the IVa2 protein would be the use of clonable labels capable of clustering metal atoms into a high-density particle with high spatial resolution, as metallothionein (Mercogliano and DeRosier, 2007). However, it is not clear if gold cluster would be formed inside the viral capsid. An alternative imaging technique for single-particle virus reconstruction would be Zernike phase-contrast EM (ZPC-EM), which produces dramatic low-resolution contrast enhancement and has been previously used to see for the first time viral portal structures as in HSV (Rochat et al., 2011) or to improve a previous model of portal vertex as in epsilon15 bacteriophage (Murata et al., 2010). A work recently published (Ostapchuk, Almond, and Hearing, 2011) reported a mutant lacking IVa2 which assembles empty capsids. A 3DEM reconstruction of these empty capsids lacking IVa2 might be a way to study the localization of IVa2, but this project would still be hindered by the predominant icosahedral symmetry of the empty particles and their heterogeneity and instability.

5.3 Reptile adenoviruses

Virus propagation

Reptile adenoviruses could be an interesting tool for clinical purposes, with a clear advantage to the most common adenoviral vectors, avoiding the pre-existing immunity. The lack of structural studies on the complete virion of any adenovirus distinct from those with mammalian hosts is in part motivated by the low availability of cell lines to propagate them in cell culture to achieve high titers of purified viruses.

This thesis shows that two *Atadenoviruses* infecting reptiles can be propagated in cell culture with efficiencies similar to those of the best characterized human AdV.

Virus stability

In human adenovirus, the presence of some minor coat proteins is patent in the disassembling products of the virus. These products are majoritarily GONs (Group Of Nine hexons). These groups of hexons are glued by proteins VIII and IX (**Figure 61**). The *Atadenoviruses* studied in this thesis (SnAdV-1 and LAdV) presented a different pattern of capsid disruption, without the presence of GONs and a more stable core structure than the human adenovirus. Also, infectivity and capsid integrity were less sensitive to high temperatures for lizard and snake adenovirus. These differences in the disassembly pattern and heat resistance between reptile adenoviruses and human adenovirus point to a greater stability of the *atadenovirus* structure under the conditions studied. The 3DEM reconstruction of SnAdV-1 and its interpretation by homology models, allowed the localization of a higher number of icosahedrally ordered capsid components than in the case of the human adenovirus. These extra-contacts might be implicated in a greater stability of the capsids in comparison with the Ad5GL.

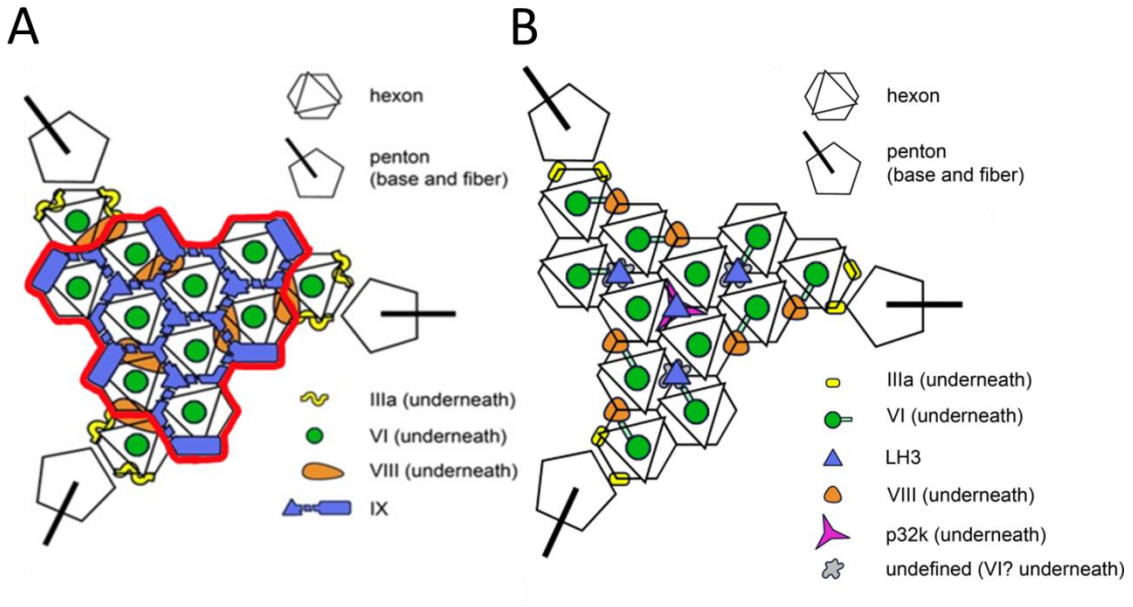

Figure 61.- GON structure in human and snake adenovirus. (A) Human adenovirus, the group of nine hexons is outlined in red color. Modified from (San Martin, 2012). (B) Snake adenovirus.

There is a human adenovirus mutant mimicking the immature stage of the virus (Ad2 *ts1*). This immature adenovirus presents a greater stability and a different uncoating pattern than the wild type (Perez-Berna et al., 2009). It has a deficient proteolytic processing and gives place to a non-infectious viral particle by hindering escape from the endosome. In Ad2 *ts1* the core conserves a spherical, compact shape when the capsid is broken and extra-densities inside the hexon cavities (assigned to the precursor of polypeptide VI) are detected. These structural characteristics are observed in parallel in the SnAdV-1 particle, also accompanied by greater stability of the virion. However, *Atadenoviruses* do infect, unlike Ad2 *ts1*, so maybe they use a different entry strategy.

Facing the reptile adenoviruses as candidates for vector therapy, their high thermo-stability might be an advantage in terms of storing and manipulation.

This work supports the identification of LH3 for the "knobs", reported for the only previous *Atadenovirus* structure published (OAdV-1) (Pantelic et al., 2008), however, assignment of p32K protein to the densities in the inner side of the capsid could not be confirmed.

Structure prediction in combination with the 3DEM map of SnAdV-1 indicated that LH3 is a trimeric protein following a beta-helix folding that is reportedly involved in oligosaccharide processing, as a bacteriophage phi29 protein (PDB ID = 3GQ7), in charge of the host-interaction (adsorption and entry). The protuberances formed by LH3 in the outside of the capsid could have a role in the viral tropism in addition to the cementing function for capsid stabilization.

5.4 Future directions in the characterization of reptile adenoviruses

The concentration obtained for SnAdV-1 (10E+11 vp/ml) and aggregation of the particles on the grid hindered image acquisition; LAdV is a good candidate to achieve a higher resolution of the 3DEM reconstruction since its purification yielded higher concentrations than the SnAdV-1(10E+12vp/ml).

CryoEM of the LAdV vertex enriched sample might help to further characterize the three fibers. The intrinsic flexibility of the fibers would not allow a full reconstruction, but the attachment to the penton base and the interaction between the three fibers at the rigid basal segment could be resolved, at least as far as the symmetry mismatch would allow.

The respiratory, digestive, urogenital and ocular tracts are major portals of entry for viruses into vertebrates. Viral infections can be initiated by specific attachment of a virus particle to protein or carbohydrate receptors projecting from the cell surface. Characterization of the receptors has relevance for the design and use of adenovirus-based gene delivery vehicles with improved properties and for the development of new antiviral strategies. The three fiber complex from LAdV, the lack of RGD loop in the penton base or the LH3 knobs characterized in SnAdV-1 might indicate different entry strategies in Atadenovirus from those described for Mastadenovirus.

Conclusions

6 Conclusions

Concerning protein IVa2 in human AdV:

1. It has been shown for the first time that IVa2 has the ability to form homo-oligomers.

2. Although *in vitro* IVa2 does not present a preferred oligomeric form, the presence of ring-shaped structures with five-fold symmetry, similar to other viral packaging ATPases, has been observed. Homology modeling in combination with a low resolution 3DEM map suggest that DNA would interact with the periphery of the ring.

3. In the virion, IVa2 is located in a position inaccessible to antibodies or proteases.

4. In the virion, IVa2 can interact with DNA binding proteins and with vertex proteins.

5. A model for the localization and organization of IVa2 within the virion has been proposed. In this model, IVa2 would be a pentameric ring located at the inner surface of one of the viral vertices, with the PS wrapped around the ring.

Concerning the characterization of AdVs infecting reptiles:

6. The production and purification of two AdVs infecting reptiles (LAdV and SnAdV-1) has been optimized for structural and molecular studies.

7. The protein composition of purified LAdV and SnAdV-1 viral particles has been characterized.

8. SnAdV and LAdV present higher thermostability and different disassembly patterns than human AdV (AdV5GL).

9. In LAdV, two fiber genes produce two fiber proteins that are incorporated into the virion, but surprisingly, they assemble three fibers per vertex complex.

10. A 3DEM map of SnAdV-1 at 12.5 Å resolution has been obtained and interpreted with the help of homology models for the major capsid proteins, revealing a set of minor proteins different from those in human AdV that could explain the increased stability. Interestingly, one of the minor coat proteins could present a fold typical of bacteriophage host attachment proteins.

Summary (in Spanish)

7 Resumen en español

7.1 Introducción

7.1.1 Adenovirus

Desde su descubrimiento en tejido adenoide humano a mediados del siglo XX (Rowe et al., 1953), un gran número de adenovirus han sido detectados en huéspedes vertebrados. El interés en el estudio de adenovirus se basa en su dualidad como patógenos (del ser humano y de animales con interés económico y ambiental) y como herramientas para terapia génica y desarrollo de vacunas.

El genoma de adenovirus humano es una molécula de ADN de cadena doble de unas 35000 pb. Los genes se codifican en unidades de transcripción superpuestas, requiriendo un "splicing" o empalme alternativo del pre-ARNm. El genoma se divide en regiones tempranas (E1A, E1B, E2A, E2B, E3 y E4) que se expresan en primer lugar durante la replicación viral, y regiones tardías (de L1 a L5) que generalmente se expresan tras el comienzo de la replicación del ADN viral (Russell, 2000).

Adenovirus es un virus sin envuelta, con cápsidas icosaédricas de unos 90 nm de diámetro. La cápsida está compuesta por tres proteínas mayoritarias (hexón, base del pentón y fibras) y cuatro proteínas minoritarias (IIIa, VI, VIII y IX) (San Martin, 2012). El "core" o núcleo del virus está compuesto por una molécula de ADN y una serie de proteínas unidas a él (V, VII, μ, PT, IVa2 y la proteasa viral).

Adenovirus infecta células epiteliales por endocitosis mediada por repector. El bajo pH del endosoma provoca cambios en la cápsida que facilitan el escape viral. A través del citoesqueleto, el virus se desplaza hacia el núcleo finalizando con la inserción del ADN viral a través de un poro nuclear. Este ADN viral se replica y se transcribe en el núcleo, donde se produce el ensamblaje de nuevos viriones (Flint, 2009). Los procesos de ensamblaje y empaquetamiento del ADN aún no se han descrito en detalle. El último

paso en la maduración viral consiste en un procesamiento proteolítico por parte de la proteasa viral.

7.1.2 Encapsidación del genoma

En purificaciones virales por gradientes de densidad, se han detectado partículas completas y partículas vacías (sin estructura de "core"), así como cápsidas de densidades intermedias con pequeños fragmentos de la molécula de ADN (Shimojo et al., 1967; Smith, 1965). Las partículas vacías podrían interpretarse como cápsidas pre-ensambladas en las que posteriormente se empaquetaría el DNA, del mismo modo que bacteriófagos; aunque un razonamiento alternativo que no puede descartarse considera a las partículas incompletas como abortos de ensamblaje.

El DNA de adenovirus se empaqueta siempre desde el extremo terminal izquierdo, donde se encuentra una secuencia específica: la secuencia de empaquetamiento (Gustin and Imperiale, 1998; Lang and Hearing, 2003). A esta secuencia se une la proteína IVa2 (Zhang and Imperiale, 2000).

IVa2 es una proteína multifuncional, activadora del promotor mayor tardío (MLP) e imprescindible para el empaquetamiento del ADN viral. En ausencia de esta proteína, se obtienen sólo cápsidas vacías. La secuencia de IVa2 presenta un alto grado de conservación entre los distintos géneros de adenovirus, con motivos comunes en ATPasas, como la "Walker Box". Este hecho junto con la probada unión a ATP (aunque no así la hidrólisis del nucleótido) (Ostapchuk and Hearing, 2008) hace pensar en IVa2 como motor de empaquetamiento del DNA viral. Su número de copia (6.3 ±1.5) y su propuesta localización en un vértice (Christensen et al., 2008) dan fuerza a esta hipotética función como motor de empaquetamiento, por homología al sistema de empaquetamiento de bacteriófagos y de algunos virus de eucariotas, como el virus de herpes simple.

Adenovirus presenta una característica atípica en el conjunto de los virus: una proteína del core (VII) está íntimamente unida al DNA viral formando estructuras de tipo histona. La presencia de esta proteína acomplejada con el DNA representa un problema

adicional para elucidar el proceso de empaquetamiento de ADN (Zhang and Arcos, 2005).

7.1.3 Otros adenovirus

Los adenovirus se clasifican en cinco géneros diferentes: *Mastadenovirus* (infectan a mamíferos), *Aviadenovirus* (infectan aves), *Atadenovirus* (infectan reptiles, aves, marsupiales y mamíferos), *Siadenovirus* (infectan anfibios y aves) e *Ichtadenovirus* (infectan peces) (ictvdb.bio-mirror.cn/Ictv/index.htm). El uso de adenovirus que no infectan de manera natural a humanos como vectores para terapias clínicas se ha propuesto como una manera de evitar la inmunidad pre-existente. La caracterización estructural de estos adenovirus aislados de tejidos no humanos está limitada al adenovirus canino de tipo 2 (Schoehn et al., 2008) y al adenovirus ovino (Pantelic et al., 2008) ; no hay datos de la estructura completa del virión de adenovirus aislados de animales no mamíferos.

Adenovirus aislado de boa constrictor (*Boa constrictor*) fue propagado en la línea celular VH-2 y completamente secuenciado (Farkas, Harrach, and Benko, 2008). Más recientemente, adenovirus aislado de un lagarto mejicano (*Heloderma horidum*) fue aislado y propagado en cultivo celular de IgH2 (Papp, Fledelius et al. 2009). La secuencia completa de su genoma ha sido obtenida por nuestros colaboradores Dra. Mária Benkö y Dr. Balázs Harrach (publicación en preparación), destacando la peculiaridad de que contiene dos genes que codificarían fibras, estructuras situadas en los vértices de la partícula viral implicadas en reconocimiento del huésped. Estos dos adenovirus aislados de reptiles han sido utilizados en el trabajo para la presente tesis doctoral.

7.2 Objetivos

Esta tesis está dividida en dos temas principales. Uno es el estudio de la proteína IVa2 como hipotético motor de empaquetamiento del DNA en adenovirus humano, y el segundo es la caracterización molecular y estructural de adenovirus aislados de reptiles.

En particular, se han perseguido los siguientes objetivos:

Proteína IVa2:

- Determinar la estructura cuaternaria de IVa2 *in vitro*.
- Determinar la localización de la proteína IVa2 en la partícula viral.

Adenovirus aislados de reptiles:

- Optimizar la propagación y la purificación de adenovirus de reptiles para su estudio estructural y molecular.
- Caracterizar la composición proteica de adenovirus aislados de reptiles.
- Caracterizar la estabilidad es los adenovirus aislados de reptiles.
- Si es posible, determinar la primera estructura de un adenovirus de huésped no mamífero.

7.3 Resultados

Análisis de la organización de la proteína IVa2 en el virión de adenovirus.

Utilizando técnicas de inmunomarcaje y de proteólisis limitada, se ha determinado que la proteína IVa2 de adenovirus humano no se encuentra expuesta en el exterior de la cápsida viral. El análisis de fragmentos de desensamblaje de cápsidas virales ha revelado que IVa2 se encuentra interaccionando con proteínas del core viral (VII) y de los vértices (IIIa). Utilizando preparaciones de IVa2 recombinante, en su forma completa y en una variante truncada en su extremo amino-terminal, se ha determinado mediante técnicas de biología molecular, microscopía electrónica y procesamiento de imagen, que esta proteína tiene la capacidad de formar homo-oligómeros pentaméricos con forma de anillo, aunque en las condiciones ensayadas no existe una forma oligomérica mayoritaria. Mediante modelado por homología y ME3D se ha obtenido un modelo pseudo-atómico del pentámero de IVa2 que permite hacer predicciones sobre la localización y el papel de los distintos motivos funcionales de la proteína en el oligómero.

Caracterización de adenovirus que infectan reptiles.

Partiendo de adenovirus aislados de boa y de lagarto, se ha optimizado su propagación y purificación en cultivo, hasta obtener preparaciones de calidad suficiente

para su estudio por técnicas de biología molecular y crio-microscopía electrónica. Mediante ensayos de infectividad y microscopía electrónica se ha caracterizado la termo-estabilidad de estos virus y comparado con la adenovirus humano. Utilizando espectrometría de masas acoplada a cromatografía líquida se ha determinado cuáles de los genes dan lugar a proteínas estructurales incorporadas a los viriones. Un resultado completamente novedoso es la presencia de dos genes para fibra en el adenovirus de lagarto, que dan lugar a un complejo de tres fibras presente en cada vértice del virión. En cuanto al adenovirus de serpiente, se han realizado estudios por crio-microscopía electrónica tridimensional que han dado lugar a un mapa a 12.5 Å de resolución, el cual se ha interpretado usando modelos por homología de las estructuras de las proteínas mayoritarias de la cápsida y mapas diferencia para revelar las proteínas minoritarias.

7.4 Discusión

Estado oligomérico de IVa2, localización e implicaciones para el empaquetamiento del DNA.

Trabajos anteriores apuntaban a un estado monomérico de la proteína IVa2 (Lutz and Kedinger, 1996) y (Yang, Yang, and Maluf, 2009). Sin embargo, los métodos de purificación de la proteína y las técnicas utilizadas en esas publicaciones para la detección de estados oligoméricos no pueden descartar los resultados obtenidos en esta tesis para la observación de estados oligoméricos.

La localización de IVa2 en un vértice, en una posición no accesible desde el exterior de la cápsida implicaría un modelo diferente al utilizado por bacteriófagos, un modelo más afín al descrito para Herpes virus (Rochat et al., 2011).

Ante la ausencia de modelos estructurales con los que contrastar la reconstrucción 3D del anillo de IVa2, se ha utilizado un modelo de homología remota para realizar el encaje. El modelo ha permitido predecir que el sitio de unión a DNA está localizado en el exterior del anillo. Un mecanismo combinado de captura y traslocación del DNA, podría explicar esta unión externa como paso previo al empaquetamiento del genoma viral.

Adenovirus de reptiles

En adenovirus humanos, la presencia de proteínas minoritarias de la cápsida se hace patente en los productos de desensamblaje del virus. La mayor parte de estos productos son los GONs (grupos de nueve hexones). Estos hexones están unidos por las proteínas minoritarias VIII y IX. El patrón de desensamblaje observado en los Atadenovirus estudiados presentan un patrón diferente de rotura de cápsida, sin la aparición de GONs y con una estructura "core" más estable que la del adenovirus humano. Estas diferencias en el desensamblaje, unidas a la mayor termo-estabilidad detectada para LAdV y SnAdV-1 apuntan a una mayor estabilidad de estos virus en las condiciones experimentadas. La reconstrucción 3D de SnAdV-1 y su interpretación con modelos por homología, han permitido la localización de un mayor número de proteínas ordenadas siguiendo simetría icosaédrica. Este mayor número de contactos podría estar implicado en la mayor estabilidad de los adenovirus de reptil.

7.5 Conclusiones

En cuanto a la proteína IVa2 en adenovirus humano:

1. Se ha mostrado por primera vez que IVa2 tiene la capacidad de formar homo-oligómeros.
2. Aunque IVa2 *in vitro* no presenta una forma oligomérica predominante, se ha observado la presencia de estructuras de tipo anillo con simetría cinco, similar a otras ATPasas virales de empaquetamiento. El modelado por homología en combinación con un mapa de ME3D, sugiere que el ADN podría interaccionar con la periferia del anillo.
3. En el virión, IVa2 está localizada en una posición inaccesible para anticuerpos y proteasas.
4. En el virión, IVa2 puede interaccionar con otras proteínas de unión a DNA y con proteínas situadas en el vértice.

5. Se ha propuesto un modelo de localización y organización de IVa2 en el virión. En este modelo, IVa2 sería un anillo pentamérico localizado en la cara interna de uno de los vértices virales, y la región del genoma que contiene la secuencia de empaquetamiento se enrollaría en torno al anillo.

En cuanto a la caracterización de adenovirus que infectan reptiles:

6. Se ha optimizado la propagación y la purificación de dos adenovirus aislados de reptiles (SnAdV-1 y LAdV) para su estudio estructural y molecular.
7. Se ha caracterizado la composición proteica de SnAdV-1 y de LAdV.
8. Tanto SnAdV-1 como LAdV, presentan una termo-estabilidad mayor que la de humano (Ad5GL) y diferentes patrones de desensamblaje.
9. En LAdV, los dos genes de fibra se traducen a dos proteínas de fibra que se incorporan en el virion pero, sorprendentemente, se ensamblan tres fibras en cada vértice.
10. Se ha obtenido un mapa 3D de SnAdV-1 a 12.5 Å de resolución. Se ha interpretado con la ayuda de modelos de homología para las proteínas mayoritarias de la cápsida, revelando un conjunto de proteínas minoritarias diferente de las de adenovirus humano. Es interesante destacar que, uno de los mapas podría presentar un plegamiento típico de una proteína de reconocimiento de huésped en bacteriófagos.

8 References

Benson, S. D., Bamford, J. K., Bamford, D. H., and Burnett, R. M. (2004). Does common architecture reveal a viral lineage spanning all three domains of life? *Mol Cell* **16**(5)**,** 673-85.

Berget, S. M., Moore, C., and Sharp, P. A. (1977). Spliced segments at the 5' terminus of adenovirus 2 late mRNA. *Proc Natl Acad Sci U S A* **74**(8)**,** 3171-5.

Bradley, P., Cowen, L., Menke, M., King, J., and Berger, B. (2001). BETAWRAP: successful prediction of parallel beta -helices from primary sequence reveals an association with many microbial pathogens. *Proc Natl Acad Sci U S A* **98**(26)**,** 14819-24.

Brown, M., and Weber, J. (1980). Virion core-like organization of intranuclear adenovirus chromatin late in infection. *Virology* **107**(1)**,** 306-10.

Burroughs, A. M., Iyer, L. M., and Aravind, L. (2007). Comparative genomics and evolutionary trajectories of viral ATP dependent DNA-packaging systems. *Genome Dyn* **3,** 48-65.

Cupelli, K., and Stehle, T. (2011). Viral attachment strategies: the many faces of adenoviruses. *Curr Opin Virol* **1**(2)**,** 84-91.

Chatterjee, P. K., Vayda, M. E., and Flint, S. J. (1986a). Adenoviral protein VII packages intracellular viral DNA throughout the early phase of infection. *EMBO J* **5**(7)**,** 1633-44.

Chatterjee, P. K., Vayda, M. E., and Flint, S. J. (1986b). Identification of proteins and protein domains that contact DNA within adenovirus nucleoprotein cores by ultraviolet light crosslinking of oligonucleotides 32P-labelled in vivo. *J Mol Biol* **188**(1)**,** 23-37.

Chatterjee, P. K., Yang, U. C., and Flint, S. J. (1986). Comparison of the interactions of the adenovirus type 2 major core protein and its precursor with DNA. *Nucleic Acids Res* **14**(6)**,** 2721-35.

Cherrier, M. V., Kostyuchenko, V. A., Xiao, C., Bowman, V. D., Battisti, A. J., Yan, X., Chipman, P. R., Baker, T. S., Van Etten, J. L., and Rossmann, M. G. (2009). An icosahedral algal virus has a complex unique vertex decorated by a spike. *Proc Natl Acad Sci U S A* **106**(27)**,** 11085-9.

Chow, L. T., Gelinas, R. E., Broker, T. R., and Roberts, R. J. (1977). An amazing sequence arrangement at the 5' ends of adenovirus 2 messenger RNA. *Cell* **12**(1)**,** 1-8.

Christensen, J. B., Byrd, S. A., Walker, A. K., Strahler, J. R., Andrews, P. C., and Imperiale, M. J. (2008). Presence of the adenovirus IVa2 protein at a single vertex of the mature virion. *J Virol* **82**(18)**,** 9086-93.

Christensen, J. B., Ewing, S. G., and Imperiale, M. J. (2012). Identification and characterization of a DNA binding domain on the adenovirus IVa2 protein. *Virology* **433**(1)**,** 124-30.

Dan, A., Ruzsics, Z., Russell, W. C., Benko, M., and Harrach, B. (1998). Analysis of the hexon gene sequence of bovine adenovirus type 4 provides further support for a new adenovirus genus (Atadenovirus). *J Gen Virol* **79 (Pt 6),** 1453-60.

Davison, A. J., Benko, M., and Harrach, B. (2003). Genetic content and evolution of adenoviruses. *J Gen Virol* **84**(Pt 11)**,** 2895-908.

Davison, A. J. H., B. (2002). Siadenovirus. *In* "In the Springer Index of Viruses", pp. 29-33. C.A. Tidona & G. Darai, New York.

Dery, C. V., Toth, M., Brown, M., Horvath, J., Allaire, S., and Weber, J. M. (1985). The structure of adenovirus chromatin in infected cells. *J Gen Virol* **66 (Pt 12),** 2671-84.

Dobbelstein, M. (2004). Replicating adenoviruses in cancer therapy. *Curr Top Microbiol Immunol* **273,** 291-334.

Draper, S. J., and Heeney, J. L. (2010). Viruses as vaccine vectors for infectious diseases and cancer. *Nat Rev Microbiol* **8**(1)**,** 62-73.

Driedonks, R. A., and Caldentey, J. (1983). Gene 20 product of bacteriophage T4. II. Its structural organization in prehead and bacteriophage. *J Mol Biol* **166**(3)**,** 341-60.

El Bakkouri, M., Seiradake, E., Cusack, S., Ruigrok, R. W., and Schoehn, G. (2008). Structure of the C-terminal head domain of the fowl adenovirus type 1 short fibre. *Virology* **378**(1)**,** 169-76.

Ewing, S. G., Byrd, S. A., Christensen, J. B., Tyler, R. E., and Imperiale, M. J. (2007). Ternary complex formation on the adenovirus packaging sequence by the IVa2 and L4 22-kilodalton proteins. *J Virol* **81**(22)**,** 12450-7.

Farkas, S. L., Harrach, B., and Benko, M. (2008). Completion of the genome analysis of snake adenovirus type 1, a representative of the reptilian lineage within the novel genus Atadenovirus. *Virus Res* **132**(1-2)**,** 132-9.

Favier, A. L., Schoehn, G., Jaquinod, M., Harsi, C., and Chroboczek, J. (2002). Structural studies of human enteric adenovirus type 41. *Virology* **293**(1)**,** 75-85.

Flint, S. J. (2009). "Principles of virology: molecular biology, pathogenesis and control." (A. Press, Ed.), Washington, D.C.

Garber, E. A., Seidman, M. M., and Levine, A. J. (1980). Intracellular SV40 nucleoprotein complexes: synthesis to encapsidation. *Virology* **107**(2)**,** 389-401.

Goncalves, M. A., and de Vries, A. A. (2006). Adenovirus: from foe to friend. *Rev Med Virol* **16**(3)**,** 167-86.

Gorman, J. J., Wallis, T. P., Whelan, D. A., Shaw, J., and Both, G. W. (2005). LH3, a "homologue" of the mastadenoviral E1B 55-kDa protein is a structural protein of atadenoviruses. *Virology* **342**(1)**,** 159-66.

Guardado-Calvo, P., Llamas-Saiz, A. L., Fox, G. C., Langlois, P., and van Raaij, M. J. (2007). Structure of the C-terminal head domain of the fowl adenovirus type 1 long fiber. *J Gen Virol* **88**(Pt 9)**,** 2407-16.

Guardado-Calvo, P., Munoz, E. M., Llamas-Saiz, A. L., Fox, G. C., Kahn, R., Curiel, D. T., Glasgow, J. N., and van Raaij, M. J. (2010). Crystallographic structure of porcine adenovirus type 4 fiber head and galectin domains. *J Virol* **84**(20)**,** 10558-68.

Gustin, K. E., and Imperiale, M. J. (1998). Encapsidation of viral DNA requires the adenovirus L1 52/55-kilodalton protein. *J Virol* **72**(10)**,** 7860-70.

Gustin, K. E., Lutz, P., and Imperiale, M. J. (1996). Interaction of the adenovirus L1 52/55-kilodalton protein with the IVa2 gene product during infection. *J Virol* **70**(9)**,** 6463-7.

Hess, M. (2000). Detection and differentiation of avian adenoviruses: a review. *Avian Pathol* **29**(3)**,** 195-206.

Jacobson, E. R., and Gardiner, C. H. (1990). Adeno-like virus in esophageal and tracheal mucosa of a Jackson's chameleon (Chamaeleo jacksoni). *Vet Pathol* **27**(3)**,** 210-2.

Jacobson, E. R., Gaskin, J. M., and Gardiner, C. H. (1985). Adenovirus-like infection in a boa constrictor. *J Am Vet Med Assoc* **187**(11)**,** 1226-7.

Juhasz, A., and Ahne, W. (1993). Physicochemical properties and cytopathogenicity of an adenovirus-like agent isolated from corn snake (Elaphe guttata). *Arch Virol* **130**(3-4)**,** 429-39.

Julian, A. F., and Durham, P. J. (1982). Adenoviral hepatitis in a female bearded dragon (Amphibolurus barbatus). *N Z Vet J* **30**(5)**,** 59-60.

Jung, W. S., Hong, C. K., Lee, S., Kim, C. S., Kim, S. J., Kim, S. I., and Rhee, S. (2007). Structural and functional insights into intramolecular fructosyl transfer by inulin fructotransferase. *J Biol Chem* **282**(11)**,** 8414-23.

Kallberg, M., Wang, H., Wang, S., Peng, J., Wang, Z., Lu, H., and Xu, J. (2012). Template-based protein structure modeling using the RaptorX web server. *Nat Protoc* **7**(8)**,** 1511-22.

Kidd, A. H., Chroboczek, J., Cusack, S., and Ruigrok, R. W. (1993). Adenovirus type 40 virions contain two distinct fibers. *Virology* **192**(1)**,** 73-84.

Kinsel, M. J., Barbiers, R. B., Manharth, A., and Murnane, R. D. (1997). Small intestinal adeno-like virus in a mountain chameleon (Chameleo montium). *J Zoo Wildl Med* **28**(4)**,** 498-500.

Lang, S. E., and Hearing, P. (2003). The adenovirus E1A oncoprotein recruits the cellular TRRAP/GCN5 histone acetyltransferase complex. *Oncogene* **22**(18)**,** 2836-41.

Lasaro, M. O., and Ertl, H. C. (2009). New insights on adenovirus as vaccine vectors. *Mol Ther* **17**(8)**,** 1333-9.

Leen, A. M., and Rooney, C. M. (2005). Adenovirus as an emerging pathogen in immunocompromised patients. *Br J Haematol* **128**(2)**,** 135-44.

Liu, H., Jin, L., Koh, S. B., Atanasov, I., Schein, S., Wu, L., and Zhou, Z. H. (2010). Atomic structure of human adenovirus by cryo-EM reveals interactions among protein networks. *Science* **329**(5995)**,** 1038-43.

Liu, H., Wu, L., and Zhou, Z. H. (2011). Model of the trimeric fiber and its interactions with the pentameric penton base of human adenovirus by cryo-electron microscopy. *J Mol Biol* **406**(5)**,** 764-74.

Loser, P., Kumin, D., Hillgenberg, M., Both, G. W., and Hofmann, C. (2002). Preparation of ovine adenovirus vectors. *Methods Mol Med* **69,** 415-26.

Ludtke, S. J., Baldwin, P. R., and Chiu, W. (1999). EMAN: semiautomated software for high-resolution single-particle reconstructions. *J Struct Biol* **128**(1)**,** 82-97.

Lutz, P., and Kedinger, C. (1996). Properties of the adenovirus IVa2 gene product, an effector of late-phase-dependent activation of the major late promoter. *J Virol* **70**(3)**,** 1396-405.

Ma, H. C., and Hearing, P. (2011). Adenovirus structural protein IIIa is involved in the serotype specificity of viral DNA packaging. *J Virol* **85**(15)**,** 7849-55.

Maizel, J. V., Jr., White, D. O., and Scharff, M. D. (1968). The polypeptides of adenovirus. I. Evidence for multiple protein components in the virion and a comparison of types 2, 7A, and 12. *Virology* **36**(1)**,** 115-25.

Marschang, R. E. M., R.; Benkö, M.; Papp, T.; Harrach, B.; Böhm, R. (August 2003). *In Proceedings of the 6th International Congress of Veterinary Virology: Virus persistence and evolution (European Society for Veterinary Virology), Saint.Malo, France*.

McGeoch, D. J. D., A.J. (1999). "The molecular evolutionary history of the herpesviruses. In Origin and Evolution of Viruses." Academic Press, London.

Mercogliano, C. P., and DeRosier, D. J. (2007). Concatenated metallothionein as a clonable gold label for electron microscopy. *J Struct Biol* **160**(1)**,** 70-82.

Morais, M. C., Koti, J. S., Bowman, V. D., Reyes-Aldrete, E., Anderson, D. L., and Rossmann, M. G. (2008). Defining molecular and domain boundaries in the bacteriophage phi29 DNA packaging motor. *Structure* **16**(8)**,** 1267-74.

Murata, K., Liu, X., Danev, R., Jakana, J., Schmid, M. F., King, J., Nagayama, K., and Chiu, W. (2010). Zernike phase contrast cryo-electron microscopy and tomography for structure determination at nanometer and subnanometer resolutions. *Structure* **18**(8)**,** 903-12.

Ogawa, M., Ahne, W., and Essbauer, S. (1992). Reptilian viruses: adenovirus-like agent isolated from royal python (Python regius). *Zentralbl Veterinarmed B* **39**(10)**,** 732-6.

Ostapchuk, P., Almond, M., and Hearing, P. (2011). Characterization of Empty adenovirus particles assembled in the absence of a functional adenovirus IVa2 protein. *J Virol* **85**(11)**,** 5524-31.

Ostapchuk, P., and Hearing, P. (2008). Adenovirus IVa2 protein binds ATP. *J Virol* **82**(20)**,** 10290-4.

Ostapchuk, P., Yang, J., Auffarth, E., and Hearing, P. (2005). Functional interaction of the adenovirus IVa2 protein with adenovirus type 5 packaging sequences. *J Virol* **79**(5)**,** 2831-8.

Pantelic, R. S., Lockett, L. J., Rothnagel, R., Hankamer, B., and Both, G. W. (2008). Cryoelectron microscopy map of Atadenovirus reveals cross-genus structural differences from human adenovirus. *J Virol* **82**(15)**,** 7346-56.

Pardo-Mateos, A., and Young, C. S. (2004). A 40 kDa isoform of the type 5 adenovirus IVa2 protein is sufficient for virus viability. *Virology* **324**(1)**,** 151-64.

Perez-Berna, A. J., Marabini, R., Scheres, S. H., Menendez-Conejero, R., Dmitriev, I. P., Curiel, D. T., Mangel, W. F., Flint, S. J., and San Martin, C. (2009). Structure and uncoating of immature adenovirus. *J Mol Biol* **392**(2)**,** 547-57.

Perez-Romero, P., Tyler, R. E., Abend, J. R., Dus, M., and Imperiale, M. J. (2005). Analysis of the interaction of the adenovirus L1 52/55-kilodalton and IVa2 proteins with the packaging sequence in vivo and in vitro. *J Virol* **79**(4)**,** 2366-74.

Pichla-Gollon, S. L., Drinker, M., Zhou, X., Xue, F., Rux, J. J., Gao, G. P., Wilson, J. M., Ertl, H. C., Burnett, R. M., and Bergelson, J. M. (2007). Structure-based identification of a major neutralizing site in an adenovirus hexon. *J Virol* **81**(4)**,** 1680-9.

Prage, L., Hoglund, S., and Philipson, L. (1972). Structural proteins of adenoviruses. 8. Characterization of incomplete particles of adenovirus type 3. *Virology* **49**(3)**,** 745-57.

Prage, L., and Pettersson, U. (1971). Structural proteins of adenoviruses. VII. Purification and properties of an arginine-rich core protein from adenovirus type 2 and type 3. *Virology* **45**(2)**,** 364-73.

Prage, L., Pettersson, U., Hoglund, S., Lonberg-Holm, K., and Philipson, L. (1970). Structural proteins of adenoviruses. IV. Sequential degradation of the adenovirus type 2 virion. *Virology* **42**(2)**,** 341-58.

Putnak, J. R., and Phillips, B. A. (1981). Differences between poliovirus empty capsids formed in vivo and those formed in vitro: a role for the morphopoietic factor. *J Virol* **40**(1)**,** 173-83.

Rao, V. B., and Feiss, M. (2008). The bacteriophage DNA packaging motor. *Annu Rev Genet* **42,** 647-81.

Reddy, V. S., Natchiar, S. K., Stewart, P. L., and Nemerow, G. R. (2010). Crystal structure of human adenovirus at 3.5 A resolution. *Science* **329**(5995)**,** 1071-5.

Rekosh, D. M., Russell, W. C., Bellet, A. J., and Robinson, A. J. (1977). Identification of a protein linked to the ends of adenovirus DNA. *Cell* **11**(2)**,** 283-95.

Rochat, R. H., Liu, X., Murata, K., Nagayama, K., Rixon, F. J., and Chiu, W. (2011). Seeing the portal in herpes simplex virus type 1 B capsids. *J Virol* **85**(4)**,** 1871-4.

Rombaut, B., Vrijsen, R., and Boeye, A. (1990). New evidence for the precursor role of 14 S subunits in poliovirus morphogenesis. *Virology* **177**(1)**,** 411-4.

Rowe, W. P., Huebner, R. J., Gilmore, L. K., Parrott, R. H., and Ward, T. G. (1953). Isolation of a cytopathogenic agent from human adenoids undergoing spontaneous degeneration in tissue culture. *Proc Soc Exp Biol Med* **84**(3)**,** 570-3.

Ruigrok, R. W., Barge, A., Albiges-Rizo, C., and Dayan, S. (1990). Structure of adenovirus fibre. II. Morphology of single fibres. *J Mol Biol* **215**(4)**,** 589-96.

Russell, W. C. (2000). Update on adenovirus and its vectors. *J Gen Virol* **81**(Pt 11)**,** 2573-604.

San Martin, C. (2012). Latest insights on adenovirus structure and assembly. *Viruses* **4**(5)**,** 847-77.

Saugar, I., Luque, D., Ona, A., Rodriguez, J. F., Carrascosa, J. L., Trus, B. L., and Caston, J. R. (2005). Structural polymorphism of the major capsid protein of a double-stranded RNA virus: an amphipathic alpha helix as a molecular switch. *Structure* **13**(7)**,** 1007-17.

Scheres, S. H., Nunez-Ramirez, R., Gomez-Llorente, Y., San Martin, C., Eggermont, P. P., and Carazo, J. M. (2007). Modeling experimental image formation for likelihood-based classification of electron microscopy data. *Structure* **15**(10)**,** 1167-77.

Schoehn, G., El Bakkouri, M., Fabry, C. M., Billet, O., Estrozi, L. F., Le, L., Curiel, D. T., Kajava, A. V., Ruigrok, R. W., and Kremer, E. J. (2008). Three-dimensional structure of canine adenovirus serotype 2 capsid. *J Virol* **82**(7)**,** 3192-203.

Seiradake, E., Lortat-Jacob, H., Billet, O., Kremer, E. J., and Cusack, S. (2006). Structural and mutational analysis of human Ad37 and canine adenovirus 2 fiber heads in complex with the D1 domain of coxsackie and adenovirus receptor. *J Biol Chem* **281**(44)**,** 33704-16.

Shimojo, H., Yamashita, T., Yamamoto, H., Suzuki, E., and Abe, C. (1967). Empty particles of Adenovirus 12. *Jpn J Med Sci Biol* **20**(2)**,** 199-203.

Shiver, J. W., Fu, T. M., Chen, L., Casimiro, D. R., Davies, M. E., Evans, R. K., Zhang, Z. Q., Simon, A. J., Trigona, W. L., Dubey, S. A., Huang, L., Harris, V. A., Long, R. S., Liang, X., Handt, L., Schleif, W. A., Zhu, L., Freed, D. C., Persaud, N. V., Guan, L., Punt, K. S., Tang, A., Chen, M., Wilson, K. A., Collins, K. B., Heidecker, G. J., Fernandez, V. R., Perry, H. C., Joyce, J. G., Grimm, K. M., Cook, J. C., Keller, P. M., Kresock, D. S., Mach, H., Troutman, R. D., Isopi, L. A., Williams, D. M., Xu, Z., Bohannon, K. E., Volkin, D. B., Montefiori, D. C., Miura, A., Krivulka, G. R., Lifton, M. A., Kuroda, M. J., Schmitz, J. E., Letvin, N. L., Caulfield, M. J., Bett, A. J., Youil, R., Kaslow, D. C., and Emini, E. A. (2002). Replication-incompetent adenoviral vaccine vector elicits effective anti-immunodeficiency-virus immunity. *Nature* **415**(6869)**,** 331-5.

Smith, K. O. (1965). Studies on Adenovirus-12. I. Quantitative Correlations between Some Physical, Antigenic and Infectious Properties. *J Immunol* **94,** 976-89.

Song, J. D., Liu, X. L., Chen, D. L., Zou, X. H., Wang, M., Qu, J. G., Lu, Z. Z., and Hung, T. (2012). Human adenovirus type 41 possesses different amount of short and long fibers in the virion. *Virology* **432**(2)**,** 336-42.

Stadtfeld, M., Nagaya, M., Utikal, J., Weir, G., and Hochedlinger, K. (2008). Induced pluripotent stem cells generated without viral integration. *Science* **322**(5903)**,** 945-9.

Stewart, P. L., Burnett, R. M., Cyrklaff, M., and Fuller, S. D. (1991). Image reconstruction reveals the complex molecular organization of adenovirus. *Cell* **67**(1)**,** 145-54.

Sun, S., Kondabagil, K., Draper, B., Alam, T. I., Bowman, V. D., Zhang, Z., Hegde, S., Fokine, A., Rossmann, M. G., and Rao, V. B. (2008). The structure of the phage T4 DNA packaging motor suggests a mechanism dependent on electrostatic forces. *Cell* **135**(7)**,** 1251-62.

Sundquist, B., Everitt, E., Philipson, L., and Hoglund, S. (1973). Assembly of adenoviruses. *J Virol* **11**(3)**,** 449-59.

Tyler, R. E., Ewing, S. G., and Imperiale, M. J. (2007). Formation of a multiple protein complex on the adenovirus packaging sequence by the IVa2 protein. *J Virol* **81**(7)**,** 3447-54.

Upton, C., Slack, S., Hunter, A. L., Ehlers, A., and Roper, R. L. (2003). Poxvirus orthologous clusters: toward defining the minimum essential poxvirus genome. *J Virol* **77**(13)**,** 7590-600.

van Oostrum, J., and Burnett, R. M. (1985). Molecular composition of the adenovirus type 2 virion. *J Virol* **56**(2)**,** 439-48.

van Raaij, M. J., Mitraki, A., Lavigne, G., and Cusack, S. (1999). A triple beta-spiral in the adenovirus fibre shaft reveals a new structural motif for a fibrous protein. *Nature* **401**(6756)**,** 935-8.

Vrati, S., Brookes, D. E., Strike, P., Khatri, A., Boyle, D. B., and Both, G. W. (1996). Unique genome arrangement of an ovine adenovirus: identification of new proteins and proteinase cleavage sites. *Virology* **220**(1)**,** 186-99.

Wadell, G., Hammarskjold, M. L., and Varsanyi, T. (1973). Incomplete virus particles of adenovirus type 16. *J Gen Virol* **20**(3)**,** 287-302.

Weber, J., and Philipson, L. (1984). Protein composition of adenovirus nucleoprotein complexes extracted from infected cells. *Virology* **136**(2)**,** 321-7.

Weber, J. M. (1995). Adenovirus endopeptidase and its role in virus infection. *Curr Top Microbiol Immunol* **199 (Pt 1),** 227-35.

Wellehan, J. F., Johnson, A. J., Harrach, B., Benko, M., Pessier, A. P., Johnson, C. M., Garner, M. M., Childress, A., and Jacobson, E. R. (2004). Detection and analysis of six lizard adenoviruses by consensus primer PCR provides further evidence of a reptilian origin for the atadenoviruses. *J Virol* **78**(23)**,** 13366-9.

Winter, N., and D'Halluin, J. C. (1991). Regulation of the biosynthesis of subgroup C adenovirus protein IVa2. *J Virol* **65**(10)**,** 5250-9.

Wood, Z. A., Schroder, E., Robin Harris, J., and Poole, L. B. (2003). Structure, mechanism and regulation of peroxiredoxins. *Trends Biochem Sci* **28**(1)**,** 32-40.

Wu, K., Orozco, D., and Hearing, P. (2012). The adenovirus L4-22K protein is multifunctional and is an integral component of crucial aspects of infection. *J Virol* **86**(19)**,** 10474-83.

Xiang, Y., Leiman, P. G., Li, L., Grimes, S., Anderson, D. L., and Rossmann, M. G. (2009). Crystallographic insights into the autocatalytic assembly mechanism of a bacteriophage tail spike. *Mol Cell* **34**(3)**,** 375-86.

Xu, L., Benson, S. D., and Burnett, R. M. (2007). Nanoporous crystals of chicken embryo lethal orphan (CELO) adenovirus major coat protein, hexon. *J Struct Biol* **157**(2)**,** 424-31.

Yamada, T., Onimatsu, H., and Van Etten, J. L. (2006). Chlorella viruses. *Adv Virus Res* **66,** 293-336.

Yamamoto, M., and Curiel, D. T. (2010). Current issues and future directions of oncolytic adenoviruses. *Mol Ther* **18**(2)**,** 243-50.

Yang, T. C., Yang, Q., and Maluf, N. K. (2009). Interaction of the adenoviral IVa2 protein with a truncated viral DNA packaging sequence. *Biophys Chem* **140**(1-3)**,** 78-90.

Zhang, W., and Arcos, R. (2005). Interaction of the adenovirus major core protein precursor, pVII, with the viral DNA packaging machinery. *Virology* **334**(2)**,** 194-202.

Zhang, W., and Imperiale, M. J. (2000). Interaction of the adenovirus IVa2 protein with viral packaging sequences. *J Virol* **74**(6)**,** 2687-93.

Zhang, W., Low, J. A., Christensen, J. B., and Imperiale, M. J. (2001). Role for the adenovirus IVa2 protein in packaging of viral DNA. *J Virol* **75**(21)**,** 10446-54.

Zhao, H., Finch, C. J., Sequeira, R. D., Johnson, B. A., Johnson, J. E., Casjens, S. R., and Tang, L. (2010). Crystal structure of the DNA-recognition component of the bacterial virus Sf6 genome-packaging machine. *Proc Natl Acad Sci U S A* **107**(5)**,** 1971-6.

Glossary

µm:	Micrometer
2D:	two dimensions
3D:	three-dimensions
3DEM:	three-dimentional electron microscopy
Å:	amstrong
A/T:	adenine/timine
AA:	aminoacid
AB:	antibody
Ad:	adenovirus
Ad2:	adenovirus type 2
Ad41:	adenovirus type 41
Ad5:	adenovirus type 5
Ad7:	adenovirus type 7
ATP:	adenosin triphosphate
bp:	base pair
CAR:	Coxsackievirus and adenovirus *receptor*
CAV-2:	Canine adenovirus type 2
ChIP:	chromatin immunoprecipitation
Cryo-EM:	Cryo-electron microscopy
CsCl:	Caesium chloride
C-terminal:	carboxi-terminal
Da:	Dalton
DBP:	adenoviral DNA binding protein
DNA:	Deoxyribonucleic acid
dsDNA:	double strand deoxyribonucleic acid
E.coli:	Escherichia coli
EM:	Electron microscopy
EMAN:	http://blake.bcm.edu/emanwiki/EMAN/
EMSA:	electrophoretic mobility shift assay
flIVa2:	full lenght IVa2 protein
GL:	glutaraldehyde
GON:	Group of nine hexons
GOS:	Group of six hexons
HVS:	Herpes virus simplex
ITR:	inverted terminal repeats
kb:	kilobase
kDa:	kilo Dalton
kpb:	kilo base pair
kV:	kilo volt
LAdV:	Lizard adenovirus

MLF2D:	2D-classification by maximum-likelihood in Fourier space
MLF3D:	3D-classification by maximum-likelihood in Fourier space
MLP:	major late promoter
mRNA:	messenger ribonucleic acid
nm:	nanometer
OAdV:	Ovine adenovirus
pol:	polimerase
PS:	Packaging sequence
px:	pixel
SnAdV:	Snake adenovirus
TP:	Terminal protein
TRIS:	tris(hydroxymethyl)aminomethane
trIVa2:	truncated IVa2 protein
UCSF CHIMERA:	http://www.cgl.ucsf.edu/chimera/
WB:	western blot
XMIPP:	http://xmipp.cnb.csic.es/twiki/bin/view/Xmipp/WebHome

Agradecimientos

Esta tesis no habría sido posible sin la ayuda y la dirección de Carmen San Martín. Agradezco la oportunidad que me ha dado para investigar junto a ella durante los últimos cinco años, su calidez humana y buen sentido del humor a lo largo de todo este tiempo.

También quiero agradecer al Prof. J. M. Carazo y a todo su grupo, por su colaboración y simpatía. A los grupos del Prof. J. L. Carrascosa y del Prof. J. M. Valpuesta por compartir conocimientos, por su disponibilidad y cercanía. (Gracias también por alguna alícuota de bacteriófago T7 para mis controles).

To our collaborators, P. Hearing, Mena Ostapchuk, Jane Flint, Rachel Marschang, Tibor Papp, Mária Benkö, Balázs Harrach.

A las personas de los servicios científicos del CNB que han participado de algún modo en la elaboración de esta tesis: a Leonor Kremer por sus buenos consejos a la hora de utilizar y entender los anticuerpos, y a Fernando Roncal, por la síntesis de las membranas para el mapeo de epítopos. A las personas del servicio de proteómica que han realizado los experimentos de espectrometría de masas, Silvia Juárez, Alberto Paradela y Rosana Navajas. A Juan Carlos Sánchez, por facilitarnos los modelos por homología para la interpretación del mapa 3D de SnAdV-1.

Párrafo aparte para el servicio de microscopía. Gracias a Cristina y a Javi por tantos años echando una mano y aclarando dudas. Gracias también a Rocío, en el breve tiempo que hemos compartido en el CNB ha sido de gran ayuda.

Kiitoksia kauhean paljon Ville Väisänen, Mari Peltola, Veikko Wahlroos (Laboratorion ensimmäinen opettajat!!).

Quiero agradecer a todas las personas que he ido conociendo durante este tiempo, por haber hecho mi estancia mucho más agradable e interesante de lo que jamás hubiese pensado. Gracias a las personas que han compartido tiempo de deporte conmigo, a los que me han acompañado a ver estrellas fugaces, a los montañeros y a los artistas.

Gracias también a mis compañeras (y ex compañer@s) de laboratorio por ser, muchas veces, más que simplemente eso. Gracias María, Ana, Marta, Cris, Ambra, Esther, Elena, Alejandro, Gabriela, Álvaro. Podría escribir capítulos completos con las cosas que me habéis aportado. Sabéis que no olvidaré cada vez que habéis sacado tiempo para facilitarme un protocolo, cada vez

que se ha hecho un apoyo técnico excelente, cada vez que me habéis aconsejado bien en lo personal.

A mi familia, por comprender la necesidad que tengo de complicarme la vida haciendo cosas como esta. En especial a mi hermana y a mi abuela, por apoyarme en todo momento, por estar siempre presentes.

A mi familia de Madrid, por abrirme sus puertas y hacerme sentir como en casa. Gracias MªÁngeles, David, Ana, Alina, Marina, Hugo, Ricardo, gracias por estos años. He aprendido mucho de vosotr@s.

Alla mia famiglia d'Italia, per avermi fatto sentire sempre benvenuta. Un grazie a Rosalinda, Marcello, Daria e la nonna. Grazie a Andrea, per stare sempre vicino.

A esas personas que han estado cerca cuando más lo he necesitado, quienes a pesar de la distancia y del paso de tantos años, siempre me han acompañado. Gracias Abel, Marco, Cape, Lorena.